

# Superfluidity in nuclear systems and neutron stars

Armen Sedrakian\*

Frankfurt Institute for Advanced Studies, Ruth-Moufang str. 1, 60438 Frankfurt am Main, Germany

John W. Clark†

Department of Physics and McDonnell Center for the Space Sciences,

Washington University, St. Louis, Missouri 63130, USA and

Centro de Investigação em Matemática e Aplicações, University of Madeira, 9020-105 Funchal, Madeira, Portugal

(Dated: 22 Jan. 2018)

Nuclear matter and finite nuclei exhibit the property of superfluidity by forming Cooper pairs due to the attractive component of the nuclear interaction. We review the microscopic theories and methods that are being employed to understand the basic properties of superfluid nuclear systems, with emphasis on the spacially extended ensembles encountered in neutron stars and in nuclear collisions. Our survey includes techniques which are based on Green functions, correlated basis functions, and Monte Carlo sampling of quantum states. Novel phases arise in nuclear and related systems (such as ultra-cold atomic gases) under imbalance in the populations of the fermions that form Cooper pairs. Such phases include current-carrying superfluid states, heterogeneous phase-separated states, and phases involving deformation of Fermi surfaces. The phase diagram of imbalanced superfluids is reviewed, focusing especially on the crossover from Bardeen-Cooper-Schrieffer (BCS) pairing to a Bose-Einstein condensate (BEC) of tightly bound dimers under increase of the coupling strength of the theory. The neutron, proton, and hyperonic condensates that may exist under conditions prevailing in neutron stars are discussed, and calculations of weak-interaction rates within the Green functions formalism are examined in detail. We close with a discussion of quantum vortex states in nuclear systems and their dynamics in neutron-star crusts.

## Contents

<b>I. Introduction</b>	1	1. BCS-BEC transition in the balanced case	25
<b>II. Basic BCS theory for nuclear systems</b>	3	2. BCS-BEC transition in the imbalanced case	26
A. Pairing Hamiltonian and the gap equation	3	F. Toward a complete phase diagram	28
B. Nucleon-nucleon pairing in different partial waves	4	G. Spin polarized neutron matter	29
C. Effects of isospin asymmetry and neutron stars	5	<b>V. Astrophysical manifestations of pairing in neutron stars</b>	31
D. Finite nuclei	7	A. Pairing patterns in neutron stars	31
E. Interface between nuclear systems and cold atomic gases	8	B. Pairing in higher partial waves	32
<b>III. Methods for strongly correlated systems</b>	9	C. Hyperonic pairing	34
A. Green Functions approach and Gor'kov formalism	9	D. Overview of neutrino radiation from compact stars	35
1. Green functions formalism	10	E. Pair-breaking and formation processes	37
2. Mean-field BCS theory	11	F. Collective modes	39
3. Polarization effects	12	G. Urca process in superfluid phases	39
4. Boson-exchange theories	13	H. Axion radiation from superfluid phases	40
B. T- and G-matrix approaches, Thouless criterion	14	<b>VI. Quantum vorticity</b>	42
C. Self-consistent Green's functions theory (SCGF)	16	A. Motivation	42
D. Correlated Basis Functions Theory	18	B. Vortex core quasiparticles	42
E. Monte Carlo methods	19	C. Vortex dynamics and pinning	43
F. Overview of the results	20	D. Mutual friction	44
<b>IV. Unconventional pairing and BCS-BEC crossovers</b>	20	<b>VII. Conclusions</b>	45
A. Formalism	21	<b>Acknowledgments</b>	46
B. Homogeneous phase	23	<b>References</b>	46
C. FFLO phases	23		
D. Deformed Fermi surface phase	24		
E. BCS-BEC crossover	25		

\*Electronic address: [sedrakian@fias.uni-frankfurt.de](mailto:sedrakian@fias.uni-frankfurt.de)

†Electronic address: [jwc@physics.wustl.edu](mailto:jwc@physics.wustl.edu)

## I. INTRODUCTION

Pairing phenomena play an important role in experimental and observational manifestations of neutron

stars and finite nuclei. Their theoretical understanding is rooted in the microscopic theory of superconductivity advanced by Bardeen, Cooper and Schrieffer (BCS) (Bardeen *et al.*, 1957). However, strong correlations, which are generic to nuclear systems, and the complex dynamics of finite systems, such as nuclei, require developments beyond this theory. The study of nuclear systems is built on our understanding of the underlying nuclear forces and the quantum many-body theory of fermionic systems – both aspects having undergone immense advances during the past several decades. In parallel with these improvements in the ingredients of the theory, the scope of the problems considered has broadened over the years and now includes such traditionally “condensed-matter” issues as the crossover from the BCS condensate to Bose-Einstein condensate (BEC), inhomogeneous phases with broken spatial symmetries, pair-breaking in strong magnetic fields or resistive flow of quantum vorticity.

In this review we concentrate on the recent developments in the quantum many-body problem associated with nuclear pairing, on novel forms of nuclear pairing that have strong overlap with the physics of ultra-cold atoms, and on the roles played by pairing in macroscopic manifestations of neutron stars. There exist a number of previous reviews that cover different stages of development of pairing theory in the nuclear context, with emphasis placed on varied aspects of pairing phenomena (Dean and Hjorth-Jensen, 2003; Gezerlis *et al.*, 2014; Lombardo and Schulze, 2001; Page *et al.*, 2013; Takatsuka and Tamagaki, 1993). The reader will benefit from consulting them for alternative exposition of selected topics.

The key insights into nuclear pairing were put forward shortly after the advent of the BCS theory (Bogoliubov, 1958; Bohr *et al.*, 1958; Migdal, 1959). The overwhelming success of the BCS theory in explaining the properties of metallic superconductors provided experimental verification of the Cooper theorem (Cooper, 1956), which asserts that attractive fermions filling a Fermi sphere will form spin-zero bound pairs with equal and opposite momenta. Since the long-range part of the nuclear interaction is attractive, it is natural to conclude that nucleons will form Cooper pairs in nuclei and neutron-star matter, as these systems contain an ensemble of quantum-degenerate states of nucleons bound by either the nuclear force (nuclei) or gravity (neutron stars). In due course, essential aspects of the modern quantum many-body theory were introduced, such as the Fermi-liquid theory of nuclear systems (Larkin and Migdal, 1964; Migdal, 1962), quantum vorticity in superfluid neutron matter (Ginzburg and Kirzhnits, 1965) and type-II superconductivity of proton matter (Baym *et al.*, 1969a).

A new impetus to the theory of fermionic pairing was provided by the discovery of pulsars in 1967 (Hewish *et al.*, 1968) and their identification with neutron stars (Gold, 1968). In particular, observations of long time scales for the recovery of regular pulse fre-

quency following pulsar glitches provided the first evidence of possible superfluidity of neutron star interiors (Baym *et al.*, 1969b). Initial many-body calculations of pairing already predicted the correct magnitude of the gap in neutron and proton fluids of about 1 MeV, although the nuclear interactions available at the time were not very realistic. The initial theoretical treatments indicated that neutron pairing in the inner crust of a neutron star would occur in the  $^1S_0$  state (Yang and Clark, 1971) and in the  $^3P_2$  state (Hoffberg *et al.*, 1970; Takatsuka and Tamagaki, 1971) at higher densities present in the stellar core. Because of the low abundance of protons relative to neutrons in  $\beta$ -stable neutron-star matter, protons were predicted to pair in the  $^1S_0$  state over some range of densities within the core (Chao *et al.*, 1972).

The uncertainty in the values of the pairing gaps predicted for various models was substantially reduced with the advent of potentials that are realistic in the sense that they provide high-precision fits to the energy dependence of the experimental scattering phase shifts (with  $\chi^2 \simeq 1$ ). There is in fact a direct relation between scattering phase shifts for nucleonic scattering and the magnitudes of the pairing gaps (Elgarøy and Hjorth-Jensen, 1998; Khodel *et al.*, 1996). Nevertheless, a quantitative microscopic understanding of the way in which gap values are affected by correlations among nucleons produced both by their interactions and Pauli exclusion, is still lacking. We shall examine this situation in some detail.

The last decade has seen impressive advances in both experimental and theoretical research on pairing in the novel fermionic systems realized in ultra-cold fermionic gases, which exhibit many features in common with nucleonic superfluids. Such atomic systems allow for remarkable control within the relevant parameter space, notably by tuning of the strength of the pairing force via a Feshbach resonance (Bloch *et al.*, 2008; Giorgini *et al.*, 2008; Leggett and Zhang, 2012). Importantly, these systems can provide a testbed for the repertoire of theoretical approaches being used to describe nucleonic pairing at the microscopic level. Existing parallels have been explored in the context of several phenomena, especially the transition from a BCS-paired state to a BEC. Another commonality arises when one studies cases of imbalanced pairing, as may occur in a nuclear system with unequal numbers of neutrons and protons. Such isospin asymmetry (or flavor asymmetry more generally) can be easily simulated in ultra-cold systems of atoms having unequal populations of different hyperfine states. A third parallel involves the quantum vortex states in ultra-cold atomic gases that can be explored *in situ* by imaging techniques; these provide a complete analog of neutron vorticity in rotating neutron stars. Accordingly, another focus of this review will be on these three phenomena as they occur in nucleonic systems, with the prospect of experimental verification in systems of ultra-cold atoms.

What can be learned about nuclear superfluidity and pairing from observations of neutron stars? In fact, the

observed rotational anomalies in pulsar spins and the X-ray measurements of their surface temperatures provide us with significant evidence of superfluidity of their interiors. The pulsed emission of pulsars (with periodicity of seconds or less) is locked to the rotation period of the star. Pulsars are nearly perfect clocks with their periods increasing gradually over time due to the secular loss of rotational energy. However, some pulsars undergo abrupt increases in their rotation and spin-down rates which are followed by slow relaxation toward their pre-glitch values, on a time scale of order weeks to years, in some cases with permanent hysteresis effects. Such behavior is attributed to a component within the star that is only weakly coupled to the rigidly rotating normal component responsible for the emission of pulsed radiation. A natural candidate for such a phase is the neutron superfluid either in the core ( $P$ -wave) or in the crust ( $S$ -wave). Furthermore, young neutron stars cool by neutrino emission from the dense interior and the cooling histories of neutron stars appear to be consistent with the existing data only if the neutrino emission rates incorporate the superfluidity of their interiors. Our discussion will focus, in part, on advances in the understanding of the role of pairing in superfluid dynamics and neutrino emission. Thus, a strong focus of this article will be on microscopic many-body methods for the computation of superfluid properties of neutron stars.

Radioactive-beam facilities have opened an exciting new arena for nuclear physics, instrumental to the study of exotic nuclei close to the proton and neutron drip lines. They enable acquisition of vital information on the nature of the pairing in neutron/proton-rich stable and unstable nuclei, which is of great importance in nuclear astrophysics, especially for an understanding neutron-star crusts. Hartree-Fock-Bogolyubov (HFB) theories have evolved into a standard tool that incorporates pairing in the description of medium-to-heavy nuclei. However, modern HFB codes still employ simplistic pairing interactions that are matched phenomenologically to more rigorous computations in infinite nuclear matter based on realistic nuclear interactions. While some consideration will be given to the role of pairing in exotic nuclei and the neutron-star crust, this will not be a topic of emphasis in the present review.

We will use natural units  $\hbar = c = 1$  throughout, unless otherwise stated.

## II. BASIC BCS THEORY FOR NUCLEAR SYSTEMS

### A. Pairing Hamiltonian and the gap equation

We start with a brief description of the simplest model of superconductivity, based on the Bogolyubov's method of canonical transformations (Bogoljubov, 1958). This method still serves as a prototype for the treatment of pairing in finite nuclei (Ring and Schuck, 1980). Consider a system of fermions with macroscopic number  $N$

described by the pairing Hamiltonian

$$H - \mu N = \sum_{\mathbf{p}, \sigma} \epsilon_p a_{\mathbf{p}\sigma}^\dagger a_{\mathbf{p}\sigma} - G \sum_{\mathbf{p}_1 + \mathbf{p}_2 = \mathbf{p}_3 + \mathbf{p}_4} a_{\mathbf{p}_3}^\dagger a_{\mathbf{p}_4}^\dagger a_{\mathbf{p}_1} a_{\mathbf{p}_2}. \quad (1)$$

The first term is the kinetic energy, with  $\epsilon_p = p^2/2m - \mu$ , while the second term is the attractive interaction energy, approximated by a contact ( $\delta$ -function-type) interaction of strength  $G$ . Here  $a^\dagger(\mathbf{p}, \sigma)$  and  $a(\mathbf{p}, \sigma)$  are respectively the creation and annihilation operators for particles having spin  $\sigma = \uparrow\downarrow$  and momentum  $\mathbf{p}$ , with  $\mu$  denoting the chemical potential. The method of canonical transformations introduces two new creation and annihilation operators  $\alpha^\dagger$  and  $\alpha$  through

$$a_{\mathbf{p}, \uparrow} = u_p \alpha_{\mathbf{p}\uparrow} + v_p \alpha_{-\mathbf{p}\downarrow}^\dagger \quad \text{and} \quad a_{\mathbf{p}, \downarrow} = u_p \alpha_{\mathbf{p}\downarrow} + v_p \alpha_{-\mathbf{p}\uparrow}^\dagger. \quad (2)$$

These new operators obey the fermionic commutation relation  $\{\alpha_{\mathbf{p}, \sigma}, \alpha_{\mathbf{p}', \sigma'}^\dagger\} = \delta_{\mathbf{p}\mathbf{p}'} \delta_{\sigma\sigma'}$  provided the Bogolyubov amplitudes  $u_p$  and  $v_p$  satisfy the normalization condition  $u_p^2 + v_p^2 = 1$ , implying that the free energy of the system is a functional of only one amplitude. The free energy is given by the standard expression

$$E - \mu N = \langle H - \mu N \rangle, \quad (3)$$

where  $\langle \dots \rangle$  denotes the mean value of the operator enclosed in brackets,  $N$  is the net particle number operator. The quasiparticle occupation numbers are defined by  $\langle \alpha_{\mathbf{p}, \downarrow}^\dagger \alpha_{\mathbf{p}, \downarrow} \rangle = n_{\mathbf{p}, \downarrow}$  and  $\langle \alpha_{\mathbf{p}, \uparrow}^\dagger \alpha_{\mathbf{p}, \uparrow} \rangle = n_{\mathbf{p}, \uparrow}$ . Minimization of the free energy (3), which requires  $\delta(E - \mu N)/\delta v_p = 0$ , leads to the gap equation

$$\Delta = G \sum_{\mathbf{p}} u_p v_p (1 - n_{\mathbf{p}, \downarrow} - n_{\mathbf{p}, \uparrow}), \quad (4)$$

where

$$u_p^2 = \frac{1}{2} \left( 1 + \frac{\epsilon_p}{E_p} \right), \quad v_p^2 = \frac{1}{2} \left( 1 - \frac{\epsilon_p}{E_p} \right). \quad (5)$$

The quasiparticle energy in the superconducting state is given by  $E_p = \sqrt{\epsilon_p^2 + \Delta^2}$ , which demonstrates the key property of superconductivity and superfluidity in fermionic systems: the spectrum of a superconductor features an energy gap  $\Delta$  separating the ground state from any excited state. Note that the variation  $\delta(E - \mu N)/\delta n_{\mathbf{p}, \uparrow}$ , with  $u_p$  and  $v_p$  held constant, yields the quantity  $E_p$ , confirming its meaning as assigned above. Consequently, excitations can be created in the system if a Cooper pair breaks, implying that an energy of at least  $2\Delta$  must be supplied to the system. The existence of gap in the spectrum  $E_p$  ensures the defining property of a superconductor – the absence of resistance to an electrical current, or the absence dissipation in fluid flow in neutral fermionic fluids such as neutron matter.

Let us now extract a standard expression for the energy gap from Eq. (4). This is done for finite temperature  $T$  by inserting the equilibrium occupation numbers for

fermion quasiparticles, i.e.,  $f(p) = (e^{E_p/T} + 1)^{-1}$ , and changing the integration measure according to  $d^3p \rightarrow m^* p_F d\epsilon_p d\Omega$ , where  $m^*$  is the effective mass and  $p_F$  is the Fermi momentum. Thereby we obtain

$$1 = \frac{\lambda}{2} \int_0^\Lambda \frac{d\epsilon_p}{\sqrt{\epsilon_p^2 + \Delta^2}} \tanh\left(\frac{\sqrt{\epsilon_p^2 + \Delta^2}}{2T}\right), \quad (6)$$

where  $\lambda = G\nu(p_F)$  is the dimensionless coupling,  $\nu(p_F) = p_F m^* / \pi^2$  is the density of quasiparticle states, and the ultraviolet cut-off  $\Lambda$  is needed to regularize the integral for large momenta. In the limit  $T \rightarrow 0$ , the tanh function becomes unity and the integral (6) is computed using the substitution  $\epsilon_p = \Delta \sinh \phi$ . Eq. (6) then reduces to  $1 = (\lambda/2) \operatorname{arcsinh}(\Lambda/\Delta)$ . For weak coupling, i.e.  $\Delta \ll \Lambda$ , application of the relation  $\lim_{x \rightarrow \infty} \operatorname{arcsinh} x = \ln(2x) + O(x^{-2})$  yields the famous gap equation of BCS theory at  $T = 0$ :

$$\Delta_0 = 2\Lambda \exp(-2/\lambda). \quad (7)$$

This result reveals a property of BCS pairing that is awkward from the computational standpoint: the exponential sensitivity of the energy gap to variation of the nuclear pairing matrix elements.

In the asymptotic regime  $T \rightarrow T_c$ , where  $T_c$  is the critical temperature for destruction of pairing, the gap equation can be linearized by setting  $\Delta = 0$  in the denominator of Eq. (6). Straightforward integration leads to  $T_c = (2\Lambda\gamma/\pi) \exp(-2/\lambda) = \gamma/\pi\Delta_0$ , where  $\gamma \equiv e^C$  and  $C = 0.57$  is the Euler constant. To next-to-leading order in the small and large temperature expansions, one finds

$$\Delta(T) = \begin{cases} \Delta_0 - \sqrt{2\pi\Delta_0 T} \exp(-\Delta_0/T), & T \rightarrow 0, \\ 2\pi\sqrt{2/7\zeta(3)} [T_c(T_c - T)]^{1/2}, & T \rightarrow T_c, \end{cases} \quad (8)$$

where  $\zeta(x)$  is the Riemann  $\zeta$  function. It follows from Eq. (8) that the temperature variations of the gap function at low temperatures are exponentially small, and that upon approach to the critical temperature, the gap closes with infinite slope.

The contact-interaction model described above can be applied to spin-1/2 fermions, characterized by free-space scattering length  $a_0$ , in the dilute gas limit  $|a_0|p_F \ll 1$ . In this case, the exponential in Eq. (7) is given by  $\lambda = \pi/4p_F|a_0|$ , whereas the scale for  $\Lambda$  is set by the Fermi energy  $\epsilon_F$ . Non-perturbative computations show that  $\Lambda = (4\epsilon_F/e^2)\beta_{GM}$ , where  $\beta_{GM} = (4e)^{-1/3}$  is a correction arising from polarization type contributions to the matrix element (Gor'kov and Melik-Barkhudarov, 1961). The pairing in the low-density neutron matter (with  $a_n \simeq -19$  fm) can be treated within the Gor'kov-Melik-Barkhudarov theory in the dilute regime ( $|a_n|p_F \ll 1$ ). Numerical studies of pairing in neutron matter within this theory and its extensions have been conducted by a number of authors (Fan *et al.*, 2017; Schulze *et al.*, 2001).

The contact-interaction model also forms the basis for the computations of BCS pairing in finite nuclei within density functional theories, to be discussed in Sec. II.D.

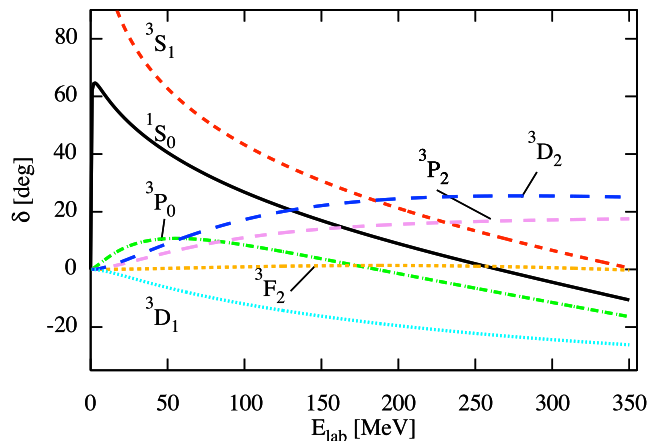


FIG. 1 Dependence of nucleon-nucleon scattering phase shifts on the laboratory energy of a two-nucleon system for the channels relevant to the pairing problem.

## B. Nucleon-nucleon pairing in different partial waves

The complexity of the problem of pairing in nuclear systems stems largely from the complexity of nuclear interactions. In practice the assumed interactions divide roughly into those employed in density functional studies and those designed for *ab initio* computations. With the pairing interaction given directly by the bare nucleon-nucleon (NN) potential, computation of the gap and other superfluid properties of infinite nuclear systems (e.g. neutron stars) is straightforward at the mean-field BCS level in the energy range where the interactions are well constrained by the elastic nucleon-nucleon scattering data, i.e.,  $E_{\text{lab}} < 350$  MeV. Such calculations performed with NN-interaction models that fit the scattering data with high precision, such as the Argonne  $v_{18}$  ( Wiringa *et al.*, 1995), Paris (Lacombe *et al.*, 1980), Nijmegen (Stoks *et al.*, 1994) and Bonn (Machleidt, 2001), converge to identical results for the pairing gaps in the low partial waves. The low-energy sector of the nuclear force is accurately described by potentials that are based on chiral perturbation theory, in which the interactions are modeled in terms of pion and nucleon fields and are organized in powers of a typical momentum scale of the nuclear problem over a cutoff  $\Lambda_{\text{QCD}} \sim 1$  GeV/c provided by the chiral symmetry breaking scale (Machleidt and Entem, 2011). At sufficiently high order, the nuclear potentials constructed using chiral effective field theory may have precision comparable to that achieved with the high-precision NN phenomenological potential models mentioned above.

The pairing patterns in nuclear matter and neutron-star matter can be understood qualitatively on the basis of partial-wave analysis of NN scattering data. Phase shifts derived from this analysis for different partial-wave channels  $^{2S+1}L_J$  of the two-nucleon scattering problem are identified using standard spectroscopic notation. The relative orbital angular momentum quantum number

$L = 0, 1, 2, \dots$  is mapped successively to  $S, P, D, F, G, \dots$ , while the total spin quantum number  $S = 0, 1$  maps to singlet and triplet spin states. The allowed values the total angular momentum quantum number,  $J = 0, 1, 2, \dots$ , follow from the quantum-mechanical vector sum of the relative orbital and total spin angular momentum operators.

The experimental scattering phases in the range of laboratory energies  $0 < E_{\text{lab}} \leq 350$  MeV are shown in Fig. 1 for partial waves that are relevant to pairing in nuclear and neutron matter. As discussed in the next subsection, isospin  $T = 1$  pairing dominates in neutron matter, whereas in symmetrical nuclear matter  $T = 0$  pairing competes with  $T = 1$  pairing. Before assessing the roles of various pairing channels, we focus on the consequences of Pauli principle for the scattering two nucleons, whose total wave function has spin and isospin components besides its spatial component.

To satisfy the Pauli principle, the total wave function, including isospin, must be antisymmetrical under interchange of the two nucleons. At low energies,  $L = 0$  states dominate. Necessarily symmetrical in spatial dependence under exchange, the allowed possibilities are the  $^1S_0$  partial wave and the  $^3S_1$ - $^3D_1$  coupled partial wave. (Coupling in the later case is due to the presence of a tensor component in the nuclear force, required to explain the quadrupole moment of the deuteron.) With  $L = 0$ , consider now the cases of neutron-neutron and proton-proton scattering, trivially implying  $T = 1$  and hence an isospin-symmetric wave function. To satisfy the Pauli principle, the spin component must then be asymmetric under exchange, thus excluding occupancy of the  $S = 1$  state of spin and hence the triplet  $^3S_1$ - $^3D_1$  coupled partial wave.

Consequently, the dominant attractive  $^3S_1$ - $^3D_1$  partial wave channel (see Fig. 1) cannot lead to pairing in neutron-dominated matter, where neutrons and protons have Fermi surfaces of vastly different radii. On the other hand, at the opposite extreme of symmetrical nuclear matter, these Fermi surfaces coincide, and one may expect strong  $T = 0$  pairing to occur in this channel. Moreover, since the deuteron is bound in this partial wave with energy  $E_d = -2.2$  MeV, one may also expect a transition to a Bose-Einstein condensate of deuterons at asymptotically low density.

At the large isospin asymmetries found in neutron stars, where the neutron number density is about 95% of the total baryonic density, only  $T = 1$  Cooper pairs can form. This will occur at relatively low densities, driven by the attraction in the  $^1S_0$ -partial wave channel. Here observe from Fig. 1 that the attractive  $^3P_0$  channel remains sub-dominant to the  $S$ -wave channel in the low-energy regime below  $E_{\text{lab}} = 70$  MeV, where this  $P$ -wave competitor is overtaken by the  $^3P_2$ - $^3F_2$  coupled partial wave as the most attractive  $L = 1$  channel. However, it is only around  $E_{\text{lab}} = 170$  MeV that the  $^3P_2$ - $^3F_2$  partial wave starts to dominate the  $T = 1$  scattering, as the  $^1S_0$ -wave interaction loses its attractive component and eventually becomes repulsive (having negative phase

shifts) for  $E_{\text{lab}} > 250$  MeV.

Thus, the dominant  $T = 1$  channel above  $E_{\text{lab}} = 200$  MeV energy is the coupled  $^3P_2$ - $^3F_2$  partial-wave channel, for which the spatial wave function is antisymmetric, whereas the total spin  $S = 1$  and isospin  $T = 1$  imply symmetrical components of the wave function in their respective spaces. Accordingly, pairing in the triplet spin-1 channel is allowed by the Pauli principle for two neutrons or protons. In contrast, if the nuclear system has equal populations of neutrons and protons,  $S = 1$  and  $T = 0$  pairs may be formed in the  $^3D_2$  channel, which applies exclusively to neutron-proton scattering, being forbidden for like-isospin particles by the Pauli principle.

To this point we have referred to specific features of the nuclear interaction exhibited in two-nucleon scattering over ranges of laboratory energy. How does one translate this behavior into density ranges in neutron stars? This can be done semi-quantitatively by observing that the center-of-mass energy of two scattering fermions, given by  $E_{\text{lab}}/2$ , should be roughly twice the Fermi energy of the nuclear medium. With applications to neutron stars in mind, we may focus on the high-density, low-temperature regime of highly degenerate nucleonic matter. Neutron Fermi energies are of the order  $E_{F_n} \simeq 60$  MeV in neutron-star matter at the nuclear saturation density,  $n_0 = 0.16$  fm $^{-3}$ . From this, we can already predict the result, born out in microscopic many-body calculations, that neutron pairing in the  $^1S_0$  partial wave will expire at depths slightly above the crust-core interface, where the density is about half  $n_0$ . The low proton fraction in the neutron-star core,  $x_p \simeq 5$ -10%, and the correspondingly low proton Fermi energies, imply that proton pairing occurs in the  $^1S_0$  state up to quite high densities. It is conceivable that at neutron-star densities in excess of a few times the nuclear saturation density, pairing can occur in higher even- $L$  partial waves such as the  $^1D_2$  channel (not shown in Fig. 1). On the other hand, isospin-symmetric nuclear matter with  $n_p = n_n$ , where  $n_n$  and  $n_p$  are the number densities of neutrons and protons, may support pairing in the attractive  $^3D_2$  partial wave, with a wave function which is symmetrical in space, antisymmetrical in isospace ( $T = 0$ ) and symmetrical in spin space ( $S = 1$ ). In some models of dense matter the densities of neutrons and protons can be forced to be equal through the emergence of a meson condensate.

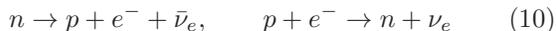
### C. Effects of isospin asymmetry and neutron stars

Much of the research on nuclear pairing is concerned with neutron stars, so it is important to review the state of matter in such objects. The interiors of neutron stars are approximately in equilibrium with respect to the weak interactions during their lifetimes. Small deviations from such equilibrium may be important in some problems, such as the bulk viscosity of matter, but for the most part we will assume strict  $\beta$ -equilibrium. The

resulting disparity between the neutron and proton numbers (breaking the  $SU(2)$  symmetry in matter) has profound influence on the pairing patterns in neutron stars. The isospin asymmetry is quantified by the asymmetry (or neutron excess) parameter

$$\alpha = \frac{n_n - n_p}{n_n + n_p}. \quad (9)$$

If the temperatures of neutron stars are below several MeV, a condition reached by at most several hours after birth, neutrinos leave the stellar interior without interaction. Hence their chemical potentials can be set to zero. Consider for illustration the simplest case of matter composed of neutrons ( $n$ ), protons ( $p$ ) and electrons ( $e$ ) in weak equilibrium. The processes of the  $\beta$ -decay and electron capture reactions



establish a certain balance between the abundances of hadrons and leptons, which requires  $\mu_e = \mu_n - \mu_p$ , where  $\mu$  refers to the chemical potentials of the three particle types involved. Given the energy density  $E_{NM}$  of asymmetric nuclear matter at baryon density  $n$  at zero temperature, these chemical potentials can be expressed as

$$\mu_{n/p} = \frac{\partial E_{NM}(n, \alpha)}{\partial n_{n/p}}, \quad (11)$$

where  $\delta\mu = \mu_n - \mu_p = \mu_e$  and  $n_i$  with  $i \in \{n, p, e\}$  are the number densities of species. Charge neutrality requires coincidence of proton and electron number densities:  $n_p = n_e$ . Treating electrons as non-interacting and massless, we have  $n_e = \mu_e^3/3\pi^2$ , which in turn means that if  $\mu_e \leq m_\mu$ , where  $m_\mu = 105.7$  MeV is the muon rest mass, the proton fraction  $Y_p = n_p/n = (1 - \alpha)/2$  (and similarly the electron fraction  $Y_e$ ) may be expressed as

$$Y_p = Y_e = \frac{8}{3\pi^2 n} S_2^3 \left( \frac{1}{2} - Y_p \right)^3, \quad (12)$$

in terms of an expansion  $E_S = S_2\alpha^2 + S_4\alpha^4 + O(\alpha^6)$  of the symmetry energy of nuclear matter. On the other hand, once  $\mu_e \geq m_\mu$ , the electrons decay into muons via the reaction  $e^- \rightarrow \mu^- + \bar{\nu}_\mu + \bar{\nu}_e$ . Equilibrium with respect to this process and its inverse implies  $\mu_e = \mu_\mu$ , where  $\mu_\mu$  is the chemical potential of muons. The proton fraction in this case is given by the parametric equation

$$Y_p = \frac{1}{3\pi^2 n} \left[ (\delta\mu^2 - m_\mu^2)^{3/2} + \delta\mu^3 \right]. \quad (13)$$

At densities exceeding nuclear saturation by factors of a few, the appearance of heavier baryons with non-zero strangeness becomes energetically favorable in many (but not all) nuclear models. To generalize the equilibrium conditions to this situation, one observes that there are

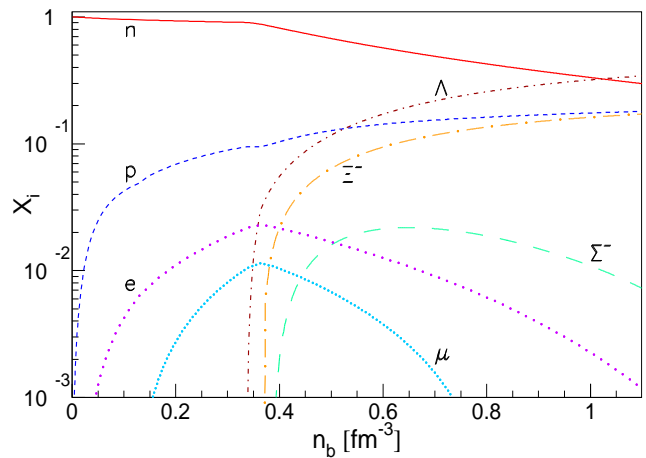


FIG. 2 Dependence of the baryon and lepton fraction on the total baryonic density  $n_b$  for DDME2 covariant density functional.

two conserved charges in matter - the total baryonic charge, which enforces baryon-number conservation, and the total electrical charge, which enforces charge neutrality of the system. (Strangeness is not conserved in weak interactions, which may convert nucleons into hyperons, therefore the strangeness chemical potential is zero). The baryon and lepton chemical potentials are obtained as

$$\mu_i = \frac{\partial E_{NM}}{\partial n_i} = -\mu_B B_i + \mu_L Q_i, \quad (14)$$

$$\mu_j = \frac{\partial E_{NM}}{\partial n_j} = \mu_L Q_j, \quad (15)$$

where  $i$  and  $j$  enumerate the baryon and lepton species respectively,  $B_i$  and  $Q_i$  are the baryon and electric charges,  $\mu_B$  and  $\mu_L$  are the associated Lagrange multipliers and  $n$  is the net baryon density.

Conventionally, the neutron and electron chemical potentials are chosen as independent parameters, i.e.,  $\mu_B = -\mu_n$  and  $\mu_L = -\mu_e$ , and the chemical potentials of arbitrary baryonic species can be read off from Eq. (14) and (15) as  $\mu_i = B_i\mu_n - Q_i\mu_e$ . For example, in a mixture consisting of  $n$ ,  $p$ ,  $\Sigma^\pm$ , and  $\Lambda^0$  baryons, the equilibrium is determined by the set of equations

$$\mu_{\Sigma^-} = \mu_n + \mu_e, \quad \mu_\Lambda = \mu_n, \quad (16)$$

$$\mu_{\Sigma^+} = \mu_n - \mu_e = \mu_p, \quad \mu_\mu = \mu_e, \quad (17)$$

$$Y_p + Y_{\Sigma^+} - (Y_e + Y_\mu + Y_{\Sigma^-}) = 0, \quad (18)$$

where  $Y_{i,j} = n_{i,j}/n$ . In Fig. 2 we illustrate the abundances of various species in a mixture of baryons and leptons in the interior of a neutron star in the case of density dependent covariant functional theory (Fortin *et al.*, 2016; Raduta *et al.*, 2017). It is seen that the neutrons and protons forming the dominant component of matter are subject to a large disparity in their densities, and hence in their chemical potentials (which in the case of  $n, p, e$  matter is given simply by the chemical potential

of electrons). This has the consequence that the pairing with quantum numbers  $S = 1$  and  $T = 0$ , specifically in the partial wave channels  ${}^3S_1$ - ${}^3D_1$  and  ${}^3D_2$ , is strongly suppressed, because  $\delta\mu \gg \Delta(\alpha = 0)$ , i.e., the energetic separation of the Fermi surfaces of neutrons and protons is much larger than the gap. Thus the two channels that provide the largest attraction in symmetrical nuclear matter are ineffective in neutron-star matter (see Fig. 1). Pairing in neutron stars is therefore dominated by the  ${}^1S_0$  and  ${}^3P_2$ - ${}^3F_2$  partial waves in the  $T = 1$  channel at low and high densities, respectively. The disparity in the neutron and proton densities also implies that the transition from  $S$ -wave to  $P$ -wave pairing takes place at quite different densities. For neutrons this transition occurs at  $n \simeq n_0$ , whereas for protons the required density is not reached in neutron-star interiors in the majority (but not all) models. Notwithstanding the arguments above, it has been argued that in the low-density and low isospin asymmetry nuclear matter that may be created in low to intermediate heavy-ion collisions supernova and proto-neutron star matter the  ${}^3S_1$ - ${}^3D_1$  pairing may persist if the pairing interaction does not differ strongly from the one in free space. We will detail the physics of  ${}^3S_1$ - ${}^3D_1$  pairing and its suppression in low-density nuclear matter in the Sec. IV.

#### D. Finite nuclei

Although this review is concerned primarily with pairing in infinite nuclear systems, it will be helpful to recapitulate the basic facts about pairing in finite nuclei. Validation of pairing theory in direct terrestrial experiments on accessible nuclides ( $N, A = N + Z$ ) provides a valuable source of constraints and methods potentially relevant to the study of infinite nuclear matter. For in-depth expositions of the pairing in finite nuclei see (Broglia and Zelevinsky, 2013; Dean and Hjorth-Jensen, 2003; Ring and Schuck, 1980).

At the most basic level, pairing correlations in finite nuclei express themselves in the odd- $A$ -even- $A$  staggering of the measured binding energies of nuclei. The neutron “pairing gaps” in the cases of odd and even mass numbers are commonly defined as

$$\Delta_{Z,N}^{\text{odd}} = \frac{1}{2} (E_{Z,N+1} + E_{Z,N-1}) - E_{Z,N}, \quad (19)$$

$$\Delta_{Z,N}^{\text{even}} = -\frac{1}{2} (E_{Z,N+1} + E_{Z,N-1}) - E_{Z,N}, \quad (20)$$

where  $E_{Z,N}$  is the binding energy of a nucleus with proton number  $Z$  and neutron number  $N$ . The pairing gaps for changes of proton number are defined by the same equations (19) and (20), with  $N$  and  $Z$  interchanged. Evaluation of these differences in the case of neutron-number increments shows that odd- $A$  nuclides are less bound than their neighboring nuclides by about 1 MeV on average. Gap values for each fixed  $N$  can fluctuate by a factor two. Enhancement of the pairing effect on binding is observed for nuclei having neutron magic numbers

$N = 28, 50, 82,$  and  $126$ . Proton pairing shows the same energetic systematics, with somewhat smaller values of gap, presumably due to the Coulomb repulsion between protons. The pairing gaps decrease with the mass number of nuclei, a behavior described phenomenologically by the fit  $\Delta_{Z,N}^{\text{even/odd}} = 12A^{-1/2} + a_{\text{even/odd}}$ , with  $a_{\text{even}} = \pm 0.28$  and  $a_{\text{odd}} = \pm 0.25$ .

Differences in the excitation spectra of the even- $N$  and odd- $N$  nuclei provide another source of evidence for pairing correlations in nuclei. For  $N$  even, the excited states are separated from the ground state by a gap that can be interpreted as the energy needed to break a pair of neutrons, whereas for  $N$  odd, the lowest discrete (but dense) energy levels are found well within the range of 1 MeV characteristic of gaps in nuclei. Additionally, it should be noted that the excited states of nuclei may have collective nature that is reminiscent of the phonon modes present in macroscopic superfluids. Because of the finite nature of nuclei these modes are not necessarily bulk modes, i.e., they could be associated with the lowest-order quadrupolar shape oscillations of the nucleus with angular momentum and parity quantum numbers  $J^\pi = 2^+$ .

Theoretical studies of pairing properties of nuclei in the range of the intermediate and large mass number are generally performed within the framework of density functional theory (DFT), for recent work see (Goriely *et al.*, 2013, 2016; Reinhard, 2017). Such approaches may be based purely on Hartree-Fock (HF) functionals, nuclear properties (energy states and associated densities and currents) being computed in the absence of pairing, with pairing included in a final step within a simple BCS approach – essentially as outlined in Sec. II.A. Alternatively, nuclear pairing studies may utilize Hartree-Fock-Bogolyubov (HFB) functionals, performing computations that iterate the normal and anomalous states of the system, in a manner that allows for feedback of pairing correlations in the resulting mean fields, guaranteeing a self-consistent solution. The pairing interactions are typically modeled as contact interactions, with the theory outlined in Sec. II.A providing the basis for their treatment. The two parameters of this theory, namely the dimensionless pairing interaction (or coupling)  $\lambda$  and the energetic range  $2\Lambda$  over which the pairing is effective, are adjusted to the phenomenology of the nuclei being considered. Alternatively, these parameters can be chosen so as to reproduce the results of pairing calculations in infinite neutron matter (Goriely *et al.*, 2013, 2016).

As we shall discuss in the later sections, there are two effects that influence the results obtained with simple two-body contact interactions. First, there could be substantial corrections to the pairing interaction coming from collective modes (polarization effects). Secondly, three-nucleon interactions are non-negligible in nuclear systems, as they have been found to be important in high-precision fits to the properties of light nuclei and to some extent for the saturation of nuclear matter. (Apart from the generic three-body forces originating at the level of quark substructure, there are also “effective” three-body

forces generated in diverse theoretical treatments of two-body interactions that feature strong short-range repulsive components). In addition, the parameter  $\Lambda$  of the contact-interaction model is expected to depend on the occupancy of states in the vicinity of the Fermi surface, when the pairing is dominated by the direct (attractive) nuclear interaction. However, when (or if) the pairing is predominantly driven by collective effects,  $\Lambda$  would reflect the frequency range of collective phonon modes.

As explained in Sec. II.B, at sub-saturation densities the dominant attractive NN interaction is in the  $^3S_1$ - $^3D_1$  channel, i.e., the channel supporting a  $np$  bound state in free space – the deuteron. However, the foregoing discussion of pairing in nuclei has involved only isospin-triplet ( $nn$  or  $pp$ ), spin-singlet pairing. Noteworthy in this connection is the empirical fact that the binding energies of nuclei on the  $N = Z$  line are larger than those of their neighbors by an amount known as Wigner energy. This could be interpreted as evidence for pairing in the  $^3S_1$ - $^3D_1$  channel, which is otherwise suppressed for  $N \neq Z$  nuclei by the mismatch in the neutron and proton energy-level occupancies. Obviously, the pairing interaction may be modified by the ambient medium differently in different isospin-spin channels, one consequence being a less attractive force in the  $^3S_1$ - $^3D_1$  than in the  $^1S_0$  channel. Moreover, the spin-orbit field of the nucleus may affect the spin coupling of nucleonic Cooper pairs differentially, suppressing the  $^3S_1$ - $^3D_1$  neutron-proton pairing more than  $S$ -wave pairing of like-isospin pairs.

Besides its influence on static properties of nuclei, pairing and the accompanying superfluidity are expected to affect the dynamics of nuclei, including rotation, shape oscillations, and fission. In contrast to neutron stars (addressed intensively in Sec. V), where the effects of nuclear superfluidity extend over macroscopic scales, the characteristic scale of Cooper pairs, i.e., the coherence length, is of the order of the size of the nucleus or somewhat larger. Accordingly, one would expect the breakdown of superfluidity in nuclei to have little or no effect on their global dynamics. Surprisingly, self-consistent cranking HFB models, which reproduce the  $2^+$  excitations of nuclei with good accuracy, require moments of inertia which are half the rigid-body value (Delaroche *et al.*, 2010).

In its study, sub-barrier fission offers another tool to access the degree to which various nuclei are superfluid. Specifically, superfluidity enhances the probability of fission, as it produces a larger overlap between different nearly degenerate configurations. Since quantum-mechanical tunneling probability depends exponentially on the energy difference between configurations, one would expect a high sensitivity of the empirical results for the fluid parameters of a given nucleus. In particular, theoretical interpretation of the fission of  $^{234}\text{U}$  and  $^{240}\text{Pu}$  requires inclusion of an enhancement through superfluidity in order to account for the observed decay lifetimes (Bertsch, 2013; Sadhukhan *et al.*, 2016).

## E. Interface between nuclear systems and cold atomic gases

The realization of BCS pairing in ultracold atoms in 2004-2006 (Greiner *et al.*, 2005; Zwierlein *et al.*, 2006) was a major development that has considerably enlarged and diversified the scope of fermionic pairing as exemplified in strongly correlated quantum many-body systems. Indeed, prior to this discovery, the domain of application of fermion pairing has been limited to specific examples considered to arise in nature, specifically in nuclei, neutron-star matter, color-superconducting quark matter, liquid  $^3\text{He}$ , and electron systems in solids. Quantum gases of fermionic atoms offer the freedom to transcend nature by tuning the interaction between atoms via the Feshbach resonance mechanism, notably to the strongly interacting regime  $p_F|a| \gg 1$ , where  $p_F$  is the Fermi momentum and  $a$  the scattering length of the interaction. In this regime the gas particles can no longer be described perturbatively as forming a weakly interacting gas. Remarkably, the maximally strong-coupling regime – the unitary limit corresponding to  $p_F|a| \rightarrow \infty$  – has become accessible for ultracold fermions because three-body collisions are strongly suppressed in these systems *precisely because* of the Pauli principle. (The opposite situation applies for the case of boson atoms, where the lifetime of such cold-atom systems tends to zero due to three-body collisions). The new possibility is of great importance to nuclear physics in that pure low-density neutron matter, with its anomalously large scattering length  $a_n \simeq -19$  fm, is close to the unitary regime.

Furthermore, by adjusting the magnitude of the magnetic field to tune Feshbach resonances, it became feasible to drive a trapped cold atomic gas experimentally from the weakly interacting BCS regime, where the gas consists of loosely bound Cooper pairs, to the strongly interacting Bose-Einstein condensate (BEC) regime of tightly bound dimers. Thus, the theoretical ideas put forward several decades ago in support of a hypothetical BCS-BEC transition (Bloch *et al.*, 2008; Leggett and Zhang, 2012; Nozières and Schmitt-Rink, 1985) have been validated in experimental realizations (Regal and Jin, 2007; Zwierlein *et al.*, 2006).

The experimental prospects opened by technique developed to manipulate cold atoms include the possibility of creating a trapped atomic gas, for example composed of  $^6\text{Li}$  atoms, having unequal populations of two different hyperfine states – thereby simulating a interacting Fermi gas with unequal numbers of spin-up and spin-down particles. Such systems are expected to exhibit a rich variety of unconventional pairing phases, such as the current-carrying FFLO phase (Fulde and Ferrell, 1964; Larkin and Ovchinnikov, 1965) predicted in 1964. Importantly, the combination of these two features outlined above – the BCS-BEC crossover and population imbalance – will allow one to explore regimes of strongly interacting paired fermionic matter that have never been accessible in other systems, yet are of high interest for

phenomenological understanding of pairing in asymmetric nuclear matter and spin-polarized neutron matter.

By placing fermions in an optical lattice of suitable design, one is now able to simulate the effect of a periodic potential on the properties of strongly correlated fermions subject to tunable interactions. So far, experimental studies of quantum many-body systems along such lines has concentrated mainly on properties of Hubbard models and the Mott transition. With dense-matter astrophysics in mind, one potential application of this new ability is a cold-atom laboratory model of the matter in the crust of a neutron star. Insight could be gained into the interplay of the periodic potential and pairing in a strongly interacting gas under freely adjustable conditions, including lattice spacing, strength of interaction, various shapes of lattice potentials that may induce non-spherical “nuclei” (pasta phases), etc.

Another area of overlap between the nuclear superfluids in neutron stars and those created in cold-atom traps involves the presence of the quantum vortices. Experimental realization of quantum fermionic vortices in trapped gases and their evolution through the BCS-BEC crossover was initially instrumental in proving the very existence of superfluidity in a Fermi gas of  ${}^6\text{Li}$  (Zwierlein *et al.*, 2006). However, the range of phenomena that can be now probed experimentally is vast and embraces, for example, studies of: (i) core quasiparticle excitations in different interaction regimes and with respect to imbalance, (ii) mutual friction in superfluid-normal mixtures of gases, (iii) higher spin vortices, and (iv) mixtures of fermionic superfluids and Fermi-Bose fluids. Macroscopic dynamics of rotating superfluids featuring vortex lattices has been investigated both theoretically and experimentally in great detail (Fetter, 2009). The corresponding studies have focused on vortex-lattice oscillations (Tkachenko modes), quadrupolar modes of oscillations, rapid-rotation induced Landau quantization of states, etc. Most of these experimental realizations find analogs in the physics of neutron stars, as will be pointed out in Section V.

### III. METHODS FOR STRONGLY CORRELATED SYSTEMS

#### A. Green Functions approach and Gor’kov formalism

In this section we outline and discuss the Green functions method for the treatment of superfluid systems. The method was originally introduced by Gor’kov and by Nambu (Gor’kov, 1958; Nambu, 1960). Their formulation is based on thermodynamic Green functions (GF) defined in the imaginary-time formalism. The starting point of this formalism is the set of coupled Dyson-Schwinger equations for the normal and anomalous propagators, which determine the self-energies of the system. Their diagrammatic representation allows for systematic account of the correlations in the system in terms of re-

summations of diagrams in the relevant dynamical channels. A variant of the zero-temperature GF theory of pairing appropriate for nuclear systems was developed by Larkin and Migdal (Larkin and Migdal, 1964), on the basis of the Landau Fermi-liquid theory for normal systems. Already in this early work a number of important aspects of the fermionic pairing problem were introduced, including wave-function renormalization and summations in the particle-hole and particle-particle channels, with results expressed in terms the phenomenological parameters of the Landau Fermi liquid theory. This approach was further adapted to finite Fermi systems (nuclei), and a number of nuclear observables were evaluated using the Landau parameters for nuclear systems (Migdal, 1967).

In the following decades the GF method was largely abandoned in the context of nuclear pairing. It was revived in the early 1990s by a number of research groups, specifically in the context of  ${}^3S_1$ - ${}^3D_1$  pairing in isospin symmetric and asymmetric systems (Baldo *et al.*, 1992a, 1995; Sedrakian *et al.*, 1997), as well as for  ${}^1S_0$  and  ${}^3P_2$ - ${}^3F_2$  pairing (Baldo *et al.*, 1998; Elgarøy *et al.*, 1996a,b,c). These studies were based on realistic (i.e., phase-shift equivalent) NN interactions.

Somewhat earlier, the real-time anomalous propagator treatment of nuclear pairing was introduced by (Su *et al.*, 1987), but the interactions were treated at the level of the Skyrme effective contact forces commonly used for computations on finite nuclei. The particle-particle and particle-hole resummations in the GF theory are related to the microscopic determination of the Landau Fermi liquid parameters (see Sec. III.A.3 for details). This task was taken up within GF theory at about the same time in Refs. (Ainsworth *et al.*, 1989; Schulze *et al.*, 1996; Wambach *et al.*, 1993).

The class of theories of *unpaired* matter formulated in terms of Green functions allow one to deduce only the critical temperature of the superfluid phase transition, as signaled by poles that emerge in the medium-modified scattering matrix of two nucleons (Alm *et al.*, 1993, 1996; Dickhoff, 1988; Schmidt *et al.*, 1990; Sedrakian, 1995; Stein *et al.*, 1995). We relegate to Section III.B the discussion of theories in which pairing is inferred indirectly from instability of the normal state.

An important feature of the of GF formation is that it admits a description beyond the concept of quasiparticles inherent to the Landau Fermi-theory by accounting for the finite width of particle states. This may strongly affect pairing when it is addressed at the level of self-energies (Božek, 2000, 2002, 2003; Božek and Czerski, 2002; Müther and Dickhoff, 2005). We relegate the discussion of these theories to subsection III.C.

Excellent reviews of GF methods applied and results obtained up to the turn of the century have been provided in Refs. (Dean and Hjorth-Jensen, 2003; Lombardo and Schulze, 2001).

The following two decades have seen wide application of GF theory to superfluid nuclear systems. One approach is to accurately incorporate many-body correc-

tions while enforcing consistency between various ingredients, especially vertex corrections and renormalization of single-particle energies, as has been done for  $S$ -wave channels (Cao *et al.*, 2006; Sedrakian and Lombardo, 2000; Shen *et al.*, 2005). Another line of development has employed soft effective interactions to account for the resummations in the particle-hole channel in the framework of Landau Fermi-liquid theory, specifically for  $S$ - and  $P$ -wave channels (Schwenk and Friman, 2004; Schwenk *et al.*, 2003). The effects of phonons and retardation of the interaction on pairing have also been explored based on effective interactions (Barranco *et al.*, 2005; Sedrakian, 2003). More recently, the following aspects of the problem of nucleonic pairing have been brought into focus: (i) Incorporation of effects on the pairing interaction and self-energies of three-body ( $3N$ ) forces, either of fundamental origin or generated by the many-body method used to treat strong correlations (Dong *et al.*, 2013; Drischler *et al.*, 2017; Papakonstantinou and Clark, 2017), (ii) calculation of pairing gaps based on a variety of soft, chiral NN interactions (Drischler *et al.*, 2017; Finelli *et al.*, 2015; Maurizio *et al.*, 2014; Srinivas and Ramanan, 2016), which explore the influence of the cutoff of these interactions, and (iii) studies of the effects on pairing of short-range correlations (Ding *et al.*, 2016a; Rios *et al.*, 2017a), as accounted for in terms of spectral functions (to be considered in Sec. III.C). The general trends that emerge from these studies will be discussed at a later stage, subsequent to an exposition of the formalism of GF pairing theory, i.e., a finite-temperature version of GF theory for superfluid Fermi systems (Larkin and Migdal, 1964) with finite-range two-body interactions, as described by us in an earlier review (Sedrakian and Clark, 2006a).

### 1. Green functions formalism

The Gor'kov propagators describing the superfluid state formally obey the Dyson-Schwinger equation

$$\mathbf{G}_{\alpha\beta}(x, x') = \mathbf{G}_{\alpha\beta}^0(x, x') + \sum_{\gamma, \delta} \int d^4 x'' d^4 x''' \mathbf{G}_{\alpha\gamma}^0(x, x''') \times \Sigma_{\gamma\delta}(x''', x'') \mathbf{G}_{\delta\beta}(x'', x') \quad (21)$$

containing the free propagator  $\mathbf{G}_{\alpha\beta}^0(x, x')$  and self-energy  $\Sigma_{\gamma\delta}(x''', x'')$ , where  $x$  represents the space-time coordinate and the Greek indices  $\alpha, \beta \dots$  label spin and isospin states. The most general treatment in real time requires time ordering along the Keldysh-Schwinger contour, which generates the familiar  $2 \times 2$  matrix GFs with components representing the causal and acausal GFs as well as two additional GFs with fixed time arguments on opposite sides of the contour. Below we will be concerned only with the equilibrium physics; hence we do not present the equations for the most general case. Instead, we restrict our attention to the retarded components of the GFs and self-energies, which can be obtained through

unitary transformation from the initial matrix Keldysh-Schwinger GFs.

To describe the superfluid state, another  $2 \times 2$  matrix structure in the particle-hole space is required to include the pairing correlations. The GFs that obey the Dyson equation Eq. (21) are then written explicitly as

$$i\mathbf{G}_{\alpha\beta}(x, x') = \begin{pmatrix} \langle T\psi_\alpha(x)\psi_\beta^\dagger(x') \rangle & i\langle T\psi_\alpha(x)\psi_\beta(x') \rangle \\ i\langle T\psi_\alpha^\dagger(x)\psi_\beta^\dagger(x') \rangle & \langle T\psi_\alpha^\dagger(x)\psi_\beta(x') \rangle \end{pmatrix} = i \begin{pmatrix} G_{\alpha\beta}(x, x') & F_{\alpha\beta}(x, x') \\ -F_{\alpha\beta}^\dagger(x, x') & \tilde{G}_{\alpha\beta}(x, x') \end{pmatrix}, \quad (22)$$

where the  $\psi_\alpha(x)$  are baryon field operators, and  $T$  and  $\tilde{T}$  signify time-ordering and inverse time-ordering of operator products, respectively. The free propagator is diagonal in the Gor'kov-Nambu space.

The matrix structure of the self-energy  $\Sigma_{\alpha\beta}(x, x')$  is identical to that of the propagators:

$$\Sigma_{\alpha\beta}(x, x') = \begin{pmatrix} \Sigma_{\alpha\beta}(x, x') & \Delta_{\alpha\beta}(x, x') \\ \Delta_{\alpha\beta}^\dagger(x, x') & \tilde{\Sigma}_{\alpha\beta}(x, x') \end{pmatrix}. \quad (23)$$

The off-diagonal self-energies  $\Delta$  and  $\Delta^\dagger$  describe the superfluid state and vanish in the unpaired limit.

The Fourier transform of Eq. (21) with respect to the relative coordinate  $x - x'$  gives a set of coupled equations

$$G_{\alpha\beta}(p) = G_{0\alpha\beta}(p) + G_{0\alpha\gamma}(p) \times [\Sigma_{\gamma\delta}(p)G_{\delta\beta}(p) + \Delta_{\gamma\delta}(p)F_{\delta\beta}^\dagger(p)], \quad (24)$$

$$F_{\alpha\beta}^\dagger(p) = G_{0\alpha\gamma}(-p) \times [\Delta_{\gamma\delta}^\dagger(p)G_{\delta\beta}(p) + \Sigma_{\gamma\delta}(-p)F_{\delta\beta}^\dagger(p)] \quad (25)$$

for the component GFs, summation over repeated being understood. The dependence of these GFs on the center-of-mass coordinate is suppressed and will not be needed until we consider current-carrying states in Sec. IV. Eq. (24) exhibits the coupling of the normal propagators  $G_{\alpha\beta}(p)$  and  $G_{0\alpha\beta}(p)$  with their anomalous counterparts  $F_{\alpha\beta}^\dagger(p)$  and  $F_{\alpha\beta}(p)$ , through processes encoded in the normal and analogous self-energies, respectively  $\Sigma_{\alpha\beta}(p)$  and  $\Delta_{\alpha\beta}(p)$ . Similar equations can be written for  $F_{\alpha\beta}^\dagger(x, x')$  and  $\tilde{G}_{\alpha\beta}(x, x')$ , but in most of the cases (for example for systems with time-reversal symmetry) these are redundant.

In the normal (unpaired) state the generalized Schwinger-Dyson equation reduces to a single equation

$$G_{\alpha\beta}^N(p) = G_{0\alpha\beta}(p) + G_{\alpha\gamma}^N(p)\Sigma_{\gamma\delta}(p)G_{0\delta\beta}(p), \quad (26)$$

which has the solution  $G_{\alpha\beta}^N(p) = \delta_{\alpha\beta}[\omega - \varepsilon(p)]^{-1}$ , in effect defining the single-particle energies  $\varepsilon(p) = \varepsilon_p + \Sigma(p)$ , where  $\varepsilon_p$  is the free single-particle spectrum. Note that the self-energy  $\Sigma(p)$  is diagonal in spin and isospin spaces, given spin-isospin conserving forces. Eqs. (24), (25) can now be expressed in a more compact form

$$G_{\alpha\beta}(p) = G_{\alpha\gamma}^N(p) \left[ \delta_{\gamma\beta} + \Delta_{\gamma\delta}(p)F_{\delta\beta}^\dagger(p) \right], \quad (27)$$

$$F_{\alpha\beta}^\dagger(p) = G_{\alpha\gamma}^N(-p)\Delta_{\gamma\delta}^\dagger(p)G_{\delta\beta}(p) \quad (28)$$

having the solution

$$G_{\alpha\beta}(p) = \delta_{\alpha\beta} \frac{\omega - E_A(p) + E_S(p)}{[\omega - E_A(p)]^2 - E_S(p)^2 - \Delta^2(p)}, \quad (29)$$

$$F_{\alpha\beta}^\dagger(p) = \frac{\Delta_{\alpha\beta}^\dagger(p)}{[\omega - E_A(p)]^2 - E_S(p)^2 - \Delta^2(p)}, \quad (30)$$

where  $E_{S/A} = \frac{1}{2}[\varepsilon(p) \pm \varepsilon(-p)]$  denotes the symmetric ( $S$ ) and antisymmetric ( $A$ ) parts of the single-particle spectrum in the normal state and  $\Delta(p)\Delta^\dagger(p) \equiv -\Delta^2(p)$ . The GFs in Eqs. (29) and (30) share the same poles at

$$\omega_\pm = E_A(p) \pm \sqrt{E_S(p)^2 + \Delta^2(p)}, \quad (31)$$

thereby determining the excitation spectrum. If the normal self-energy is invariant under reflections in space (i.e. even under  $\mathbf{p} \rightarrow -\mathbf{p}$ ) and time-reversal invariant (i.e. even under  $\omega \rightarrow -\omega$ ), the  $E_A$  component is zero. Thus there is a non-zero energy cost  $\sim 2\Delta$  for creating an excitation from the ground state of the system – a signature of superconductors leading to the flow of current without resistance. If by some physical mechanism it happens that  $E_A \neq 0$ , the superconductivity is *gapless*. The realization of this eventuality in nuclear systems will be exemplified in Section IV.

Our methodological considerations have so far been general, in that as we have not been explicit about the properties of interactions or correlations in the system under study. Superconductivity is inherently a Fermi-surface phenomenon, so one natural approximation entails an expansion of the self-energy  $\Sigma(\omega, \mathbf{p})$  around its on-shell value assuming that the off-mass-shell contribution is small. Since the imaginary part of the self-energy vanishes quadratically on the mass shell, the expansion is carried out for the real part by writing

$$\text{Re}\Sigma(\omega, \mathbf{p}) = \text{Re}\Sigma(\varepsilon_p) + \left. \frac{\partial \text{Re}\Sigma(\omega, \mathbf{p})}{\partial \omega} \right|_{\omega=\varepsilon_p} (\omega - \varepsilon_p), \quad (32)$$

where  $\varepsilon_p = \epsilon_p + \text{Re}\Sigma(\varepsilon_p)$  is the on-mass-shell single-particle spectrum in the normal state, i.e., the solution to Eq. (26).

Within this approximation, the self-energies in Eqs. (26) contain only on-shell self-energies  $\Sigma(\varepsilon_p, \mathbf{p})$  and are multiplied by a wave-function renormalization, i.e.,  $G_{\alpha\beta} \rightarrow Z(\mathbf{p})G_{\alpha\beta}$  and  $F_{\alpha\beta} \rightarrow Z(\mathbf{p})F_{\alpha\beta}$ , where

$$Z(\mathbf{p})^{-1} \equiv 1 - \left. \frac{\partial \text{Re}\Sigma(\omega, \mathbf{p})}{\partial \omega} \right|_{\omega=\varepsilon_p}. \quad (33)$$

A similar expansion may be implemented for the anomalous self-energy. It should be noted, however, that for time-local pairing interactions (essentially all bare or effective soft NN interactions) the gap function is energy-independent. Non-local interactions are naturally generated from local ones, if they are constructed via summations of series, as in models of medium polarization (cf. see Sec. III.A.3.) If the pairing interaction is modelled

in terms of boson exchange, the dependence of  $\Delta(\omega)$  on frequency shows significant structure off the mass shell, as will be seen in Sec. III.A.4.

The existence of a Fermi surface also implies an approximation of the momentum dependence of the self-energy, although this approximation can be trivially avoided. Expanding the normal self-energy at the Fermi surface one finds

$$\varepsilon(p) = v_F(p - p_F) - \mu^*, \quad \frac{m}{m^*} = 1 + \left. \frac{m}{p} \frac{\partial \text{Re}\Sigma(p)}{\partial p} \right|_{p=p_F} \quad (34)$$

where  $\mu^* \equiv -\varepsilon(p_F) + \mu - \text{Re}\Sigma(p_F)$ ,  $v_F$  is the Fermi velocity, and  $m^*$  is an effective mass. The spectrum (34) now has the proper form for a Fermi liquid, although there are no significant computational gains from this effective-mass approximation.

## 2. Mean-field BCS theory

The next essential step is to establish the prescription for computing the self-energies. BCS theory is a mean-field theory for the anomalous self-energy, which in its most general form can be written as

$$\Delta(p) = -2 \int \frac{d^4 p'}{(2\pi)^4} \Gamma(p, p') \text{Im}F(p') f(\omega'), \quad (35)$$

where  $\Gamma(p, p')$  is a four-point vertex function to be determined from the nucleon-nucleon interaction and  $f(\omega) = [1 + \exp(\beta\omega)]^{-1}$  is the Fermi distribution at inverse temperature  $\beta$ . Up to a constant, the factor  $2\text{Im}F(p')f(\omega')$  may be identified as the off-diagonal Green function in the Keldysh-Schwinger formalism. Thus, as expected, the anomalous self-energy is given by a convolution of the interaction vertex and a GF.

Consider next time-local (but space non-local) interactions, in which case the replacement  $\Gamma(p, p') \rightarrow V(\mathbf{p}, \mathbf{p}')$  can be made and, moreover,  $V(\mathbf{p}, \mathbf{p}')$  can be expanded in partial waves. Performing wave-function renormalization of the propagator, integrating over the energy variable, and considering a single uncoupled channel, we arrive at an integral equation

$$\Delta(p) = Z(p) \int \frac{dp p^2}{(2\pi)^2} V(p, p') Z(p') \frac{\Delta(p')}{\omega_+(p')} [f(\omega_+) - f(\omega_-)], \quad (36)$$

for the gap function depending only on the modulus of the momentum, with  $\omega_\pm = \pm \sqrt{\varepsilon_p^2 + \Delta^2}$ . In a number of cases, e.g. in low-density nuclear systems, it is necessary to solve for the density

$$\begin{aligned} \rho &= -2 \sum_\alpha \int \frac{d^4 p}{(2\pi)^4} \text{Im}G(p) f(\omega) \\ &= \frac{1}{2} \sum_\alpha \int \frac{d^3 p}{(2\pi)^3} Z(\mathbf{p}) \sum_{i=+,-} \left( 1 + \frac{\varepsilon_p}{\omega_i} \right) f(\omega_i) \end{aligned} \quad (37)$$

to obtain the chemical potential, which is modified by the effects of pairing on the single-particle energies. (Here  $\alpha$  denotes a sum over all spin/isospin states.) This “back-reaction” of the density on the chemical potential is small in the weak-coupling regime, but becomes important with strong coupling. For an input pairing interaction  $V(p, p')$  and the spectrum  $\varepsilon_p$  in the unpaired state, Eqs. (36) and (37) fully determine the gap and the chemical potential from which all the thermodynamic functions of the system can be computed.

The simple model of Sec. II can be recovered assuming a momentum-independent pairing interaction, the gap at the Fermi momentum being given by

$$\Delta(p_F) \simeq 8\mu^* \exp\left(-\frac{2}{\lambda}\right), \quad (38)$$

with effective coupling  $\lambda = \nu(p_F)|V(p_F, p_F)|$  and a density of states  $\nu(p_F) = m^* Z^2(p_F) p_F / \pi^2$ . It is seen that the main effect of wave-function renormalization is to modify the density of states at the Fermi surface. It is important to note that in the case of an NN interaction, the matrix element of the effective pairing interaction  $V(p_F, p_F)$  on the Fermi surface can have the “wrong” sign, implying a dominant repulsive interaction component. However, Eq. (36) may still have a pairing solution because the momentum dependence of  $V(p, p')$  be can sufficiently attractive away from the Fermi-surface (Khodel *et al.*, 1996).

In the foregoing development, we implicitly assumed that the normal self-energy  $\Sigma(p)$  and hence the normal-state spectrum  $\varepsilon(p)$  do not depend on the properties of the paired state, e.g., the gap  $\Delta(p)$ . The replacement of  $G(p)$  by  $G^N(p)$  when computing the normal-state spectrum is an approximation (known as the *decoupling approximation*), which is only valid when the pairing is a small perturbation on the normal ground-state. This approximation should work well for nuclear systems at high densities (implying weak coupling), but might not be adequate at lower densities where the strong-coupling corrections are significant.

Qualitatively, the renormalization of the single-particle spectrum in momentum space (accounted for, in particular, through the effective mass ratio  $m^*/m$  for nucleons) acts to reduce the density of states, therefore the magnitude of the gap, by factors up to two or three, depending on density. Additional reduction comes from the wave-function renormalization  $Z(\mathbf{p}) \leq 1$ .

### 3. Polarization effects

The interaction between nucleons is modified in the nuclear medium. Therefore the replacement  $\Gamma(p, p')$  by the free-space interaction, which describes correctly only the asymptotic states of the nucleons, is an approximation that needs further elaboration. The leading class of modifications of the pairing interaction in medium arises

from “polarization effects” or “screening.” Let us examine this type of modification.

We start with a simple but instructive approach based on ideas from the Landau theory of Fermi liquids. Consider the following integral equation which sums the particle-hole diagrams to all orders

$$\Gamma(\mathbf{p}, \mathbf{p}', \mathbf{q}) = U(\mathbf{p}, \mathbf{p}', \mathbf{q}) - i \int \frac{d^4 p''}{(2\pi)^4} U(\mathbf{p}, \mathbf{p}'', \mathbf{q}) G^N(p'' + q/2) G^N(p'' - q/2) \Gamma(\mathbf{p}'', \mathbf{p}', \mathbf{q}), \quad (39)$$

where  $\mathbf{q}$  is the momentum transfer. The driving term  $U(\mathbf{p}, \mathbf{p}', \mathbf{q})$  must be devoid of blocks that contain particle-particle ladders to avoid double summation in the gap equation. In general this driving interaction depends on spin and isospin and can be decomposed as

$$U_{\mathbf{q}} = f_{\mathbf{q}} + g_{\mathbf{q}}(\boldsymbol{\sigma} \cdot \boldsymbol{\sigma}') + [f'_{\mathbf{q}} + g'_{\mathbf{q}}(\boldsymbol{\sigma} \cdot \boldsymbol{\sigma}')] (\boldsymbol{\tau} \cdot \boldsymbol{\tau}'), \quad (40)$$

where  $\boldsymbol{\sigma}$  and  $\boldsymbol{\tau}$  are the vector observables represented by Pauli matrices in the spin and isospin spaces. Eq. (40) is written assuming the block  $U_{\mathbf{q}}$  depends only on the momentum transfer, which is a good approximation for highly degenerate Fermi systems. For illustrative purposes, the tensor component of the interaction and the spin-orbit terms are ignored in Eq. (40). The solution of (39) is given by

$$\begin{aligned} \nu(p_F) \Gamma_{\mathbf{q}} &= \frac{F_{\mathbf{q}}}{1 + L(q)F_{\mathbf{q}}} + \frac{G_{\mathbf{q}}}{1 + L(q)G_{\mathbf{q}}} (\boldsymbol{\sigma} \cdot \boldsymbol{\sigma}') \\ &+ \left[ \frac{F'_{\mathbf{q}}}{1 + L(q)F'_{\mathbf{q}}} + \frac{G'_{\mathbf{q}}}{1 + L(q)G'_{\mathbf{q}}} (\boldsymbol{\sigma} \cdot \boldsymbol{\sigma}') \right] (\boldsymbol{\tau} \cdot \boldsymbol{\tau}'), \end{aligned} \quad (41)$$

where  $F_{\mathbf{q}} = \nu(p_F) f_{\mathbf{q}}$ ,  $G_{\mathbf{q}} = \nu(p_F) g_{\mathbf{q}}$ ,  $F'_{\mathbf{q}} = \nu(p_F) f'_{\mathbf{q}}$ , and  $G'_{\mathbf{q}} = \nu(p_F) g'_{\mathbf{q}}$  are the dimensionless particle-hole interactions (Landau parameters), whereas

$$L(q) = \nu(p_F)^{-1} \int \frac{d^4 p''}{(2\pi)^4} G^N(p'' + q/2) G^N(p'' - q/2), \quad (42)$$

is the polarization tensor, given by in the present case by the Lindhard function. The momentum transfer is related to the scattering angle  $\theta$  and Fermi momentum  $p_F$  according to  $q = 2p_F \sin \theta/2$ , assuming that the momenta of particles are restricted to the Fermi surface. The parameters  $F$ ,  $F'$ ,  $G$ , and  $G'$  can be expanded in spherical harmonics with respect to the scattering angle, writing

$$\begin{pmatrix} F(q) \\ G(q) \end{pmatrix} = \sum_l \begin{pmatrix} F_l \\ G_l \end{pmatrix} P_l(\cos \theta), \quad (43)$$

and similarly for  $F'(q)$  and  $G'(q)$ . The Landau parameters  $F_l$ ,  $G_l$ ,  $F'_l$ , and  $G'_l$  depend on the Fermi momentum. In neutron matter one has  $\boldsymbol{\tau} \cdot \boldsymbol{\tau}' = 1$ , and the number of independent Landau parameters for each  $\mathbf{q}$  or  $l$  can be reduced to two by defining  $F^n = F + F'$  and  $G^n = G + G'$ .

Keeping the dominant lowest-order harmonics in the expansion (43), the interaction in a singlet pairing state (total spin of the pair  $S = 0$  and  $\boldsymbol{\sigma} \cdot \boldsymbol{\sigma}' = -3$ ) becomes

$$\begin{aligned} \nu(p_F)\Gamma_q &= F_0^n \left[ 1 - \frac{L(q)F_0^n}{1 + L(q)F_0^n} \right] \\ &- 3G_0^n \left[ 1 - \frac{L(q)G_0^n}{1 + L(q)G_0^n} \right]. \end{aligned} \quad (44)$$

In general, the polarization tensor  $L(q)$  is complex-valued. However, it is real in the limit of zero energy transfer (at fixed momentum) and at zero temperature, being given by

$$L(q) = -1 + \frac{p_F}{q} \left( 1 - \frac{q^2}{4p_F^2} \right) \ln \left| \frac{2p_F - q}{2p_F + q} \right|. \quad (45)$$

The pairing interaction (44) consists of two pieces – the direct part generated by the terms  $\propto 1$  inside the square brackets and the remaining induced part, arising from density and spin-density fluctuations, respectively the term  $\propto F_0^n$  and that  $\propto G_0^n$ .

Given the Landau parameters, the effect of polarization can be assessed by defining a pairing interaction averaged over the momentum transfers,

$$\Gamma(q, q') = \frac{1}{2qq'} \int_{|q-q'|}^{q+q'} dp p \Gamma(p). \quad (46)$$

The impact of the fluctuations on pairing has been established using the formalism described above for neutron matter below saturation by (Clark *et al.*, 1976), who showed that the density fluctuations enhance the attraction between neutrons, whereas the spin-density fluctuations reduce it. Using the values of Landau parameters in neutron matter they concluded that the suppression of pairing via spin-density fluctuations is the dominant effect (Clark *et al.*, 1976).

We turn now to studies that employ more refined approximations for the induced part of the interaction (Ainsworth *et al.*, 1989; Schulze *et al.*, 1996; Schwenk *et al.*, 2003; Wambach *et al.*, 1993). First, while the structure of Eqs. (44) and (46) remains the same, the replacement

$$F_0^n - 3G_0^n \rightarrow V_s - 3V_a = \Gamma_{\text{dir}}(p) \quad (47)$$

is made, with  $V_s$  and  $V_a$  set equal to the spin symmetrical and anti-symmetrical parts of the bare (phase-shift equivalent) nuclear potential or its low-momentum reduction. Then the induced interaction is written as

$$\nu(p_F)\Gamma_{\text{ind}}(p) = \frac{F(p)^2 L(p)}{1 + L(p)F(p)} - \frac{3G(p)^2 L(p)}{1 + L(p)G(p)}, \quad (48)$$

where we have dropped the subscript  $n$  on the particle-hole interactions  $F(q)$  and  $G(q)$ , which now depend on the magnitude of the momentum transfer  $q$ .

The method used to compute the induced interaction was developed in the 1970s and accounts for the mostly repulsive effect of screening on the direct interaction (Babu and Brown, 1973; Bäckman *et al.*, 1985, 1973; Schulze *et al.*, 1996), which by itself contains sufficient attraction to guarantee pairing.

In these approaches the driving term in the series summing up the induced interaction is computed from the Brueckner-Bethe-Goldstone theory of nuclear matter (Bethe, 1971) and is represented by the  $\mathcal{G}$ -matrix. For example, the spin-symmetric interaction  $F(q)$  is determined through the coupled integral equations

$$F = \mathcal{G} - \mathcal{A}G_{ph}F, \quad \mathcal{A} = F + FG_{ph}\mathcal{A}, \quad (49)$$

(written for simplicity in operator form), where  $\mathcal{A}$  represents the particle-hole scattering amplitude and  $G_{ph}$  is the two-body particle-hole propagator. [See (Ainsworth *et al.*, 1989; Wambach *et al.*, 1993) for details.] The spin-antisymmetric channel is treated in complete analogy.

Numerical computations of the  $^1S_0$  gap in neutron matter that include the induced interaction at various levels of sophistication indicate that its dominant repulsive character produces a strong reduction of the gap. The resulting upper bound on the magnitude of the gap is around 1 MeV; however, the density at which the maximum is attained varies substantially, c.f. (Ainsworth *et al.*, 1989; Schulze *et al.*, 1996; Schwenk *et al.*, 2003; Wambach *et al.*, 1993).

#### 4. Boson-exchange theories

In reality, the pairing interaction is retarded in time, not only because the mesons, as mediators of the nuclear force, propagate at finite speed, but also because any induced interaction which embodies resummation of a certain class of diagrams is frequency dependent. Such induced pairing interactions can also be framed within a theory of effective phonon exchange between nucleons, as is commonly done in the theories of pairing in finite nuclei. Therefore it is of interest to consider boson-exchange theories in general and leave the nature of bosons arbitrary for the time being. We will comment on possible variants of the theory at the end of this subsection.

Generic theories of pairing based on a boson-exchange model originated in the work of Eliashberg (Eliashberg, 1960) on electron-phonon superconductivity in metals. The Dyson-Schwinger Eqs. (24) and (25) remain intact in this model. However it is now convenient to split the retarded self-energy into components even ( $S$ ) and odd ( $A$ ) in  $\omega$ , i.e.  $\Sigma(p) = \Sigma_S(p) + \Sigma_A(p)$ , and define the wavefunction renormalization  $Z(p) = 1 - \omega^{-1}\Sigma_A(p)$ . The single-particle energy is then renormalized as  $E_S = \epsilon_p + \Sigma_S(E_S, \mathbf{p})$ . Accordingly, the propagators now take the forms

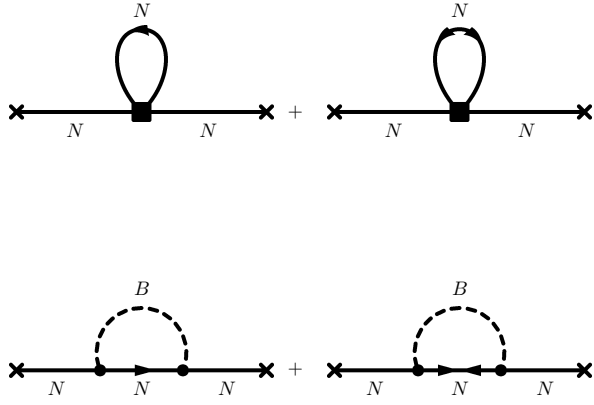


FIG. 3 Examples of Hartree (top) and Fock (lower panel) self-energies for normal (left) and anomalous (right) sectors. The solid lines correspond to nucleons ( $N$ ) and the dashed to bosonic mode ( $B$ ) (the single/double arrowed lines refers to the normal and anomalous  $F^\dagger$  propagators). The square vertex stands for time-local part of pairing interaction; crossed propagators do not belong to self-energies and are shown for clarity.

$$G(p) = \frac{\omega Z(p) + E_S(p)}{(\omega + i\eta)^2 Z(p)^2 - E_S(p)^2 - \Delta(p)^2}, \quad (50)$$

$$F(p) = -\frac{\Delta(p)}{(\omega + i\eta)^2 Z(p)^2 - E_S(p)^2 - \Delta(p)^2}, \quad (51)$$

where  $\Delta\Delta^\dagger \equiv -\Delta^2$ . Next we need to characterize the pairing interaction. It consists of (a) its local part, which enters the Hartree self-energy (Fig. 3, upper diagrams) and (b) the retarded boson-exchange interaction, which contributes to the Fock term to lowest order (Fig. 3, lower diagrams).

We do not discuss the Hartree self-energies, as they can be readily calculated from any given nuclear interaction that is local in time (e.g., a phase-shift equivalent nuclear potential). Using the fact that neutron matter is a highly degenerate Fermi system, the normal and anomalous Fock self-energies can be expressed in the following form:

$$\begin{aligned} \Sigma(p_F, \omega) = & -\int_0^\infty d\omega' K(\omega') \left\{ g(\omega') \left[ G(\omega + \omega') \right. \right. \\ & \left. \left. + G(\omega - \omega') \right] + \int_{-\infty}^\infty \frac{d\epsilon}{\pi} \text{Im} [G(\epsilon)] J(\omega, \omega', \epsilon) \right\}, \quad (52) \end{aligned}$$

$$\begin{aligned} \Delta(p_F, \omega) = & \int_0^\infty d\omega' K(\omega') \left\{ g(\omega') \left[ F(\omega + \omega') \right. \right. \\ & \left. \left. + F(\omega - \omega') \right] + \int_{-\infty}^\infty \frac{d\epsilon}{\pi} \text{Im} [F(\epsilon)] J(\omega, \omega', \epsilon) \right\}, \quad (53) \end{aligned}$$

where  $\Sigma(\omega, p_F)$  and  $\Delta(\omega, p_F)$  are respectively the normal and anomalous retarded self-energies, while

$$J(\epsilon, \omega, \omega') = \frac{f(\epsilon)}{\epsilon - \omega - \omega' - i\eta} + \frac{1 - f(\epsilon)}{\epsilon - \omega + \omega' - i\eta}, \quad (54)$$

where  $g(\omega)$  and  $f(\omega)$  and the Bose and Fermi distribution functions. Additionally, we have introduced a

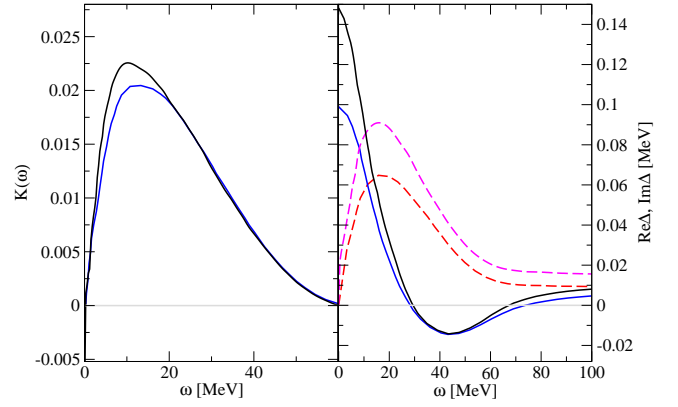


FIG. 4 Left panel: Frequency dependence of the effective interaction kernel  $K(\omega)$ , Eq. (55), for two different strengths of pairing interaction. Right panel: real (solid lines) and imaginary (dashed lines) components of the pairing gap in neutron matter for Fermi-momentum  $p_F = 0.4 \text{ fm}^{-1}$  for pairing interactions given in the left panel. In the on-shell limit  $\omega \rightarrow 0$  one finds  $\text{Im}\Delta \rightarrow 0$  and  $\text{Re}\Delta \rightarrow \Delta_0$ , where  $\Delta_0$  is the on-shell value of the gap; for details see (Sedrakian, 2003).

momentum-averaged (real) interaction kernel defined by

$$K(\omega) = \frac{m^*}{(2\pi)^3 p_F} \int_0^{2p_F} dq q \int_0^{2\pi} d\phi B(\mathbf{q}, \omega) \text{Tr} \{ \Gamma_0(\mathbf{q}) \Gamma(\mathbf{q}) \}, \quad (55)$$

in which  $\Gamma_0$  and  $\Gamma$  are the bare and full boson-fermion vertices and  $B(\omega, \mathbf{q})$  is the spectral function of the bosons. Eqs. (52) and (53) provide a set of nonlinear coupled integral equations for the complex pairing amplitude and the normal self-energy (or, equivalently the wavefunction renormalization). To illustrate some numerical solutions, consider a model in which neutrons interact via soft-pion exchange (Pankratov *et al.*, 2015; Sedrakian, 2003). Given a spectral function for the bosons, the kernel (55) is constructed as input to Eqs. (52) and (53). The input kernel for this specific model is shown in the left panel of Fig. 4, while its right panel shows the zero-temperature solutions of Eqs. (52) and (53). The imaginary component of the gap tends to zero on the mass shell ( $\omega = 0$ ); its real part gives the on-shell value of the gap. For non-zero energies these functions have complex structure that reflects the features of the input kernel  $K(\omega)$ . Knowledge of the frequency dependence of the pairing gap in nuclear and neutron matter could be important for the analysis of frequency-dependent observables, especially for the description of their dynamical response to various perturbations. Examples include the dynamical (i.e. frequency-dependent) Meissner effect and transport coefficients such as the shear and bulk viscosities.

## B. T- and G-matrix approaches, Thouless criterion

The onset of pairing correlations, and in particular the critical temperature of the superfluid phase transition, can be determined from properties of the normal

(unpaired) state, notably from the *scattering matrix*, defined here as an extension of the free-space  $T$ -matrix to a medium of strongly correlated fermions. As considered in more detail below, generalization to the medium can be implemented at different levels. An important class of  $T$ -matrix theories is obtained when propagation of particles and holes in intermediate states is included symmetrically (Galitskii, 1958). An alternative extension, introduced historically in context of nuclear matter calculations, is based on the  $K$ -matrix (or reaction matrix) – or in current notation the  $\mathcal{G}$ -matrix – in which only particle-particle propagation is taken into account (Brueckner and Gammel, 1958). The relation between superconductivity and singularities of the  $T$ - and  $\mathcal{G}$ -matrices was recognized quite early in the development of quantum many-body theory and considered in detail by (Emery, 1959, 1960). Singular behavior of the  $T$ -matrix is directly related to the pairing properties of the system, as it signals the vicinity of a superfluid phase transition. In fact, the critical temperature  $T_c$  for the onset of pairing in attractive fermionic systems, including nuclear systems, can be extracted as the temperature at which the  $T$ -matrix diverges as the system is cooled down in its normal state. This condition for the determination of the onset of superconductivity is known as Thouless criterion (Thouless, 1960).

In vacuum, both these choices for the scattering matrix reduce trivially to the  $T$ -matrix of two nucleons interacting in vacuum, which is fitted to the experimental NN phase shifts for laboratory energies below 350 MeV. In the case of  $\mathcal{G}$ -matrix, the singularities are not directly related to the coherently paired state. This has the consequence that it is still meaningful to perform calculations in nuclear matter based on the  $\mathcal{G}$ -matrix at  $T \leq T_c$ , without introducing a pairing gap in the fermion energy spectrum (Bethe, 1971).

With the advent of phase-shift equivalent, high-precision NN potentials,  $T$ -matrix theory was revived and employed to deduce the critical temperature of the phase transition to the superfluid state in nuclear matter in the attractive interaction channels (Alm *et al.*, 1993, 1990, 1996; Röpke *et al.*, 1998; Rubtsova *et al.*, 2017; Schmidt *et al.*, 1990; Sedrakian *et al.*, 1995; Stein *et al.*, 1995). It is interesting that evidence of a di-neutron bound state has been revealed in  $\mathcal{G}$ -matrix calculations that exhibit poles of this quantity lying below the Fermi energy (Arellano *et al.*, 2016; Isaule *et al.*, 2016). The conditions for such singular behavior are analogous to those for  $T$ -matrix poles, the difference being in the treatment of the intermediate states.

We now examine these scattering-matrix approaches in some detail. The integral equation determining the  $T$ -matrix can be written in momentum space as

$$T(\mathbf{p}, \mathbf{p}'; P) = V(\mathbf{p}, \mathbf{p}') + \int \frac{d\mathbf{p}''}{(2\pi)^3} V(\mathbf{p}, \mathbf{p}'') \times G_2(\mathbf{p}'', P) T(\mathbf{p}'', \mathbf{p}'; P), \quad (56)$$

where  $V(\mathbf{p}, \mathbf{p}'')$  is the two-particle interaction and the

two-particle propagator is given by

$$G_2(\mathbf{p}; P) = \int \frac{d^4 P'}{(2\pi)^4} \int \frac{d\omega}{(2\pi)} \left[ G^>(p_+) G^>(p_-) - G^<(p_+) G^<(p_-) \right] \frac{(2\pi)^3 \delta(\mathbf{P} - \mathbf{P}')}{\Omega - \Omega' \pm i\eta}, \quad (57)$$

having introduced the four-vectors  $p_{\pm} = P/2 \pm p$ , with  $P = (\mathbf{P}, \Omega)$  denoting the center-of-mass four-momentum. Eq. (56) has the familiar form of the Bethe-Salpeter integral equation appearing in scattering theory. The propagators  $G^{>,<}(p)$  are the off-diagonal GFs in the non-equilibrium Keldysh-Schwinger formalism. In equilibrium they can be written identically as

$$\begin{aligned} -iG^<(p) &= a(p, x) f(p), \\ iG^>(p) &= a(p, x) [1 - f(p)], \end{aligned} \quad (58)$$

where  $a(p)$  is the spectral function of fermions and  $f(p)$  is the equilibrium Fermi distribution function. The spectral function of quasiparticles (in the normal state) is given by

$$a(p) = 2\pi Z(\mathbf{p}) \delta(\omega - \epsilon(\mathbf{p})), \quad \epsilon(p) = v_F(p - p_F) - \mu^*. \quad (59)$$

Here the wave-function renormalization  $Z(\mathbf{p})$  is defined in terms of the normal-state self-energy by Eq. (32), while the effective mass and chemical potential are as defined in Eq. (34). With these approximations, Eq. (57) reduces to

$$G_2(\mathbf{p}; P) = Z(\mathbf{p}_+) Z(\mathbf{p}_-) \frac{Q(\mathbf{p}_+, \mathbf{p}_-)}{\Omega - \epsilon(\mathbf{p}_+) - \epsilon(\mathbf{p}_-) + i\eta}, \quad (60)$$

where

$$Q(\mathbf{p}_+, \mathbf{p}_-) = [1 - f(\mathbf{p}_+)] [1 - f(\mathbf{p}_-)] - f(\mathbf{p}_+) f(\mathbf{p}_-) \quad (61)$$

is the Pauli-blocking function, which accounts for the phase-space occupation in the intermediate scattering states of the  $T$ -matrix. The first and second terms of this expression refer to particle-particle and hole-hole propagations, respectively

In Bruckner-Bethe-Goldstone theory, a diagrammatic expansion of the normal ground-state energy is carried out in the number of hole lines, and the hole-hole propagation terms are neglected, i.e., one considers a  $\mathcal{G}$ -matrix equation

$$\begin{aligned} \mathcal{G}(\mathbf{p}, \mathbf{p}'; P) &= V(\mathbf{p}, \mathbf{p}') + \int \frac{d\mathbf{p}''}{(2\pi)^3} V(\mathbf{p}, \mathbf{p}'') \\ &\times \frac{\tilde{Q}(\mathbf{p}_+, \mathbf{p}_-)}{\Omega - \epsilon(\mathbf{p}_+) - \epsilon(\mathbf{p}_-) + i\eta} \mathcal{G}(\mathbf{p}'', \mathbf{p}'; P), \end{aligned} \quad (62)$$

with  $\tilde{Q}(\mathbf{p}_+, \mathbf{p}_-) = [1 - f(\mathbf{p}_+)] [1 - f(\mathbf{p}_-)]$ .

Returning to the  $T$ -matrix equation (56), we consider the poles that this equation might develop as the temperature is reduced, starting in the normal phase. This process can be illustrated analytically by assuming a rank-one separable interaction  $V(\mathbf{p}, \mathbf{p}') = \lambda_0 v(\mathbf{p}) v(\mathbf{p}')$ . The

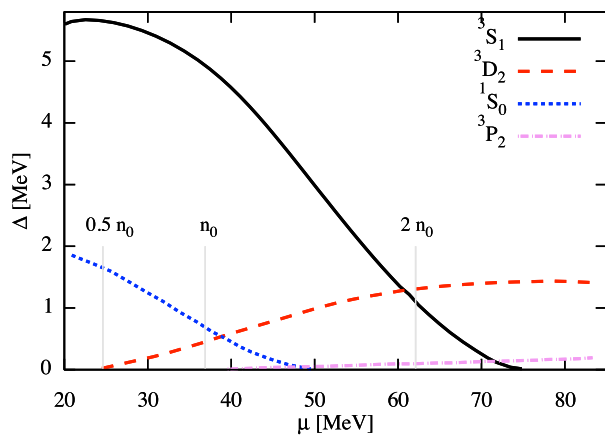


FIG. 5 Dependence of the critical temperature  $T_c$  of superfluid phase transitions on the chemical potential in symmetrical nuclear matter in attractive NN channels, as determined from the  $T$ -matrix instability (Sedrakian *et al.*, 1995). Vertical lines indicate densities in units of the nuclear saturation density  $n_0$ .

solution of Eq. (56) is then given trivially by

$$T(\mathbf{p}, \mathbf{p}', P) = \frac{V(\mathbf{p}, \mathbf{p}')}{1 - J(\mathbf{P})}, \quad (63)$$

$$J(\mathbf{P}) = \lambda_0 \int \frac{d\mathbf{p}}{(2\pi)^3} v^2(\mathbf{p}) G_2(\mathbf{p}, P), \quad (64)$$

noting that the  $T$ -matrix depends parametrically on the chemical potential the temperature of the fermionic matter through  $G_2(\mathbf{p}, P)$  in the denominator. At the critical temperature of a phase transition to the superfluid state, the  $T$ -matrix develops a pole for the energy-momentum arguments  $\Omega_c = 2\mu^*$ , and  $\mathbf{P} = 0$ , which is equivalent to the conditions

$$\text{Re } J(\mathbf{P}) = 1 \quad \text{and} \quad \text{Im } J(\mathbf{P}) = 0. \quad (65)$$

We conclude that for the given interaction, the critical temperature of the superfluid phase transition can be determined as the temperature  $T_c$  at which the  $T$ -matrix is divergent (Thouless, 1960).

Figure 5 shows the critical temperatures of the dominant channels of pairing in nuclear matter as a function of chemical potential. Among isospin-singlet ( $T = 0$ ) states, the highest critical temperatures are obtained in the  ${}^3S_1$ – ${}^3D_1$  and  ${}^3D_2$  partial-wave channels at low and high densities, for isospin-symmetric nuclear matter. In neutron-rich matter, these channels are suppressed by the strong isospin asymmetry, such that the  $T = 1$  channels  ${}^1S_0$  and  ${}^3P_2$ – ${}^3F_2$  become dominant, at low and high densities respectively.

Pursuing the example of the separable interaction, we observe that the Ansatz  $\Delta(\mathbf{p}) = C v(\mathbf{p})$ , with  $C$  a constant to be determined, reduces the BCS gap equation

(36) (with  $Z \equiv 1$ ) to the form

$$1 = -\lambda_0 \int \frac{d\mathbf{p}}{(2\pi)^3} \frac{v^2(\mathbf{p})}{2\omega_+} [1 - 2f(\omega_+)], \quad (66)$$

Taking the limit  $T \rightarrow T_c$ , i.e.,  $\omega_+ \equiv \sqrt{\epsilon(\mathbf{p})^2 + \Delta^2} \rightarrow \epsilon(\mathbf{p})$ , we recover the condition (65). Thus we see that BCS theory and the  $T$ -matrix resummation instability (activating the Thouless criterion) lead to the same condition for the critical temperature  $T_c$ .

In the case of  $\mathcal{G}$ -matrix, the absence of hole-hole propagation in the intermediate states breaks particle-hole symmetry. Consequently, the instability of the  $T$ -matrix that signals the onset of the superfluid state is suppressed and the  $\mathcal{G}$ -matrix can be computed at temperatures below  $T_c$ , down to  $T = 0$ . Brueckner-Bethe-Goldstone theory utilizes the  $\mathcal{G}$ -matrix as an effective interaction in generating the perturbative hole-line expansion. That is, the diagrams in the expansion for the energy are ordered according to the number of hole lines present, each hole line implying a convergence factor given roughly by the volume, per particle, excluded by the repulsive component of the NN interaction to the mean volume per particle. On one hand, this has the apparent virtue of wiping away the instability associated with pairing; on the other, the resulting theory is non-conserving in that it entails self-energies and scattering amplitudes that are asymmetric with respect to interchange of particles and holes. In fact, if conservation laws are to be enforced, any collision integral constructed from scattering amplitudes (or non-equilibrium self-energies in the language of the Keldysh-Schwinger formalism) must vanish in the equilibrium limit, fails to be the case if particle-hole symmetry is broken. A consequence of such non-conservation is seen in violation of the Hugenholtz-van Hove Theorem (equality of the chemical potential to the Fermi energy in the presence of arbitrarily strong interactions) in theories of nuclear matter based on the  $\mathcal{G}$ -matrix, in which only particle-particle propagation is taken into account (Brueckner and Gammel, 1958). At the same time, as long as the hole-line expansion is valid, such violation ought to be small.

### C. Self-consistent Green's functions theory (SCGF)

The foundation of self-consistent Green's functions (SCGF) theory were established long ago [see for example (Kadanoff and Baym, 1962)]. It can be applied to nuclear matter at finite temperatures above the critical temperature for pairing, see e.g. (Botermans and Malfliet, 1990). We start by reviewing the underlying formalism. SCGF theory is a microscopic approach to properties of the normal (unpaired) state in which the interactions between nucleons are accounted for via the two-body  $T$ -matrix constructed from the bare NN interaction. The single-particle spectrum is obtained from the self-energies computed in the  $T$ -matrix approximation, as illustrated

diagrammatically in Fig. 6. Eqs. (56)-(58) which determine the  $T$ -matrix remain intact, but the spectral function are now completely general, i.e.,

$$\begin{aligned} a(p) &= i [G^R(p) - G^A(p)] = i [G^>(p) - G^<(p)] \\ &= -\frac{2\Im\Sigma(p)}{[\omega - \epsilon(p) - \Re\Sigma(p)]^2 + [\Im\Sigma(p)]^2}, \end{aligned} \quad (67)$$

where  $G^{R/A}(p)$  are the retarded and advanced GFs and  $\Sigma(p)$  is the self-energy. Consequently, in SCGF theory the two-body propagator is given by

$$G_2(\mathbf{p}; P) = \int \frac{d\Omega' d\omega}{(2\pi)^2} a(p_+) a(p_-) \frac{Q(p_+, p_-)}{\Omega - \Omega' + i\eta}, \quad (68)$$

where  $Q(p_+, p_-) = [1 - f(p_+) - f(p_-)]$ . The self-energy in the  $T$ -matrix approximation is expressed as

$$\begin{aligned} \Sigma(p) &= \int \frac{d^4 p'}{(2\pi)^4} \left[ T(\mathbf{q}, \mathbf{q}; p + p') a(p') f(\omega') \right. \\ &\left. + 2g(\omega + \omega') \Im T(\mathbf{q}, \mathbf{q}; p + p') \int \frac{d\bar{\omega}}{2\pi} \frac{a(\mathbf{p}', \bar{\omega})}{\omega' - \bar{\omega}} \right], \end{aligned} \quad (69)$$

with  $\mathbf{q} \equiv (\mathbf{p} - \mathbf{p}')/2$ . Eqs. (56), (68), and (69) form a closed system of coupled integral equations requiring as input the interaction between the nucleons. These equations can be solved numerically by iteration for phase-shift equivalent two-body potentials (Bożek and Czerski, 2002; Frick and Müther, 2003; Frick *et al.*, 2004; Rios *et al.*, 2006, 2009) and two-body plus three-body potentials (Carbone *et al.*, 2013).

To obtain a closed set of equations for the investigation of pairing, it is necessary to specify an approximation to the anomalous self-energy. In the mean-field (BCS) approximation (i.e., for the on-shell gap),

$$\begin{aligned} \Delta^\dagger(p) &= i \int V(\mathbf{p}, \mathbf{p}') F^\dagger(\mathbf{p}') \frac{d^4 p'}{(2\pi)^4} \\ &= i \int V(\mathbf{p}, \mathbf{p}') G^N(-p') \Delta^\dagger(p') G(p') \frac{d^4 p'}{(2\pi)^4}, \end{aligned} \quad (70)$$

where in the second step we have eliminated the anomalous propagator using Eq. (28). Thus, in the on-shell limit we have

$$\Delta^\dagger(\mathbf{p}) = i \int \frac{d\mathbf{p}'}{(2\pi)^3} V(\mathbf{p}, \mathbf{p}') \Delta^\dagger(\mathbf{p}') G_2^S(\mathbf{p}'), \quad (71)$$

where the two-particle propagator in the superfluid state is given by

$$G_2^S(\mathbf{p}) = \int \frac{d\omega}{2\pi} G^N(-\omega, \mathbf{p}) G(\omega, \mathbf{p}). \quad (72)$$

The BCS gap equation (36) is recovered if the two-particle propagator  $G_2^S(\mathbf{p})$  is taken in the quasiparticle

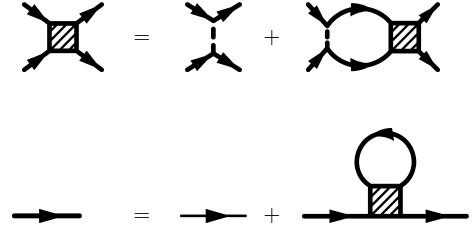


FIG. 6 Diagrammatic representation of the coupled equations for the  $T$ -matrix (top relation) and Green's function of fermions (bottom relation) in the self-consistent Green function (SCGF) theory. The vertical dashed line stands for bare interaction, while the thick and thin lines correspond respectively to the full and bare propagators.

approximation. Going beyond the quasiparticle approximation within the SCGF theory entails the replacement of the two-particle propagator in the superfluid state  $G_2^S(\mathbf{p})$  by its counterpart in the normal state (68). The main advantage of the SCGF approach is that the gap equation is solved while keeping the off-mass-shell information contained in the full spectral function of the normal state.

However, we learned that the  $T$ -matrix from which the spectral function is computed in SCGF theory is divergent below  $T_c$ . Accordingly, the spectral function apparently needs to be computed at temperatures *above*  $T_c$ . This problem is circumvented by extrapolating the imaginary part of the normal-state self-energies to temperatures  $T \leq T_c$  using the fact that  $\Im\Sigma(\omega)$  must vanish on the Fermi surface at  $T = 0$ . The real part of the self-energy is then computed from the Kramers-Kronig dispersion relation and, in this way, the complete spectral function is constructed below  $T_c$ .

The procedure so outlined allows one to feed information on the spectral function of nucleonic system, which embodies crucial effects of short range correlations, into the computation of pairing correlations. We may observe that this procedure relies on the basic strategy of the decoupling approximation: the single-particle properties of the system are computed in the normal state, and the pairing correlations are added in the second step neglecting their back-reaction on the single-particle energies.

Numerical calculations demonstrate that upon going beyond the approximation that employs on-shell quasiparticles with a renormalized spectrum, by adopting the GF given by Eq. (68), the pairing gap is suppressed by about ten percent in the isospin-singlet  ${}^3S_1$ - ${}^3D_1$  state, as well as in the isospin-triplet  ${}^1S_0$  and  ${}^3P_2$ - ${}^3F_2$  channels. These results can be attributed to the shift of some spectral weight from the quasiparticle peak toward other energies, upon implementing full spectral functions (Ding *et al.*, 2016a; Rios *et al.*, 2017a); the corresponding numerical results are discussed below in Sec. III.F for the  $S$ -wave and in Sec. V.B for the  $P$ -wave channels.

#### D. Correlated Basis Functions Theory

The variational correlated basis functions (CBF) theory was applied to nucleonic pairing at the very early stages of theoretical development of the field (Chao *et al.*, 1972; Yang and Clark, 1971). A variational theory of the superfluid ground state of uniform, infinite nucleonic systems was developed for a trial correlated BCS state later on (Krotscheck and Clark, 1980). An important further advance in the CBF approach to pairing was the variational description extended to create a correlated-basis perturbation theory for the exact superfluid ground state (Krotscheck *et al.*, 1981). Within the decoupling approximation, a sequence of approximations to the grand-canonical energy was defined, each preserving under variation the standard form of the gap equation, but with successive improvements on the effective pairing matrix elements and dressed self-energies. This method was implemented in nuclear system to treat the short- and long-range correlations consistently within the same approach in a series of works (Chen *et al.*, 1993, 1986).

An independent approach to CBF description of pairing based on the trial superfluid state was developed to treat short-range and long-range correlations consistently within the same framework and applied to extended nuclear systems in (Fantoni, 1981). This approach was further generalized to include state-dependent correlations and to use Monte-Carlo sampling of configurations to obtain the  $^1S_0$  neutron gap (Fabrocini *et al.*, 2005, 2008).

The CBF method has been applied in combination with the central parts of the phase-shift equivalent Argonne  $V'_4$  potential to obtain the ground state and  $^1S_0$  pairing gap in neutron matter recently (Fan *et al.*, 2017). This has been achieved by determining the optimal Jastrow-Feenberg correlations and corresponding effective pairing interactions by using Fermi hypernetted-chain (FHNC) techniques. The major advance of this approach is the simultaneous summation of particle-particle and particle-hole diagrams, however in an approximation which treats the correlations between particles in the Fermi sea in an average way.

The CBF theory for uniform, infinite nucleonic systems uses a trial correlated BCS state given by

$$|\Psi_s\rangle = \sum_N \sum_{m^{(N)}} \hat{F}^{(N)} |\Phi_m^{(N)}\rangle \langle \Phi_m^{(N)} | \Psi_{\text{BCS}} \rangle, \quad (73)$$

where  $\hat{F}^{(N)}$  is an unspecified correlation operator meeting certain minimal conditions and  $\{|\Phi_m^{(N)}\rangle\}$  is a complete set of Fermi-gas Slater determinants, both referred to the  $N$ -particle Hilbert space. Thus, the correlated normal states  $\{\hat{F}^{(N)}|\Phi_m^{(N)}\rangle\}$  are superposed with the same amplitudes as the model states  $|\Phi_m^{(N)}\rangle$  have in the corresponding grand-canonical representation of the original BCS state given by

$$\Psi_{\text{BCS}} = \prod_{\mathbf{p}} \left[ (1 - h_{\mathbf{p}})^{1/2} + h_{\mathbf{p}}^{1/2} \psi_{\mathbf{p}\uparrow}^\dagger \psi_{-\mathbf{p}\downarrow}^\dagger \right] |0\rangle, \quad (74)$$

where the real function  $h_{\mathbf{p}}$ , which gives the occupation probability of the pair state ( $\mathbf{p}\uparrow, -\mathbf{p}\downarrow$ ), is subject to variation

This then yields a theory having the same structure as ordinary BCS theory, when the decoupling approximation is applied. In this approximation, only one Cooper pair at a time is considered, while treating the background as normal. Formally, the expectation value of the grand-canonical Hamiltonian is expanded in terms of the deviations of the Bogolyubov amplitudes  $u_{\mathbf{p}}$  and  $v_{\mathbf{p}}$  about their normal-state values, retaining deviant terms to leading order in  $v_{\mathbf{p}}^2 - \theta(p)$  and second order in  $u_{\mathbf{p}}v_{\mathbf{p}}$ , where  $\theta(p)$  is the Fermi step function.

Because nuclear systems are characterized by a bare two-body interaction containing a strong inner repulsive core along with longer-range attractive components, their treatment calls for an improved superfluid trial state. To obtain a reasonable energy expectation value, the trial function must adequately describe the short-range geometric correlations induced by the repulsion, which inhibits the close approach of a pair of particles (Chen *et al.*, 1993, 1986; Krotscheck and Clark, 1980). The simplest such choice is the Jastrow correlation factor

$$F_J = \prod_{i<j}^N f(r_{ij}), \quad \lim_{r \rightarrow 0} f(r) \rightarrow 0, \quad \lim_{r \rightarrow \infty} f(r) \rightarrow 1, \quad (75)$$

which is suited to efficient description of state-independent two-body correlations, especially the short-range repulsive effects. A proper optimization of the two-body function  $f(r)$  allows for the Jastrow factor to incorporate also the effects of virtual phonon excitations and reproduce the correct asymptotic behavior of long-range correlations. With the state-independent Jastrow choice  $F_J$  of Eq. (75) the correlation operator  $\hat{F}$ , the effective pairing interaction and the single-particle energies can be evaluated by FHNC methods (Krotscheck and Clark, 1979, 1980).

As alluded to above, the gap equation retains its standard form

$$\Delta(\mathbf{p}) = -\frac{1}{2} \sum_{\mathbf{p}'} \mathcal{V}_{\mathbf{p}\mathbf{p}'} \frac{\Delta(\mathbf{p}')}{\sqrt{(E_{\mathbf{p}'} - \mu)^2 + \Delta_{\mathbf{p}'}^2}}, \quad (76)$$

the key difference being the definition of the effective pairing interaction  $\mathcal{V}_{\mathbf{p}\mathbf{p}'}$ , which is given by

$$\mathcal{V}_{\mathbf{p}\mathbf{p}'} = \mathcal{W}_{\mathbf{p}\mathbf{p}'} + (|E_{\mathbf{p}} - \mu| + |E_{\mathbf{p}'} - \mu|) \mathcal{N}_{\mathbf{p}\mathbf{p}'}, \quad (77)$$

with

$$\mathcal{W}_{\mathbf{p}\mathbf{p}'} = \langle \mathbf{p}\uparrow, -\mathbf{p}\downarrow | \mathcal{W}(r) | \mathbf{p}'\uparrow, -\mathbf{p}'\downarrow \rangle_a, \quad (78)$$

$$\mathcal{N}_{\mathbf{p}\mathbf{p}'} = \langle \mathbf{p}\uparrow, -\mathbf{p}\downarrow | \mathcal{N}(r) | \mathbf{p}'\uparrow, -\mathbf{p}'\downarrow \rangle_a, \quad (79)$$

where the index  $a$  implies antisymmetrization. In general the two-body operators  $\mathcal{N}$  and  $\mathcal{W}$  are non-local, but to leading order depend on the relative separation

$r$  of the nucleons. In the decoupling approximation these operators are computed from the theory of correlated normal state. If one chooses to work within the Fermi-Hypernetted-Chain (FHNC) theory, the induced interaction can be expressed as (Krotscheck, 2000)

$$\mathcal{W}(r) = \frac{1}{m} \left| \nabla \sqrt{1 + \mathcal{N}(r)} \right|^2 + [V(r) + W_{\text{ind}}(r)] [1 + \mathcal{N}(r)], \quad (80)$$

where the first term is associated with changes in the kinetic energy due to the short range correlation, the term  $\propto V(r)$ , with  $V(r)$  being the bare interaction, incorporates short-range correlations, whereas the term  $\propto W_{\text{ind}}(r)$  includes the long-range collective mode-exchange. The Fourier images of  $W_{\text{ind}}(r)$  and  $\mathcal{N}(r)$  are related to the static structure function  $S(k)$  of the correlated state according to (Fan *et al.*, 2017)

$$W_{\text{ind}}(k) = -\frac{T(k)}{2S_F(k)^2} \left[ 1 - \frac{S_F(k)}{S(k)} \right]^2 \left[ 1 + \frac{2S(k)}{S_F(k)} \right], \quad (81)$$

$$\mathcal{N}(k) = [S(k) - S_F(k)] S_F^{-2}(k), \quad (82)$$

where  $S_F(k)$  is the static structure function of the free Fermi gas and  $T(k) = k^2/2m$  is the kinetic energy. Finally, the structure function obeys an Euler-Lagrange equation that incorporates effects of both the long-range and short-range correlations

$$S(k) = S_F(k) \left\{ 1 + \frac{2S_F^2(k)}{T(k)} [\mathcal{W}(k) - W_{\text{ind}}(k)] \right\}^{-\frac{1}{2}}. \quad (83)$$

The explicit expression for the single particle energy in the CBF gap equation (76) likewise can be expressed in terms of the Fourier images of the functions  $\mathcal{W}(r)$  and  $\mathcal{N}(r)$  thus closing the system of equations (Fan *et al.*, 2017).

The recent reappraisal of the pairing gaps in low-density neutron matter within the CBF theories finds much less suppressed gaps (Benhar and De Rosi, 2017; Fan *et al.*, 2017; Pavlou *et al.*, 2017) compared to those found in the earlier computations (Chen *et al.*, 1993, 1986). Numerical results for pairing in neutron matter from these efforts based on CBF theory are displayed below in Sec. III.F.

## E. Monte Carlo methods

Our survey of the many-body methods for *ab initio* computational exploration of pairing behavior in nuclear systems would not be complete without the important class of stochastic approaches based on Monte Carlo (MC) algorithms. While MC methods have been extensively applied to normal (unpaired) state of neutron and nuclear matter over an extended period (Gandolfi *et al.*, 2009b), the much more challenging problem of pairing

has been addressed in only a handful of studies during the last decade (Fabrocini *et al.*, 2005; Gandolfi *et al.*, 2008, 2009a; Gezerlis and Carlson, 2008, 2010). These studies have focused on phase-shift equivalent interactions, especially the Argonne-Urbana class of potentials. The essence of the MC method is the solution of non-relativistic Schrödinger equation using stochastic sampling of configurations, as the system is advanced in imaginary time. In practice, an infinite system is simulated in a finite box containing a fixed number of particles subject to periodic boundary conditions. Of specific interest for this review are the Green Function Monte Carlo (GFMC) and auxiliary field Diffusion Monte Carlo (AFDMC) algorithms. The latest GFMC computations of bulk energy and pairing gaps in nuclear matter have been performed for systems of  $\sim 60$  nucleons; larger numbers of particles can be accommodated in AFDMC simulations.

AFDMC is a special kind of GFMC method in which spin/isospin configurations are sampled instead of explicitly summed, allowing extension the the calculation to higher density (Fabrocini *et al.*, 2005). The most recent computations of this kind use a fixed-phase approximation, which resolves the technical difficulties associated with the presence of a tensor interaction (Gandolfi *et al.*, 2008, 2009a; Gezerlis and Carlson, 2008). This work also employs the full Hamiltonian instead of projecting the interaction on some specific partial-wave channel (e.g.,  $^1S_0$  for low-density neutron matter). Depending on forms of the initial or trial correlated superfluid and normal states, the energy difference between their evolved versions can be under 4% (Gandolfi *et al.*, 2009a). The starting superfluid state is taken as the product of a Jastrow correlation factor  $\Pi_{i<j} f(r_{ij})$  and a Pfaffian of pair wave functions  $\phi(ij)$  obeying the prescribed boundary conditions, the pair functions being determined from a variational CBF calculation of the energy expectation value using extended FHNC techniques. In the case of odd neutron number, the energy of the unpaired neutron is chosen to minimize the energy.

The standard Green function MC (GFMC) method and the simpler variational MC (VMC) procedure sample only spatial configurations (Gandolfi *et al.*, 2015; Gezerlis and Carlson, 2008, 2010). VMC calculations use Monte Carlo integration to minimize the expectation value of the Hamiltonian, optimizing the trial wave function. In the GFMC approach the Schrödinger equation is brought to the diffusion form with respect to imaginary time and the initial trial wave function is evolved to obtain the lowest energy eigenstate. As in the AFDMC approach, the starting wave function is taken to be of the Jastrow-Pfaffian form with a fixed number of particles subject to periodic boundary conditions. The Jastrow part of the wave function is obtained from a lowest-order constrained-variational (LOCV) method.

As is done in the case of finite nuclei, the energy gap in pure neutron matter is determined from the odd-even

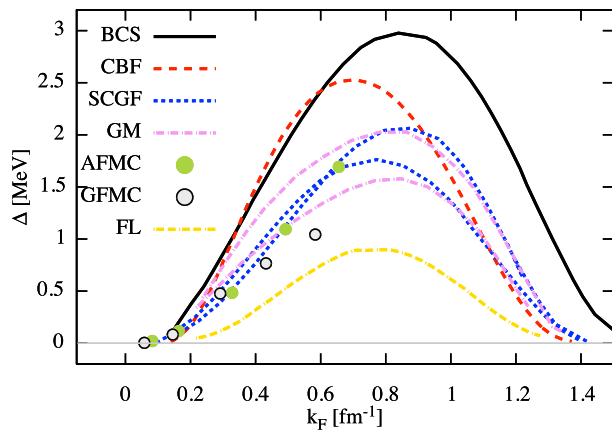


FIG. 7 Dependence of the  $^1S_0$  pairing gap in the low-density neutron matter on the Fermi momentum in different many-body theories: “BCS” corresponds to the solution of the BCS gap equation with a free single-particle spectrum; “CBF” corresponds to the results of an FHNC-optimal correlated basis calculation (Fan *et al.*, 2017); “SCGF” corresponds to self-consistent GF computations including only short-range correlations (higher-maximum curve) and both short- and long-range correlations (Ding *et al.*, 2016a); “GM” is based on solutions of the gap equation with self-energies derived from a  $G$ -matrix without (higher maximum curve) and with long-range correlations (Cao *et al.*, 2006); “AFMC” corresponds to auxiliary field Monte Carlo computations (Gandolfi *et al.*, 2008); “GFMC” shows GF Monte-Carlo results (Gezerlis and Carlson, 2008); “FL” refers to the results obtained from Fermi-liquid theory which includes long-range polarization effects (Wambach *et al.*, 1993). The “BCS”, “SCGF” and “GM” results were obtained with the Argonne  $V_{18}$  potential and the “CBF” result was obtained with the  $V'_4$  version of the same potential.

staggering formula for odd neutron number  $N$ , thus

$$\Delta(N) = E(N) - \frac{1}{2} [E(N+1) + E(N-1)]. \quad (84)$$

More recent GFMC computations (Gezerlis and Carlson, 2008, 2010) predict gaps which are about 30% smaller than those obtained with AFDMC. Furthermore, the gaps obtained by the two MC methods are suppressed compared to bare BCS result, as is usually the case with the other methods (SCGF, CBF, etc.) discussed above. One may anticipate that within their error bars the MC computations faithfully account for the strong short-range repulsion of phase-shift equivalent NN interactions. Simulations with larger number of particles may provide further insight into the accuracy of the extrapolations to infinite matter and the role of long-range correlations.

## F. Overview of the results

We close this section with an overview of the results obtained for the simplest problem, namely the neutron  $^1S_0$  pairing gap; discussion of  $^3P_2 - ^3F_2$  pairing is relegated to Sec. V.B. We show in Fig. 21 the results of computations of this quantity, all of which are based on versions of the Argonne family of NN potentials, implying that the observed differences are due mainly to differences between the many-body methods applied. All these methods (except the Monte Carlo approaches, which provide data only in the lower-density domain) predict a peak value of the gap  $\Delta_F$ , i.e.  $\Delta_{\mathbf{k}}$  evaluated for  $k = k_F$ , close to  $0.8 \text{ fm}^{-1}$ , the peak value itself varying in the range 0.8 to 2.5 MeV. The CBF, SCGF and GM theories predict gap values within a factor of 0.5 MeV around the average value 2 MeV. The Fermi-liquid (FL) methods predicts  $\Delta_F$  values smaller by about 1 MeV, which is attributed to the suppression of pairing by spin-density fluctuations. The MC results at lower densities are consistent with the results obtained within non-MC theories, but we recall that the gap in the MC computations is extracted from the difference in the energies of the normal and paired states, extrapolated to the thermodynamical limit, rather than from solution of the gap equation.

Solution of the gap equation with a bare realistic nuclear interaction does not pose conceptual problems if the phase space far from the Fermi surface is covered in the numerical procedure. However, a number of effective models of two-body interaction have been tested on the pairing problem in neutron matter. These interactions are designed and well-suited for computation of properties of finite nuclei. Calculations based on effective interactions such as the Gogny,  $V_{\text{low-k}}$  potentials (Kuckei *et al.*, 2003; Ramanan *et al.*, 2007; Sedrakian *et al.*, 2003; Sun and Pan, 2013), and chiral potentials with varying cut-off (Drischler *et al.*, 2017; Finelli *et al.*, 2015; Kaiser *et al.*, 2005; Maurizio *et al.*, 2014; Rios *et al.*, 2017b) predict gaps in neutron matter that are close numerically to those obtained from realistic full (un-truncated) interactions. Particular features of these interactions (e.g. localization at small momenta) could be utilized to achieve advances in the many-body description of pairing in neutron matter and neutron-star matter.

## IV. UNCONVENTIONAL PAIRING AND BCS-BEC CROSSOVERS

New classes of superfluid fermionic states arise when the pairing is between fermions residing on different Fermi surfaces. Such a situation arises generically in multi-component systems with cross-species pairing. The simplest example is an electronic superconductor in spin polarizing  $B$ -field which induces an imbalance between the number of spin-up and down electrons. In nuclear physics we encounter such situation when pairing oc-

curs between neutrons and protons in isospin asymmetric matter or among neutrons (or protons) placed in a strong magnetic field.

Mathematically, the novelty of such phases is associated with a non-zero anti-symmetric piece  $E_A$  of the quasiparticle spectrum in Eq. (31), which by definition requires  $\varepsilon(p) \neq \varepsilon(-p)$ , i.e., breaking of the invariance with respect to reversal of time or spatial symmetry. We shall refer to such systems below as imbalanced superfluids, a term that has become common in theory of cold fermionic atoms, where these systems can be tested experimentally.

Historically, the studies of imbalanced superfluids begun shortly after the advent of the BCS theory in the context of electronic materials containing paramagnetic impurities (Chandrasekhar, 1962; Clogston, 1962; Sarma, 1963). The effect of impurity scattering on electrons, on average, was modeled in terms of an effective magnetic field, which then induces an imbalance between the spin-up and spin-down electrons.

The initial studies were carried in the weak-coupling formalism, where the back-reaction of the pairing on the chemical potential of the system can be ignored. The imbalance was parametrized in terms of the difference in the chemical potentials of the species  $\delta\mu$ , which led to the following picture for the gap  $\Delta$  as a function of  $\delta\mu$  (Chandrasekhar, 1962; Clogston, 1962; Sarma, 1963). It is a double-valued function, the upper branch of the two solutions being constant  $\Delta(\delta\mu) = \Delta(0)$  in the range  $0 \leq \delta\mu \leq \Delta(0)$  and zero beyond the point  $\delta\mu = \Delta(0)$ . The lower branch exists in the range  $\Delta(0)/2 \leq \delta\mu \leq \Delta(0)$ , with the gap increasing from zero at the lower limit to  $\Delta(0)$  at the upper limit. Only the portion  $\delta\mu \leq \Delta(0)/\sqrt{2} = \delta\mu_1$  of the upper branch is stable in the sense that the superconducting state lowers ground-state energy of the superfluid (Sarma, 1963). In the remaining region of imbalance, the superconducting state is unstable (Sarma instability).

Imbalanced pairing in infinite nuclear systems naturally became of interest in the context of  ${}^3S_1$ - ${}^3D_1$  and  ${}^3D_2$  pairing in isospin asymmetrical nuclear matter (Alm *et al.*, 1993, 1996), and the critical temperatures in these channels were computed using  $T$ -matrix theory and realistic interactions. The full BCS formulation was applied at about the same time (Sedrakian *et al.*, 1997), and subsequently the single-particle energies  $\varepsilon_p$  were renormalized within Brueckner theory, resulting in a major reduction of the gap values and more realistic values of critical isospin asymmetries (Sedrakian and Lombardo, 2000).

The ground state of an imbalanced superfluid may entail breaking of global symmetries, notably translational or rotational symmetries, in some range of parameter space. Breaking of translational invariance was first proposed and studied independently by Fulde and Ferrell (Fulde and Ferrell, 1964) and Larkin and Ovchinnikov (Larkin and Ovchinnikov, 1965), who discovered that the superconducting state where the

Cooper pairs carry a finite center of mass (CM) momentum can extend to imbalances beyond those restricted by the Chandrasekhar-Clogston limit. In the weak coupling case, the maximum shift in the Fermi surfaces for the FFLO type of pairing is  $\delta\mu_2 = 0.755 \Delta(0) [ > \delta\mu_1 = 0.707 \Delta(0) ]$ . The condensate predicted by Fulde and Ferrell (Fulde and Ferrell, 1964) assumes  $\Delta(\mathbf{r}) = \Delta_0 \exp(-i\mathbf{P} \cdot \mathbf{r})$  for the gap function, where  $\mathbf{P}$  is the CM momentum. Larkin and Ovchinnikov (Larkin and Ovchinnikov, 1965) explored various lattice types and concluded that the body-centered-cubic lattice is the most stable configuration near the critical temperature. Imbalanced pairing involving finite-momentum of pairs of neutrons and protons in infinite nuclear systems has been studied in  ${}^3S_1$ - ${}^3D_1$  and  ${}^3D_2$  pairing channels, both within  $T$ -matrix theory (Alm *et al.*, 1996) and in extensions of the BCS theory to account for violation of spatial symmetries (Mao *et al.*, 2009; Sedrakian, 2001; Stein *et al.*, 2012, 2014a).

Two alternative to FFLO realizations of phases of imbalanced superfluids, proposed later, find their application in nuclear systems. One involves deformations of the Fermi surfaces of the fermion species in population imbalance, with the aim of improving the ground-state energy of the paired system compared with the standard configuration of Fermi spheres (Müther and Sedrakian, 2002, 2003). Another possibility is the separation of phases, originally suggested in the context of cold atomic gases (Bedaque *et al.*, 2003a), and studied thereafter in infinite nuclear systems in  ${}^3S_1$ - ${}^3D_1$  channel (Stein *et al.*, 2012, 2014a).

Extensive work on imbalanced superfluids was carried out within the area of ultra-cold atomic gases starting shortly after the observation of Bose-Einstein condensates in trapped atomic gases (Bedaque *et al.*, 2003a; Combescot, 2001; Forbes *et al.*, 2005; Liu and Wilczek, 2003; Sedrakian *et al.*, 2005; Stoof *et al.*, 1996); for a review and further references see (Bloch *et al.*, 2008). These systems offer a unique possibilities for testing the physics of imbalanced superfluidity under controllable conditions in laboratory experiments (Partridge *et al.*, 2006; Zwierlein *et al.*, 2006).

Furthermore, imbalanced superfluids have been extensively studied in the context of color superconductivity of cold quark matter in compact stars, where the three lightest flavors of quarks and three quark colors make the possible patterns of pairing especially interesting; for reviews and further references see (Alford *et al.*, 2008; Anglani *et al.*, 2014; Rajagopal and Wilczek, 2001).

## A. Formalism

Proceeding to the examination of imbalanced phases in more detail in terms of the underlying many-body theory and application to nuclear matter, we start with a brief outline of the formalism based on the extension of the

GF method to imbalanced systems. [For more details, see (Stein *et al.*, 2014a)].

The Green function of the superfluid, written in the Nambu-Gor'kov basis, is given by

$$i\mathcal{G}_{12} = i \begin{pmatrix} G_{12}^+ & F_{12}^- \\ F_{12}^+ & G_{12}^- \end{pmatrix} = \begin{pmatrix} \langle T_\tau \psi_1 \psi_2^+ \rangle & \langle T_\tau \psi_1 \psi_2 \rangle \\ \langle T_\tau \psi_1^+ \psi_2^+ \rangle & \langle T_\tau \psi_1^+ \psi_2 \rangle \end{pmatrix}, \quad (85)$$

where  $G_{12}^\pm \equiv G_{\alpha\beta}^\pm(x_1, x_2)$ , etc., and  $x = (t, \mathbf{r})$  is the four-dimensional space-time coordinate. The Greek indices label discrete spin and isospin variables. The operators in (85) can be viewed as a bi-spinors, i.e.,  $\psi_\alpha = (\psi_{n\uparrow}, \psi_{n\downarrow}, \psi_{p\uparrow}, \psi_{p\downarrow})^T$ , where the indices  $n, p$  label the particle's isospin and  $\uparrow, \downarrow$  label its spin.

The solutions of Dyson equation for the Green functions (GFs) defined in (85) are

$$G_{n/p}^\pm = \frac{ik_\nu \pm \epsilon_{p/n}^\mp}{(ik_\nu - E_{\mp/\pm}^+)(ik_\nu + E_{\pm/\mp}^-)}, \quad (86)$$

$$F_{np}^\pm = \frac{-i\Delta}{(ik_\nu - E_\pm^+)(ik_\nu + E_\mp^-)}, \quad (87)$$

$$F_{pn}^\pm = \frac{i\Delta}{(ik_\nu - E_\mp^+)(ik_\nu + E_\pm^-)}. \quad (88)$$

There are four branches of the quasiparticle spectra, which are given by

$$E_r^a = \sqrt{E_S^2 + \Delta^2} + r\delta\mu + aE_A, \quad (89)$$

where  $a, r \in \{+, -\}$  and

$$E_S = \frac{Q^2/4 + k^2}{2m^*} - \bar{\mu}, \quad E_A = \frac{\mathbf{k} \cdot \mathbf{Q}}{2m^*}, \quad (90)$$

are the symmetrical and anti-symmetrical parts of the quasiparticle spectrum,  $\bar{\mu} \equiv (\mu_n + \mu_p)/2$  is the average of neutron and proton chemical potentials,  $\mathbf{Q}$  is the center-of-mass momentum of the Cooper pair. To generate their retarded counterparts, denoted  $G_{n/p}^{R\pm}$  and  $F_{n/p}^{R\pm}$ , we analytically continue the GFs of Eqs.(86), taking  $ik_\nu \rightarrow k_0 + i0^+$ . The densities of neutrons and protons are defined in a standard fashion through these GFs:

$$n_{n/p}(\mathbf{Q}) = -2 \int \frac{d^4 k}{(2\pi)^4} \text{Im}[G_{n/p}^{R+}(k, \mathbf{Q}) - G_{n/p}^{R-}(k, \mathbf{Q})]f(\omega), \quad (91)$$

where  $k = (k_0, \mathbf{k})$  is the four-momentum.

If the interaction is time-local, the pairing gap is given by

$$\Delta(\mathbf{k}, \mathbf{Q}) = 2 \int \frac{d^4 k'}{(2\pi)^4} V(\mathbf{k}, \mathbf{k}') \times \text{Im}i[F_{np}^{R+}(k, \mathbf{Q}) - F_{pn}^{R-}(k, \mathbf{Q})]f(\omega), \quad (92)$$

where  $V(\mathbf{k}, \mathbf{k}')$  is the neutron-proton interaction. This interaction could be a bare or effective version, depending on the level of approximation; we will illustrate the

physical content of the theory using bare interactions as a benchmark.

Performing a partial-wave expansion of the interaction Eq. (92) and an energy integration, one arrives at the gap equation

$$\Delta_l(Q) = \frac{1}{2} \sum_{a,r} \int \frac{d^3 k'}{(2\pi)^3} V_{l,l'}(k, k') \times \frac{\Delta_{l'}(k', Q)}{2\sqrt{E_S^2(k') + \Delta^2(k', Q)}} [1 - 2f(E_a^r)], \quad (93)$$

where  $V_{l,l'}(k, k')$  is the interaction in the  ${}^3S_1$ - ${}^3D_1$  partial wave and  $\Delta^2 = \sum_l \Delta_l$ . Note that the magnitude of the vector  $\mathbf{Q}$  enters Eqs. (91) and (93) parametrically and should be determined from the minimization of the free energy of nuclear matter. Its direction is chosen by the ensemble spontaneously. This minimum condition leads in fact to an additional equation for  $Q$  that should be solved along with Eqs. (91) and (93).

Quite generally, the ground state of nuclear matter is obtained from the minimization of the respective free energy of the phases

$$F_S = E_S - TS_S, \quad F_N = E_N - TS_N, \quad (94)$$

where indices  $S$  and  $N$  refer to the superfluid and normal phases,  $E$  is the internal energy (statistical average of the system Hamiltonian), and  $S$  is the entropy.

The formalism developed to this point covers also the treatment of the heterogeneous, phase-separated (hereafter PS) phase proposed in (Bedaque *et al.*, 2003a) and implemented in the context of nuclear matter in (Stein *et al.*, 2012, 2014a). Allowing for separation of the phases implies that we can choose to maximize pairing by having isospin-symmetrical superfluid domains, with all the excess neutrons accommodated in normal regions. Then we already have all the necessary ingredients for evaluating the free energy of such state, using the simple construction

$$\mathcal{F}(x, \alpha) = (1-x)F_S(\alpha=0) + xF_N(\alpha \neq 0), \quad (Q=0), \quad (95)$$

where  $x$  is the filling fraction of the unpaired component. Here  $\alpha$  is the isospin asymmetry parameter defined by Eq. (9). In the superfluid phase (S), one has by definition  $n_n^{(S)} = n_p^{(S)} = n^{(S)}$ . In the unpaired phase (N), the densities of neutrons and protons need not be equal and are assigned the values  $n_{n/p}^{(N)}$ . Thus, the net densities of neutrons/protons per unit volume are given by  $n_{n/p} = (1-x)\rho^{(S)} + xn_{n/p}^{(N)}$ .

In the preceding discussion of imbalanced phases we considered a particular realization of the FFLO phase with single plane-wave modulation of the gap parameter in space, which corresponds to the original FF phase. This phase in fact breaks only the rotational symmetry along the direction of the vector  $\mathbf{Q}$ , but in many respects

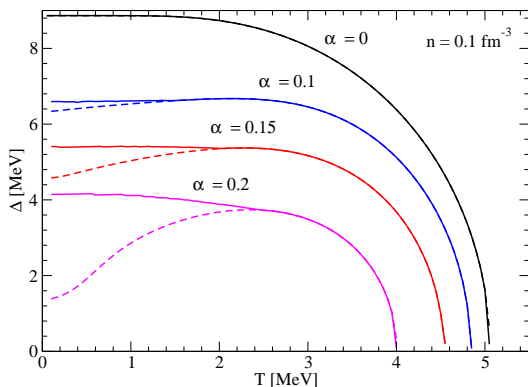


FIG. 8 Dependence of the pairing gap on temperature in the homogeneous phase (dashed lines) and FF phase (solid lines) for nuclear matter density  $n = 0.1 \text{ fm}^{-3}$ . The curves are labeled by the values of density asymmetry  $\alpha$ .

this phase is a representative for other realizations of the FFLO phases.

To summarize this section, we have surveyed the formalism for imbalanced superfluids and its realization in superfluid nuclear matter in which four possible distinct phases can be understood. These can be classified according to the three parameters below as follows

$$\begin{cases} Q = 0, \Delta \neq 0, x = 0, \text{ BCS phase,} \\ Q \neq 0, \Delta \neq 0, x = 0, \text{ FFLO phase,} \\ Q = 0, \Delta \neq 0, x \neq 0, \text{ PS phase,} \\ Q = 0, \Delta = 0, x = 1, \text{ unpaired phase.} \end{cases} \quad (96)$$

The competition between these phases is decided on the basis of minimization of the ground state energy.

These four phases are based on the notion of spherically symmetrical Fermi surfaces of the species; below we will amend our discussion with yet another phase that breaks the spatial symmetries by deformations of the Fermi surfaces away from spherical shape (Müther and Sedrakian, 2002, 2003), see Sec. IV.D below.

## B. Homogeneous phase

Eqs. (91) and (92) have to be solved simultaneously in general because the value of the chemical potential is affected by the change in the quasiparticle spectrum from the normal to the paired form, which contains the gap. In weakly coupled superfluids this back-reaction on the chemical potential is small and can be neglected, but this is not the case in nuclear systems at low densities where the coupling can be large. Once the solutions are found, the free energy can be evaluated and a specific phase can be assigned to a given temperature and density. We start our discussion with the simplest case, the homogeneous imbalanced superfluids. Their realization essentially depends on the difference in the chemical potentials of the components  $\delta\mu = \mu_n - \mu_p \geq 0$ , assuming a neutron excess. A sufficiently large  $\delta\mu$  value will

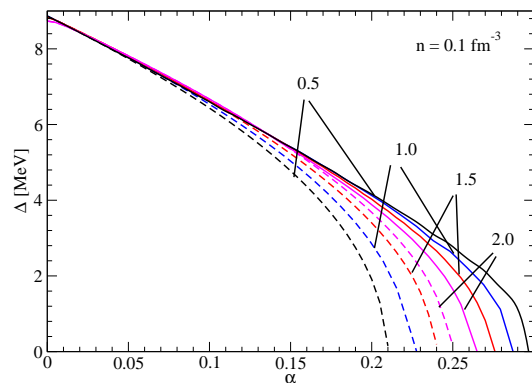


FIG. 9 Dependence of the gap on density asymmetry in the homogeneous phase (dashed lines) and FF phase (solid lines) for several temperatures values indicated in the plot. The nuclear matter density is fixed at  $n = 0.1 \text{ fm}^{-3}$ .

disrupt pairing since fermions lying on different Fermi surfaces cannot overlap to form Cooper pairs, due to the lack of phase-space overlap. Finite temperature can counteract the disruptive effect of  $\delta\mu$  because it increases the “diffuseness” of the Fermi surfaces and hence the phase-space overlap between the paired fermions. This physics is illustrated in Fig. 8, where we see that the gap has a maximum as a function of temperature as a consequence of the interplay of two effects: the disruption by  $\delta\mu$  and phase-space expansion by temperature. For large enough asymmetries there exists a lower critical temperature  $T_c^*$  (Sedrakian *et al.*, 1997; Sedrakian and Lombardo, 2000) (not shown in the figure). This phenomenon has been also observed in the context of small superconducting systems (finite nuclei, in fact) and is referred as “re-entrance” (Balian *et al.*, 1998). It should be mentioned that the “anomalous” behavior of the BCS gap below the temperature which corresponds to the maximum of the gap (see Fig. 8) leads to a number of anomalies in the thermodynamic quantities, such as negative superfluid density or an anomalous jump in the specific heat, which can be a signature of a (metastable) low-temperature homogeneous phase (Sedrakian *et al.*, 2006).

We also observe in Fig. 8 that at temperatures close to the critical homogeneous imbalanced superfluids show the same dependence of the gap on the temperature; consequently, the thermodynamics in this regime is analogous to the ordinary BCS case. Computation of the free energy of the homogeneous imbalanced phase and its comparison to other phases listed in (96) shows that it is preferred in a domain of temperatures adjacent the critical temperature, where the disruptive effects are small (Stein *et al.*, 2012, 2014a).

## C. FFLO phases

Our next example is the FF phase of nuclear matter paired in the  ${}^3S_1$ - ${}^3D_1$  channel. The physics of this

phase can be understood by observing that the finite momentum  $\mathbf{Q}$  affects the spectrum of particles in a twofold manner: there is a shift in the symmetric part of the spectrum  $E_S \rightarrow E_S + (Q^2)/8m^*$  and moreover  $E_A \neq 0 = \pm(\mathbf{k} \cdot \mathbf{Q})/2m^*$ . Thus, in the FF phase there is a positive increase in the quasiparticle kinetic energy  $\propto Q^2$ , which disfavors it relative to the BCS state. However, the anisotropic term  $\propto \mathbf{k} \cdot \mathbf{Q}$  changes the phase-space overlap of the fermions and promotes pairing in certain directions. Clearly, the FF phase is stabilized when the increase in the kinetic energy loss caused by moving the condensate is overcome by the gain in the potential energy of pairing due to the increase in the phase-space overlap.

The mechanism leading to a stable FF phase significantly affects the low-temperature behavior of the imbalanced superfluid as illustrated in Fig. 8. It is seen that the FF and homogeneous solutions coincide above a certain temperature, but there is a bifurcation at low temperatures. The high-temperature segment corresponds to the BCS state, with the temperature dependence of the gap given by the standard asymptotic behavior  $\Delta(\alpha) \sim [T_c(\alpha)(T_c(\alpha) - T)]^{1/2}$  [see also Eq. (8)], where  $T_c(\alpha)$  is the (upper) critical temperature. The quenching of the BCS gap (dashed lines) discussed above is replaced in the FF phase by solutions which are self-similar to the BCS solutions with  $d\Delta(T)/dT \leq 0$  (He *et al.*, 2006). Also the anomalies in the thermodynamic quantities found in the homogeneous phase are absent in the FF state (Jin *et al.*, 2007).

Figure 9 illustrates the competition between the FF phase and the homogeneous BCS phase by showing the dependence of the gap on asymmetry for several constant temperatures. There exist two segments for each temperature: the low- $\alpha$  segment where both phases predict the same  $\alpha$  dependence, and the large- $\alpha$  segment, where the gap values for the FF phase systematically extend to larger  $\alpha$  values. The small- $\alpha$  region is characterized by linear dependence of the gap on  $\alpha$ ; the large- $\alpha$  asymptotic behavior is  $\Delta(\alpha) \sim \Delta_{00} (1 - \alpha/\alpha_c)^{1/2}$ , where  $\alpha_c$  is the critical asymmetry characteristic of a given phase.

#### D. Deformed Fermi surface phase

The deformed Fermi surface phase restores pairing correlations in imbalanced systems via deformations of the Fermi surfaces of the two fermion species away from the perfectly spherical shape (Müther and Sedrakian, 2002, 2003; Sedrakian *et al.*, 2005). The agent of these deformations could be the non-central component of the interaction which, in principle, should be already present in the unpaired state, but can be strongly magnified by the superconducting state. The deformations can be spontaneous, as conjectured in (Müther and Sedrakian, 2002, 2003; Sedrakian *et al.*, 2005), in the sense that the original Hamiltonian is O(3) symmetric, but the ground state breaks this symmetry down to a subgroup, for example

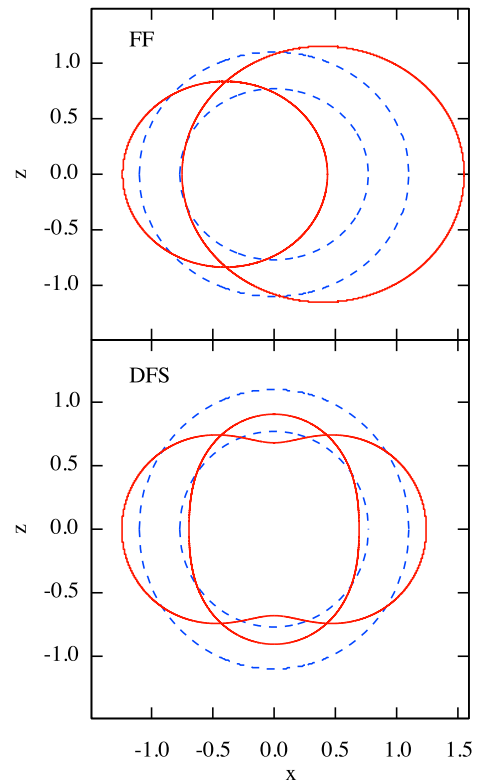


FIG. 10 Illustration of Fermi surfaces in the FF (upper panel) and DFS (lower panel) phases. The concentric (dashed) circles represent projections of spherical Fermi surfaces of neutrons and protons under imbalance in the  $x$ - $z$  plane.

to O(2). To explore whether deformations lead to improvements of the ground state energy of the system it is useful to consider spontaneous deformations which are parametrized as

$$E_r^{a,a'} = E_r^a + a' \epsilon_2 P_2(\cos \theta) \quad (97)$$

where the  $E_r^a$  are given by Eq. (89) and  $a' = \pm$ ,  $P_2(x)$  is the  $n = 2$  Legendre polynomial, and  $\theta$  the angle formed by the particle momentum and the direction of the spontaneous breaking of rotational symmetry.

The gap equation has been solved and the free energy computed for a deformation parameter defined as the relative deformation of the two Fermi surfaces  $\delta\epsilon = (\epsilon_{2,+} - \epsilon_{2,-})/2$ . This parameter is the analog of the total momentum  $\mathbf{Q}$  in the analysis of the FFLO phase. Computations for nuclear matter and cold atoms show that, in a certain domain of asymmetries, the energy is minimized for non-zero  $\delta\epsilon$ , i.e., there is a stable minimum corresponding to a state with deformed Fermi surfaces of the components.

The Fermi surfaces in the FF and DFS phases are shown in Fig. 10 along with those in imbalanced homogeneous phase. The visible intersections of Fermi surfaces of the components in the FF and DFS phases reveal the mechanisms of increased of the phase space overlap be-

FIG. 11 Illustration of the BCS-BEC transition. Left: Weakly coupled BCS state characterized by loosely bound Cooper pairs. Center: Intermediate coupling, with strongly interacting pairs. Right: Tightly bound dimers (deuterons) forming a BEC state.

tween the components and the enhancement of pairing correlations achieved in these phases.

### E. BCS-BEC crossover

Weakly coupled BCS superfluids form Cooper pairs with characteristic size of the order of the coherence length, which is much larger than the interparticle distance. The pairs are weakly bound, as the scale of binding energy set by the gap  $\Delta$  is much smaller than the Fermi energy. It was conjectured long ago that such BCS superfluids will smoothly evolve into a Bose-Einstein condensate (BEC) of tightly bound bosonic dimers, with a size which is much smaller than the interparticle distance, in what amounts to a strong-coupling limit (Eagles, 1969; Nozières and Schmitt-Rink, 1985); see Fig. 11 for an illustration. This conjecture has been confirmed in experiments on cold atomic gases, where the coupling parameter can be manipulated via tuning the magnetic field to the Feshbach resonance and thus effectively changing the magnitude of the scattering length and its sign (Regal and Jin, 2007; Zwierlein *et al.*, 2006). High-density isospin-symmetric nuclear matter forms a weakly coupled BCS condensate in the dominant  ${}^3S_1$ - ${}^3D_1$  channel. The BCS-BEC crossover in such a condensate can be achieved by diluting the system, in which case the reduction of the density of states will eventually lead to a transition to BEC state, which in this case is a condensate of deuterons (Alm *et al.*, 1993; Baldo *et al.*, 1995; Huang, 2010; Jin *et al.*, 2010; Sedrakian and Clark, 2006b; Stein *et al.*, 1995). The BCS-BEC crossover is also expected in imbalanced systems, in particular in isospin-asymmetric nuclear matter, unless the pairing is completely disrupted by the mismatch in the Fermi surfaces of protons and neutrons (Lombardo *et al.*, 2001; Mao *et al.*, 2009; Shang and Zuo, 2013; Stein *et al.*, 2012, 2014a,b; Sun and Pan, 2013). The main modification of the original Nozières-Schmitt-Rink theory (Nozières and Schmitt-Rink, 1985) involves the gaseous mixture of neutrons and deuterons in the strong-coupling low-density limit. The evidence for isospin-singlet pairing in nuclear phenomenology is scarce, but it has been conjectured that large enough nuclei may feature spin-aligned  $np$  pairs on the basis of recent experimental studies of the excited states in  ${}^{92}\text{Pd}$  (Cederwall *et al.*, 2011). Intermediate energy heavy-ion collisions produce large amounts of deuterons

in final states, which can be an asymptotic state reached once the initially formed BCS condensate in the  ${}^3S_1$ - ${}^3D_1$  channel crosses over to a BEC of deuterons (Baldo *et al.*, 1995). It has been also speculated that deuteron condensates can be formed in the dilute nuclear matter found in supernova and hot proto-neutron-star matter at sub-saturation densities, see for example (Clark *et al.*, 2016; Gulminelli and Raduta, 2015; Heckel *et al.*, 2009; Hempel and Schaffner-Bielich, 2010; Oertel *et al.*, 2012; Pais *et al.*, 2015; Raduta and Gulminelli, 2010; Sumiyoshi and Röpke, 2008; Typel *et al.*, 2010; Wu *et al.*, 2017).

The emergence of a BEC in the isospin-singlet channel at asymptotically low densities is straightforward because in the vacuum there is a bound state in this channel – the deuteron. In contrast, the BEC limit in the isotriplet  ${}^1S_0$  pairing channel is not obvious. Nevertheless the unusually large scattering length in this channel for neutron-neutron scattering,  $a_n \simeq -19$  fm, suggests traces of a BEC in neutron-rich systems such as the halo nuclei or neutron matter in compact objects (Abe and Seki, 2009; Isayev, 2008; Kanada-En'yo *et al.*, 2009; Margueron *et al.*, 2007; Matsuo, 2006; Ramanan and Urban, 2013; Salasnich, 2011; Stein *et al.*, 2016; Sun *et al.*, 2010, 2012).

#### 1. BCS-BEC transition in the balanced case

Consider first the basics of the BCS-BEC crossover in the  ${}^3S_1$ - ${}^3D_1$  pairing channel for the case of isospin symmetrical nuclear matter. The equations that are solved in this case for the densities and the gap are respectively (91) and (93) in the symmetrical limit. Results from simultaneous solution of the gap and density equations (Sedrakian and Clark, 2006b) are plotted in Fig. 12 at fixed values of the ratio  $f = n_0/n$  (we recall that  $n_0 = 0.16$  fm $^{-3}$  is the saturation density of symmetrical nuclear matter). The low- and high-temperature asymptotics of the gap function can be fitted by the BCS-like relations (8):  $\Delta(T) = \Delta(0) - [2\pi c_1 \Delta(0)T]^{1/2} \exp(-\Delta(0)/T)$  for  $T \rightarrow 0$  and  $\Delta(T) = 3.06 c_2 [T_c(T_c - T)]^{1/2}$  for  $T \rightarrow T_c$ , where  $T_c$  is the critical temperature and  $c_1, c_2$  are adjustable parameters. The values of the parameters yielding a fit,  $c_1 \simeq 0.2$  and  $c_2 \simeq 0.9$ , deviate from the predictions  $c_1 = c_2 = 1$  of BCS theory. As a consequence, the value of the ratio  $\Delta(0)/T_c$  deviates from the BCS prediction of 1.76. Clearly, the discrepancy depends on the inverse density measure  $f$  and reflects the breakdown of the weak-coupling Ansatz.

The transition from the BCS to BEC regime can be traced in terms of several characteristic quantities. One such parameter is the ratio  $\Delta(0)/|\mu|$ . Using this measure, we can now infer from Fig. 12 that the strong-coupling regime characterized by  $\Delta \gg \mu$  sets in for  $f \geq 40$ . For small values of  $f$  ( $\sim 20$ ), where  $\Delta \sim \mu$ , the system is in the transition region intermediate between BCS to BEC. A second signature of the crossover from weak to strong

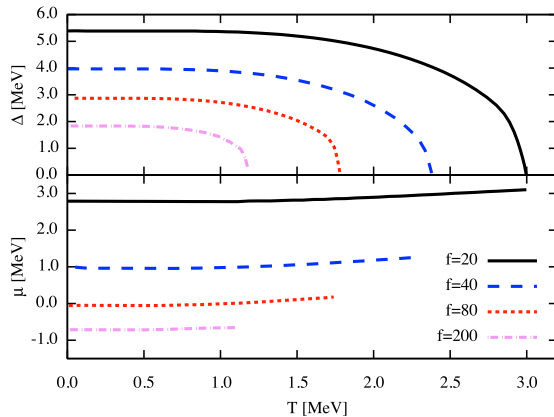


FIG. 12 Upper panel: Pairing gap  $\Delta(p_F)$  as a function of temperature  $T$  at different values of the parameter  $f = n_0/n$ , defined in the text. Lower panel: associated chemical potential  $\mu$  at the same values of  $f$ . The quoted  $f$ -values translate into the value of diluteness parameter  $na^3_{np} = 1.26, 0.63, 0.32,$  and  $0.13$ , for the neutron-proton scattering length  $a_{np} = 5.41$  fm.

coupling is the sign of the chemical potential of nucleons. Indeed, it changes sign for  $f \simeq 80$ , which is somewhat below the crossover density between weak-coupling and strong-coupling regimes deduced above. A third method, rather appealing physically, is direct comparison of the size of Cooper pairs, taking the ratio of the coherence length  $\xi$  to the interparticle distance  $d \sim n^{1/3}$ . In the BCS limit, one has by definition  $\xi \gg d$ ; conversely, in the BEC limit  $\xi \ll d$ . We use this criterion below in identifying the transition parameters.

Finally, we note that in the context of dilute atomic gases, domains of weak and strong coupling are distinguished by the parameter  $n|a|^3$ , where  $a$  is the scattering length. In nuclear matter, the strong-coupling regime was assigned to  $f \geq 40$ , which translates to  $na^3 \simeq 0.6 < 1$  if we use  $a_{np} = 5.41$  fm for the  $n$ - $p$  scattering length. Thus one may conclude that symmetrical nuclear matter is indeed in the strong coupling regime at low densities.

Another interesting feature seen in Fig. 12 is that the asymptotical value of the chemical potential  $\mu$  (i.e., at  $f \rightarrow \infty$  or  $n \rightarrow 0$ ) is  $-1.1$  MeV. This value of the chemical potential is just half the binding energy of the deuteron in free space. Formally, this result can be verified by transforming the gap equation into the eigenvalue problem, in which case it becomes a Schrödinger equation for a two-body bound state described by the anomalous correlation function, with the chemical potential as its energy eigenvalue.

We conclude that the BCS condensate of Cooper pairs in the  ${}^3S_1$ - ${}^3D_1$  state evolves into a BEC of deuterons under dilution of nuclear matter. The crossover is smooth, taking place without change of symmetry of the many-body wave function in the case of the sym-

metric nuclear matter (Alm *et al.*, 1993; Baldo *et al.*, 1995; Huang, 2010; Jin *et al.*, 2010; Sedrakian and Clark, 2006b; Stein *et al.*, 1995).

## 2. BCS-BEC transition in the imbalanced case

How does the physics of the BCS-BEC crossover change under imbalance between the populations of fermionic species that pair? As we have seen, the condition of imbalance introduces some new and unconventional phases in the BCS limit, and it is natural to ask about their counterparts (if present) in the strong-coupling limit. This problem has been addressed recently in a series of papers (Stein *et al.*, 2012, 2014a,b), in which the equations for the gap and densities [Eqs. (91) and (93)] were solved in a framework that provides for description of both the BCS phase and its low-density BEC counterpart, as well as two unconventional phases which may arise within a range of isospin asymmetries. The FF phase was chosen as a representative for phases with broken space symmetries and the collection of phases was supplemented by the heterogeneous phase in which the normal fluid and superfluid occupy separate spatial domains.

Before discussing the phase diagram containing these phases, we survey the intrinsic properties of the BCS-BEC crossover under isospin imbalance (Lombardo *et al.*, 2001; Stein *et al.*, 2012, 2014a,b). These properties include primarily the Cooper-pair wave function, the occupation probabilities of particles, the coherence length, and the quasiparticle spectra. Their quantitative study provides additional physical insight and understanding of how the system evolves from weak coupling to strong coupling under isospin asymmetry. We note that in the case of phase separation, the only non-trivial phase is the isospin symmetrical BCS phase. Therefore, its intrinsic features, apart from heterogeneity, are identical with those of the standard BCS theory and hence need not be addressed separately.

Recall that in ultracold atomic gases the imbalance is achieved by trapping different amounts of atoms in different hyperfine states, and the crossover is achieved by varying their effective interaction strength via the Feshbach mechanism. In contrast, in an extended nuclear system, a BCS-BEC crossover is induced by variation of its density and the isospin asymmetry is fixed by the minimization of the energy or the initial conditions, as e.g. in nuclear collisions. As a result, the pairing interaction strength changes, in accord with changes in the relevant energies for in-medium scattering of two nucleons set by the Fermi energy of the system. In consonance, the density of states changes. The BCS-BEC crossover in the nuclear system is therefore governed by the combination of these two effects. In contrast to ultracold atoms, it cannot be manipulated at will. To set the stage, we ex-

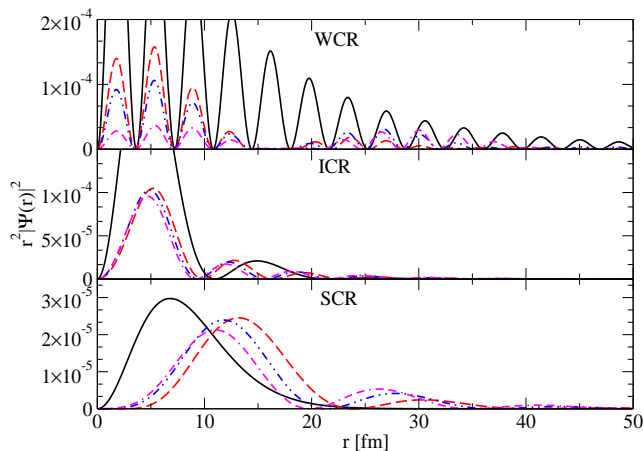


FIG. 13 Typical dependence of  $r^2|\Psi(r)|^2$  on  $r$  in the three coupling regimes, weak coupling (WCR), intermediate coupling (ICR), and strong coupling (SCR), evaluated for asymmetries  $\alpha = 0.0$  (black solid line),  $0.1$  (red dashed line),  $0.2$  (blue dashed dot-dot line),  $0.3$  (magenta dashed dot line).

tract the kernel of the gap equation,

$$K(p) \equiv \sum_{a,r} \frac{1 - 2f(E_r^a)}{4\sqrt{E_S(p)^2 + \Delta^2(p, Q)}} \quad (98)$$

[cf. Eq. (93)]. Physically,  $K(p)$  is the momentum-space wave function of the Cooper pairs, because it obeys a Schrödinger eigenvalue equation in strong coupling. In terms of its configuration-space image, we may write the wave function of a Cooper pair as

$$\Psi(r) = \sqrt{N} \int \frac{d^3p}{(2\pi)^3} [K(\mathbf{p}, \Delta) - K(\mathbf{p}, 0)] e^{i\mathbf{p}\cdot\mathbf{r}}. \quad (99)$$

Here  $N$  is a constant determined by the standard normalization of a wave function to unity, and the value  $K(\mathbf{p}, 0)$  in the normal state is subtracted to regularize the integral, which is otherwise divergent. It is useful also to define the quantities

$$\langle r^2 \rangle = \int d^3r r^2 |\Psi(r)|^2, \quad \xi_{\text{rms}} = \sqrt{\langle r^2 \rangle}, \quad (100)$$

where  $\xi_{\text{rms}}$  is the coherence length, i.e., the spatial extension of a Cooper pair. This definition can be contrasted to the weak-coupling BCS analytical formula  $\xi_a = k_F/(\pi m^* \Delta)$ . The root-mean-square definition (100) allows one to extend the notion of the coherence length into the strong-coupling regime; therefore, it can be compared to the mean interparticle distance  $d = (3/4\pi n)^{1/3}$  in the entire range of the BCS-BEC crossover.

Figure 13 shows the integrand of  $\langle r^2 \rangle$  in Eq. (100) as a function of radial distance  $r$  at densities representative for the three coupling regimes involved in the BCS-BEC crossover. At densities corresponding to the weak-coupling regime (labeled WCR,  $\log n/n_0 = -0.5$ ),

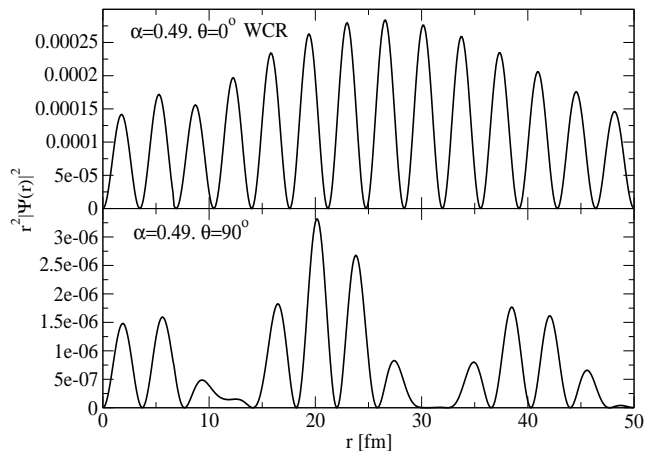


FIG. 14 Dependence of  $r^2|\Psi(r)|^2$  on  $r$  in the coupling regime WCR for  $\theta = 0^\circ$  (upper panel) and  $\theta = 90^\circ$  (lower panel) for the indicated asymmetry at which the FF phase is the ground state.

this function (as well as the wave function  $\Psi(r)$  itself, not shown) has a well-defined oscillatory form of period  $2\pi/k_F$ , which persists for multiple tens of fermis. The behavior of such a state is conforming with the long-range order inherent to BCS picture, where the spatial extension of pairs, measured by the coherence length  $\xi$ , is much greater than the interparticle distance  $d$ . For intermediate- and strong-coupling regimes (ICR and SCR,  $\log n/n_0 = -1.5$  and  $-2.5$ , respectively) the wave function becomes concentrated at the origin, possibly showing a few oscillations indicative of the transition between limiting cases. This behavior is descriptive of particles well-localized in space, a distinctive characteristic of the BEC regime.

In Fig. 14 we show the same quantity  $r^2|\Psi(r)|^2$  in the FF phase at two different angles  $\theta$ , evaluated for an asymmetry  $\alpha = 0.49$  ( $\delta\mu = 6.45$  MeV), where this phase is the ground state of the matter with  $\Delta = 1.27$  MeV and  $Q = 0.4$  fm $^{-1}$ . At  $\theta = 0$  the perfect oscillatory behavior of the BCS case is intact, with a slight modulation due to non-zero  $Q$ . At  $\theta = 90^\circ$ , the amplitude of the oscillations is modulated by a second oscillatory mode with period  $2\pi/Q \sim 20$  fm, in addition to the first mode having of period  $2\pi/k_F$ . In the FF phase and for  $\theta = 0^\circ$  the term  $\propto \cos\theta$  renders the quasiparticle spectrum and therefore the Cooper pair wave function close to the one expected from ordinary BCS state. In contrast, for  $\theta = 90^\circ$ , the term  $\propto \cos\theta$  is zero and the marked differences are seen, in particular damping of the amplitude of oscillations.

Also of central interest are the occupation numbers  $N_{n/p}(k)$  of proton and neutron states, which are identified as the integrands of Eq. (91). At zero temperature and in unpaired matter, the functions  $N_{n/p}(k)$  are discontinuous at the Fermi surface. Numerical results for balanced and imbalanced superfluids are shown in the three coupling regimes of inter-

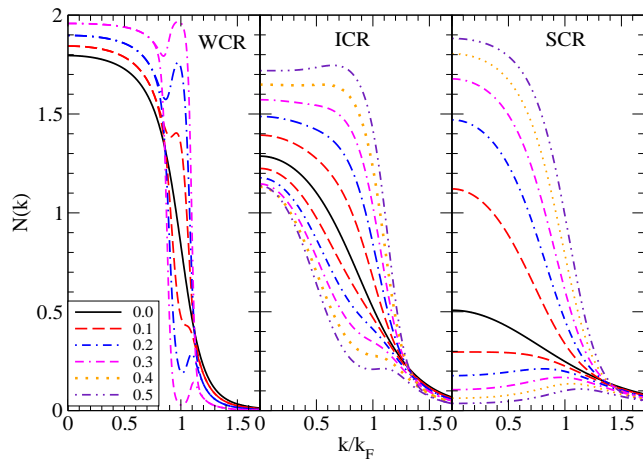


FIG. 15 Dependence of the neutron and proton occupation numbers on momentum  $k$  (in units of Fermi momentum) at densities within the three coupling regimes, for a range of asymmetries indicated in the legend.

est in Fig. 15. A key feature of this figure that is universal for imbalanced superfluids and nuclear systems is the appearance of a “breach” (Forbes *et al.*, 2005; Gubankova *et al.*, 2003; Liu and Wilczek, 2003) or “blocking region” (Lombardo *et al.*, 2001) for large asymmetries. These designations refer to the entire expulsion of the minority component (in this case the protons,  $N_p = 0$ ) from a region around the Fermi momentum of the balanced system, accompanied by maximal occupancy ( $N_n/2 = 1$ ) of the majority component (here the neutrons). Examination of  $N_{n/p}(k)$  in the FF phase for different angles shows that for small enough  $\theta$  the breach disappears and the occupation numbers resemble each other in shape. This enforces the evidence that for certain directions the effects of asymmetry are mitigated by the non-zero  $Q$ .

The ICR (middle panel) is characterized by loss of the Fermi character of the occupation numbers and vanishing of the breach. In addition, for large enough  $\alpha$ , the occupation numbers of the minority component becomes non-monotonic. In the SCR (rightmost panel) one is dealing with a BEC of strongly coupled pairs, in which the minority component is reorganized at larger asymmetries into a distribution in which the modes are populated starting from a certain nonzero value. Consequently, the Fermi sphere of the weakly coupled BCS condensate transforms into a shallow shell structure in the strongly coupled BEC.

Quasiparticle spectra are other intrinsic properties that illuminate the nature of superfluid states. In the balanced case, one finds a dispersion relation with a minimum  $E_+^+ = E_-^+ = \Delta$  for  $k = k_F$  [the spectra with lower  $\pm$  indices are degenerate, see Eq. (89)]. For non-zero asymmetries one has  $E_{\pm}^+ = E_S \pm \delta\mu$ , which induces a shift in the minima. For protons the spectrum becomes gapless: no energy is required to create excitations for

two modes (say  $k_1$  and  $k_2$ ) for which the dispersion relation intersects the zero-energy axis. This phenomenon is referred as gapless superconductivity. The momentum interval  $k_1 \leq k \leq k_2$  is in fact the interval where the “breach” in the occupation of the minority component exists.

Finally, in the SCR, the balanced limit corresponds to simply a gas of deuterons, and the dispersion relation has a minimum at the origin that corresponds to the (average) chemical potential, which in the low density limit tends to the value  $-1.1$  MeV, as discussed above. Imbalance changes the position of the average chemical potential downwards and separates the quasiparticle spectra by an amount  $\delta\mu$ . Because there is unique minimum, the dispersion relation crosses zero only once at a finite  $k$ . Upon introducing the FF phase, if one again considers different values of the angle  $\theta$ , it turns out that for  $\theta = 0^\circ$  out of four branches of quasiparticle spectra, two have a spectra closely resembling that of the ordinary BCS phase. For large  $\theta \leq 90^\circ$  dispersion relations supported by this phase are close to the imbalanced BCS case, which implies strong suppression of pairing. This behavior again points toward the key mechanism of by which the FF phase enhances pairing – the restoration of pairing correlations through an improved overlap between the Fermi surfaces of neutrons and protons in certain directions.

## F. Toward a complete phase diagram

A central problem in the physics of imbalanced many-fermion systems is the concrete realization of their phase diagram in the parameter space spanned by the density (or in cold-atom physics by the scattering length), the temperature and the degree of imbalance. While the details of the phase diagram will certainly depend on the specifics of the interactions (contact vs finite range, purely central or complicated by tensor and spin-orbit components), the generic structure of the phase diagram should be universal. It is also expected to exhibit universal features across diverse systems including cold atomic gases, nuclear systems, and dense quark matter.

Results of a detailed study of the phase diagram of the imbalanced systems presented by generally asymmetric nuclear matter, which admits the four phases listed in Eq. (96) and discussed above, were reported in a series of two papers (Stein *et al.*, 2012, 2014a). The resulting phase diagram is shown in Fig. 16. The phases are arranged in the temperature-density plane, and the phase boundaries have been computed for several values of isospin asymmetry  $\alpha$ . The generic structure of the phase diagram is as follows. (a) Above the critical temperature  $T_{c0}(n)$  for the normal-to-superfluid phase transition at  $\alpha = 0$ , the nuclear matter is in the unpaired phase. (b) At low temperatures, high densities, and moderate to large asymmetries, the FF phase forms the ground state in the triangular regions indicated in

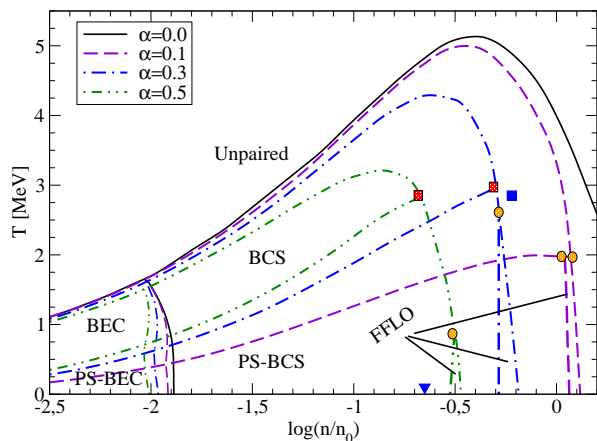


FIG. 16 Phase diagram of dilute nuclear matter in the temperature-density plane for several isospin asymmetries  $\alpha$ , where the density is normalized by the nuclear saturation density  $n_0$ . For each fixed  $\alpha$  there are two tri-critical points, the point bordering the LOFF phase being always a Lifshitz point (Hornreich, 1980). In the special case  $\alpha_4 = 0.255$ , these tri-critical points merge into a tetra-critical for  $\log(n/n_0) = -0.22$  and  $T = 2.85$  MeV (square dot). The LOFF phase completely disappears to the left of the point  $\log(n/n_0) = -0.65$  and  $T = 0$  (shown by the triangle) for  $\alpha = 0.62$ . The transition from BCS pairing to BEC, identified by the change of sign of the chemical potential  $\bar{\mu}$ , occurs on the vertical lines for  $\log(n/n_0) = -2$ .

Fig. 16. (c) Moving to stronger couplings (lower densities), one finds the domain of phase separation (PS) at sufficiently low temperatures. (d) The ordinary BCS phase with isospin asymmetry intervenes at higher temperatures. It is remarkable that the boundaries of these phases are not very sensitive to the temperature.

As seen in Fig. 16 the extreme low-density (strong coupling) limit, there are two counterparts of the weakly coupled phases: first, the BCS phase at intermediate temperatures evolves into the BEC phase of deuterons; second, the PS-BCS phase transforms into the PS-BEC phase, in which the superfluid domains contain a BEC of deuterons. These transitions are indicated in the figure by phase boundaries, although we should stress that the BCS-BEC transition and the PS-BCS to PS-BEC transition are smooth crossovers. The transition to the normal state and the phase transitions between the superfluid phases are always second order and are indicated by thin solid lines in Fig. 16. The only exception to this rule is the PS-BCS to FF phase transition, which is of first order (thick solid lines in Fig. 16). We further notice that at finite asymmetry a locus where three of the four phases meet corresponds to a tri-critical point. For each fixed  $\alpha$  there are two tri-critical points. Of these, one is a Lifshitz point, as one of the adjacent phases represents a modulated phase. We observe also that at low temperatures, the ordinary BCS-BEC crossover, which is a smooth crossover to an asymptotic state correspond-

ing to a mixture of a Bose condensate of deuterons and a gas of excess neutrons, is replaced by a new type of transition, where the fragmented superfluid contains a deuteron BEC which is surrounded by a phase containing neutron-rich unpaired nuclear matter.

### G. Spin polarized neutron matter

Another important scenario in which unconventional nuclear superfluidity arises is spin-polarized neutron matter in strong magnetic fields. Strongly magnetized neutron stars, known as magnetars, are characterized by surface fields of order  $B \sim 10^{15}$  G (Thompson and Duncan, 1995; Turolla *et al.*, 2015) and may feature fields by some factor larger in their interiors. Magnetic fields of this magnitude can suppress the pairing of neutrons and protons in the  $S$ -wave state (Sinha and Sedrakian, 2015; Stein *et al.*, 2016), but the mechanisms of suppression for charged and neutral condensates are different. The proton  $S$ -wave pairing is quenched because of the Landau diamagnetic currents of protons induced by the field; this happens once the Larmor radius of a proton in the  $B$ -field becomes of the order of the coherence length of the proton condensate. The neutron pairing is suppressed when the  $S$ -wave neutron gap becomes of the order of the Pauli-paramagnetic interaction of the neutron spin with the magnetic field. The magnitude of this interaction is  $|\tilde{\mu}_N|B$ , the neutron spin magnetic moment being given by  $\tilde{\mu}_N = g_n(m_n/m_n^*)\mu_N$ , where  $g_n = -1.91$  is the neutron  $g$  factor,  $m_n^*$  its effective mass, and  $\mu_N = e\hbar/2m_n c$  the nuclear magneton.

Thus, the physics of neutron matter in strong magnetic fields would parallel that of the  ${}^3S_1$ - ${}^3D_1$  condensate discussed in previous section, with the paramagnetic interaction playing role of the isospin asymmetry. This possibility was anticipated for the FFLO phase (Sedrakian, 2001), and the phase-separated phase of neutron matter has also been investigated (Gezerlis and Sharma, 2012). More recently, signatures of the BCS-BEC crossover in spin-polarized neutron matter and the emergence of dineutron correlations in the presence of a magnetic field have received attention (Stein *et al.*, 2016), generalizing the previous studies of this phenomenon in unmagnetized neutron matter (Abe and Seki, 2009; Isayev, 2008; Kanada-En'yo *et al.*, 2009; Margueron *et al.*, 2007; Matsuo, 2006; Salasnich, 2011; Sun *et al.*, 2010, 2012).

The critical field of unpairing of  $S$ -wave superfluidity in neutron matter is of great phenomenological interest for physics of magnetar crusts. The magnitude of the  $B$  fields in the crust and outer-core regions of magnetars cannot be determined directly from observations. One may anticipate that their interior fields are somewhat larger than the surface fields  $B \sim 10^{15}$  G based on the modeling of magnetar equilibrium figures. Some magnetar models suggest that strong toroidal  $B$ -fields are confined to the crust. Therefore, if local fields are larger than the critical field for unpairing, neutron superfluidity will

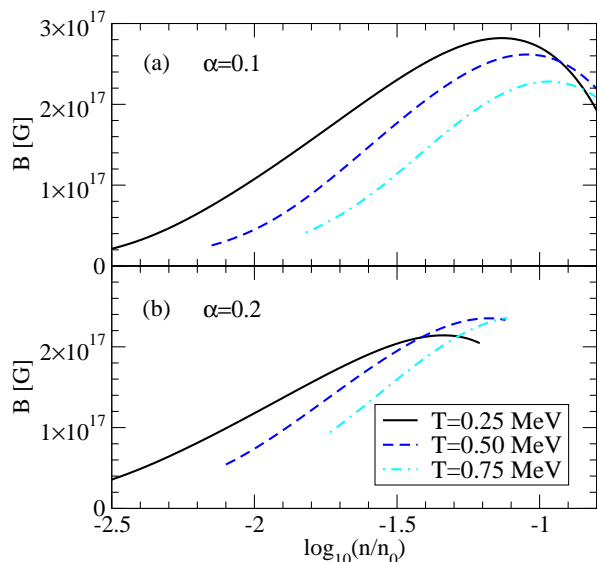


FIG. 17 Magnetic field required to create a specified spin polarization plotted as a function of density (normalized by  $n_0$ ), at two fixed values of polarization,  $\alpha = 0.1$  (panel a) and  $0.2$  (panel b), and for temperatures  $T = 0.25$  (solid line),  $0.5$  (dashed line), and  $0.75$  (dash-dotted line).

be absent. Computation of the critical field (Stein *et al.*, 2016) indicates that at a temperature  $T = 0.05$  MeV characteristic of neutron stars, it is of order  $10^{16}$  G at the base of the inner crust, i.e., at  $\log(n/n_0) = -3$ , and increases up to  $10^{17}$  G for densities one order of magnitude larger.

Thus, in contrast to the analogous case of asymmetric nuclear matter, the interest in spin-polarized neutron matter lies primarily in the dependence of pairing on the magnetic field, rather on the spin polarization *per se*. Figure 17 shows the magnitude of the field needed to generate a prescribed polarization in neutron matter; it is seen that at low densities lower magnetic fields are required. It is also to be noted that the magnetic field required to produce a specified polarization increases with decreasing temperature. The combined effect of variation of the gap and the polarization with density produces critical magnetic fields that are maximal at about  $n/n_0 = -1$ , as discussed above.

The phase diagram of neutron matter at fixed polarization is displayed in Fig. 18. It resembles the phase diagram of asymmetric nuclear matter shown in Fig. 16, but it contains only the BCS and unpaired phase. The possibility of the FFLO phase filling the low-temperature and high-density pockets formed by the critical lines for  $\alpha \neq 0$  requires further study.

Analysis of the principal intrinsic features of the spin-polarized neutron condensate – which include the Cooper-pair wave function, occupation numbers, and quasiparticle spectra – shows that their behavior runs parallel to those of asymmetrical nuclear matter, already discussed in some detail. In particular, one finds

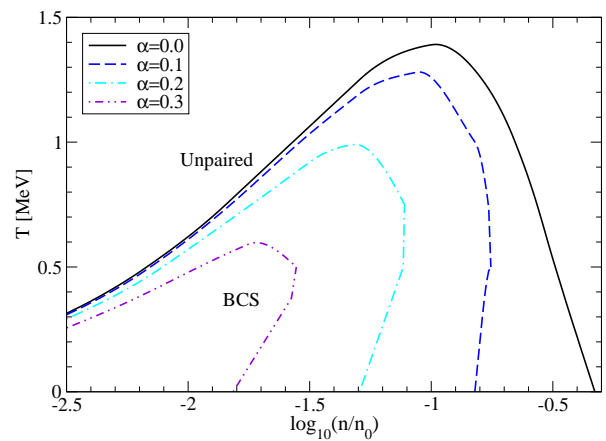


FIG. 18 Phase diagram of neutron matter in the temperature-density plane for several values of the spin polarization  $\alpha$ , showing the spin-asymmetric BCS phase and the unpaired phase at low and high temperatures respectively. Note that the phase-separation lines have double-valued character for  $\alpha \neq 0$ .

$\log_{10}(n/n_0)$	$k_{Fn}$ [fm $^{-1}$ ]	$\Delta$ [MeV]	$m^*/m$	$\mu_n$ [MeV]	$d$ [fm]	$\xi_{rms}$ [fm]
-1.0	0.78	2.46	0.967	12.94	2.46	4.87
-1.5	0.53	1.91	0.989	5.65	3.61	3.55
-2.0	0.36	1.07	0.997	2.49	5.30	2.36

TABLE I Parameters of the  $^1S_0$  condensate for  $T = 0.25$  MeV and  $\alpha = 0$  at selected values of the total particle density  $n$  (in units of  $n_0$ ). Other table entries are the Fermi momentum  $k_F = (3\pi^2 n)^{1/3}$ , pairing gap  $\Delta$ , effective mass (in units of the bare mass), chemical potential  $\mu_n$ , interparticle distance  $d$ , and coherence length  $\xi_{rms}$ .

(Stein *et al.*, 2016) that the Cooper-pair wave functions and the function  $r^2|\Psi(r)|^2$  exhibit oscillatory behavior characteristic of long-range order, the wave vector of the oscillations being  $2\pi/k_{Fn}$ , where  $k_{Fn}$  is the neutron Fermi wave number. The quasiparticle occupation numbers likewise display a breach around the Fermi momentum  $k_F$ , which is most pronounced in the high-density and low-temperature limit where the matter is highly degenerate. Furthermore, the feature of gapless superfluidity is again observed in this case: at large polarizations, the energy spectrum of the minority-spin particles crosses the zero-energy level, where modes can be excited without any energy cost.

As argued above, neutron matter exhibits the features of a BCS-BEC crossover, although at asymptotically low densities two neutrons are not bound. Evidence of this transition is clearly seen in Table I by comparing (a) the first row (high-density entry) showing  $\xi_{rms}/d > 1$  and  $\Delta/\mu \ll 1$ , which is characteristic to the BCS phase, with the third row (low-density entry), where  $\xi_{rms}/d < 1$  and

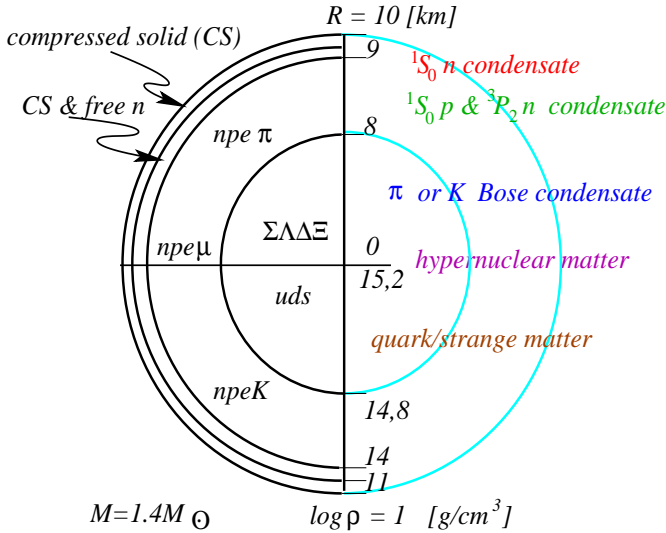


FIG. 19 Schematic interior of a  $M = 1.4M_{\odot}$  mass neutron star. Values of the radial coordinate  $r$  are indicated along the upper half of the vertical line, with values of  $\log \rho$  indicated along the lower half (density  $\rho$  is in units  $\text{gfm}^{-3}$ ). (The figure is not to scale, low- $\rho$ /large- $r$  domains being strongly expanded.) Key phases of dense matter listed, including superfluid condensates, are detailed in the text.

$\Delta/\mu \sim 1$ . The behavior at low density is interpreted as a precursor state to a (non-existent) dineutron.

## V. ASTROPHYSICAL MANIFESTATIONS OF PAIRING IN NEUTRON STARS

### A. Pairing patterns in neutron stars

So far we have concentrated on the microscopic physics of superfluidity in extended nuclear systems in a rather abstract setting, over broad ranges of density, temperature and isospin/spin asymmetry. Our next task is to adapt these considerations to the conditions prevailing in neutron stars. The matter in neutron stars is characterized by conserved charges, specifically baryon number and electrical charge. Also, at the microscopic level, the interior of a neutron star is considered to be in approximate electro-weak equilibrium. This condition, subject to charge conservation, determines the phase and composition of neutron-star matter at any given depth in the star (cf. Sec.II.C).

Figure 19 shows a schematic cross-section of the interior of a neutron star of mass  $M = 1.4M_{\odot}$ . Among the multitude of possible phases occurring at different densities, the locations of nucleonic superfluid and superconducting phases are indicated in order of increasing depth in the star, along with possible hypernuclear and quark domains in the core regime.

We now discuss briefly the key phases that exist inside a neutron star, beginning just below its surface and

moving toward the center. At densities  $\rho \simeq 10^6 \text{ g cm}^{-3}$ , neutron-star matter is fully ionized, being composed of ions of  $^{56}\text{Fe}$  and relativistic electrons. Such matter, much like that in a white dwarf but involving heavier isotopes, solidifies below a melting temperature  $T_m \sim 10^9 - 10^{10} \text{ K}$ , such that we anticipate a correlated solid phase in mature neutron stars. We note that this solid phase may have a very thin blanket (several cm in total) made up of lighter elements including H, He, etc., in ionized, atomic, or molecular form. The composition of this cover blanket can, in principle, be extracted from observations of photoemission from the surface of the star.

Under the constraints of neutrality and equilibrium, the matter becomes more neutron-rich as the depth and hence the density increases. The outer crust of the star, which spans the density range  $10^7 \leq \rho \leq 10^{11} \text{ g cm}^{-3}$ , is made up of a sequence of nuclei, their neutron fraction increasing with depth, a characteristic sequence being  $^{62}\text{Ni}$ ,  $^{86}\text{Kr}$ ,  $^{84}\text{Se}$ ,  $^{82}\text{Ge}$ ,  $^{80}\text{Zn}$ ,  $^{124}\text{Mo}$ ,  $^{122}\text{Zr}$ ,  $^{120}\text{Sr}$ , and their neutron-rich isotopes. The lattice formed by these nuclei may not be perfect and may contain nuclei with mass numbers different from those predicted for the ground state. Nucleonic superfluidity in the outer crust exists inside the individual bound finite nuclei and can be described using standard methods, such Hartree-Fock plus BCS or Hartree-Fock-Bogolyubov theories.

At a density  $\rho \simeq 4 \times 10^{11} \text{ g cm}^{-3}$ , neutrons drip out of the nuclei and start filling continuum states. Consequently a degenerate neutron gas occupies the space between the nuclear clusters. The resulting phase, which features neutron-rich nuclei immersed in an electronic background and a dilute neutron gas, occupies the inner crust of a neutron star and extends in density up to half the saturation density of symmetrical nuclear matter,  $\rho_0 = 2.8 \times 10^{14} \text{ g cm}^{-3}$ . Here one finds sequences of nuclei that are neutron-rich isotopes of Zr and Sn, which have proton numbers  $Z = 40$  and  $50$  respectively. As a rule, the mass number of the nuclei increases with density and lies in the range  $100 \leq A \leq 1500$ . Since the unbound low-energy neutrons tend to fill a Fermi sphere and their interaction in the  $^1S_0$  channel is attractive, they form a superfluid, which is the main object of applications of the theories discussed in Sec. III. The neutron condensate in the inner crust plays a fundamental role in theories of neutron-star cooling as well as in theories of their rotational dynamics.

The inner crust terminates with a first-order phase transition at the point where the clusters merge together to form a continuum. The new phase, occupying the outer core of the star, is a fluid mixture of neutrons ( $n$ ), protons ( $p$ ), and electrons ( $e$ ), along with muons ( $\mu$ ) appearing at somewhat higher densities.

As depicted in Fig. 19, the actual phase structure of matter that exists in the densest part of the core ( $\rho > 3\rho_0$ ) is uncertain. A number of conjectured phases have been explored. One possibility is hyperonization of matter, which has attracted much attention in recent years. The mechanism driving the hyperonization pro-

cess is the Pauli exclusion principle: once the Fermi energies of neutrons and electrons become of the order of the in-medium masses of  $\Sigma^{\pm,0}$ ,  $\Lambda$ , or  $\Xi^{\pm,0}$  hyperons, their formation becomes energetically more favorable with increasing density, than further increase in the Fermi energies of the neutron and electron constituents. If the hyperons experience mutual attractive interactions, they will form condensates by the same BCS mechanism that operates for non-strange baryons – a possibility that will be considered below.

Depending on the equation of state of matter, the central densities in the most massive neutron stars can lie in the range (5-10) times  $\rho_0$ , and deconfinement of hadrons into quarks becomes a plausible outcome. Deconfinement may set in after the hyperonization of matter or even before, depending on the unknown density for the deconfinement transition. We will not discuss quark color superconductivity in this review, although it may have profound implications for neutron-star phenomenology; the interested reader is referred to the reviews (Alford *et al.*, 2008; Anglani *et al.*, 2014; Rajagopal and Wilczek, 2001). Medium-modification of meson properties may also lead to their Bose-Einstein condensation and, consequently, their superfluidity. For pions, such condensation can arise through an instability of the particle-hole nucleonic excitations in the medium having pion quantum numbers. The interplay between pion condensation and nucleonic pairing has been covered extensively in the literature; see the reviews (Takatsuka and Tamagaki, 1981, 1993).

Turning to the superfluid phases within neutron stars identified in Fig. 19, we first concentrate on neutron and proton condensates at low (partial) densities (respectively in the inner crust and outer core), for which more reliable computations can be made. Keeping in mind the uncertainties involved in the many-body methods outlined in Sec. III, a good starting point is the BCS theory of pairing with renormalized single-particle energies of the constituent fermions. Quantum many-body calculation of pairing gaps can usually be simplified by adopting the decoupling approximation, i.e., by computing the single-particle energies in the normal state.

Figure 20 displays the neutron and proton pairing gaps as a function of the baryon density, for the composition shown in the same figure. The bands for neutrons are chosen to show the range of reasonable values bounded by actual computations taken from the literature (see Figure caption). Neutron  $S$ -wave superfluidity occurs at lower densities corresponding to the neutron crust. It is described essentially by the result for pure neutron matter, because at these densities the protons are confined in the nuclear clusters. It should be noted, however, that the coupling between the neutron fluid and crustal phonon modes can alter the value of the gap. The  $^1S_0$  neutron gap closes in the vicinity of crust-core interface. In the outer core, where the proton density becomes comparable to the neutron density in the inner crust, the protons also pair in the  $^1S_0$  state, with a gap of order of 1MeV,

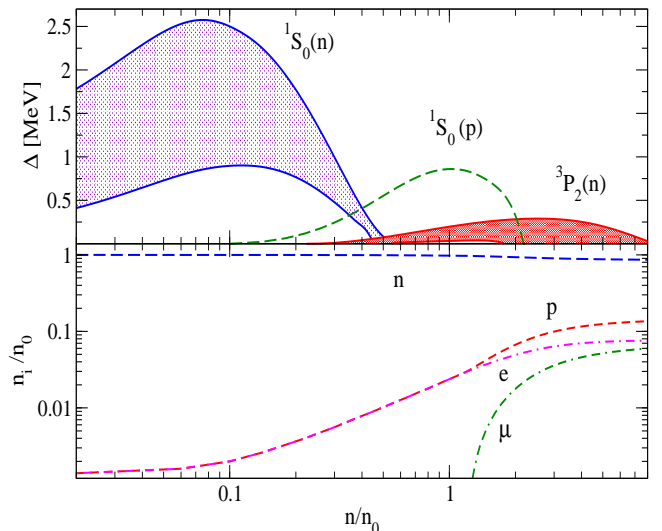


FIG. 20 Upper panel: Dependence of pairing gaps for neutrons ( $^1S_0$  and  $^3P_2$ - $^3F_2$  channels) and for protons ( $^1S_0$  channel) on baryonic density in units of nuclear saturation density. The neutron  $S$ -wave gap range is bound from above by the result of (Fan *et al.*, 2017) and from below by (Wambach *et al.*, 1993). The proton gap was computed by that of (Baldo *et al.*, 1992b). The neutron  $^3P_2$ - $^3F_2$  gap range is bound from above and below by the results of (Baldo *et al.*, 1998) and (Ding *et al.*, 2016b) respectively. Lower panel: Composition of the outer core of a neutron star at  $T = 0$ , as constructed from a relativistic density functional (Colucci and Sedrakian, 2013), which was used to map the pairing gaps to the net baryon density  $n$  of neutron star matter. The particle abundances  $n_i/n_b$  with  $i \in \{n, p, e, \mu\}$  are normalized by the net baryon density  $n_b$ , which is measured in units of the nuclear saturation density  $n_0$ .

whereas the neutrons pair with much smaller gaps of order of 100 keV. While the gap magnitude depends on the NN interaction and the underlying many-body theory, this dependence is weak in the BCS approximation. However, its dependence on the density of stellar matter could hinge strongly on the underlying model that provides the equation of state and the particle fractions. Nevertheless, the general arrangement of the pairing gaps depicted in Fig. 20, such as the transition from  $S$ - to  $P$ -wave neutron pairing around the crust-core interface, and a proton gap larger than the neutron  $P$ -wave gap in the core, is rather robust.

## B. Pairing in higher partial waves

From the preceding overview of neutron-star structure it is clear that, if present,  $^3P_2$ - $^3F_2$  pairing in neutron matter is phenomenologically important, since the neutron fluid in the core of the star occupies a large volume fraction. We now review the computations of this version of triplet pairing, as it involves a number of new aspects relative to  $^1S_0$  pairing. In this case there can be

competition between states involving various projections  $M$  of the orbital angular momentum  $L$ . Additional complications arise from spin-orbit and tensor coupling of  ${}^3P_2$  partial wave to the  ${}^3F_2$  state (Baldo *et al.*, 1992b, 1998; Khodel *et al.*, 2004, 2001a,b; Maurizio *et al.*, 2014; Papakonstantinou and Clark, 2017; Schwenk and Friman, 2004; Srinivas and Ramanan, 2016; Zverev *et al.*, 2003).

To solve the gap equation in the  $P$ -wave channel one starts with the expansion of the pairing interaction in partial waves,

$$V(\mathbf{p}, \mathbf{p}') = 4\pi \sum_L (2L+1) P_L(\hat{\mathbf{p}} \cdot \hat{\mathbf{p}}') V_L(p, p'), \quad (101)$$

where the  $P_L$  are in Legendre polynomials, and an associated expansion of the gap function

$$\Delta(\mathbf{p}) = \sum_{L,M} \sqrt{\frac{4\pi}{2l+1}} Y_{LM}(\hat{\mathbf{p}}) \Delta_{LM}(p) \quad (102)$$

in spherical harmonics  $Y_{LM}$ , where  $L$  is the orbital quantum number and  $M$  the corresponding magnetic quantum number. It is apparent that the non-linearity of the gap equation couples the various gap components of  $\Delta_{LM}(p)$ . Regarding the  $M$  dependence, this problem is simplified by performing an angle average within the denominator of the kernel of the gap equation, by focusing on real solutions and replacing  $\sqrt{\epsilon^2(\mathbf{p}) + \Delta^2(\mathbf{p})}$  by  $\sqrt{\epsilon^2(p)^2 + D^2(p)}$ , where the ‘‘angle-averaged’’ gap is given by

$$D^2(p) \equiv \int \frac{d\Omega}{4\pi} \Delta^2(\mathbf{p}) = \sum_{L,M} \frac{1}{2L+1} [\Delta_{LM}(k)]^2 \quad (103)$$

and  $\epsilon(p)$  is a single-particle energy. With this approximation the angular integrals are trivial, and we obtain a one-dimensional gap equation for the  $L$ -th component of the gap:

$$\Delta_L(p) = - \int_0^\infty \frac{dp' p'}{\pi} \frac{V_L(p, p')}{\sqrt{\epsilon(p')^2 + \sum_{L'} [\Delta_{L'}(p')]^2}} \Delta_L(p'). \quad (104)$$

In a first approximation one may neglect the terms in the sum on the right-hand side of (104) having  $L' \neq L$ , based on the common assumption that a specific pairing channel is dominant over the density concerned, an assumption that gains credence from the rule-of-thumb argument in Sec. II.B relating densities (more precisely  $k_F$  ranges) to dominant in-medium collision energies, and hence to the characteristic energy dependence of NN phase shifts in different interaction channels. However, a ‘‘specific pairing channel’’ may involve coupling of different  $L$  states through spin dependence of the interaction. In the present case there is a strong coupling to the  ${}^3F_2$  wave due to the spin-orbit and tensor components of the pairing force, which must be included to obtain quantitative results. Thus the gap equation to be solved takes the

form of coupled equations for  $P$ - and  $F$ -wave components of the gap, as in

$$\begin{pmatrix} \Delta_L \\ \Delta_{L'} \end{pmatrix} = \int_0^\infty \frac{dp' p'^2}{\pi E(p')} \begin{pmatrix} -V_{LL} & V_{LL'} \\ V_{L'L} & -V_{L'L'} \end{pmatrix} \begin{pmatrix} \Delta_L \\ \Delta_{L'} \end{pmatrix}, \quad (105)$$

where  $E(p) = \sqrt{\epsilon^2(p) + D^2(p)}$  with  $D^2(p) \equiv [\Delta_L(p)]^2 + [\Delta_{L'}(p)]^2$ . Note that this coupling is analogous to that in the  ${}^3S_1$ - ${}^3D_1$  channel discussed in Sections II.B and III.B.

Quantitative understanding of  $P$ -wave pairing, or more precisely  ${}^3P_2$ - ${}^3F_2$  pairing, is further complicated by the presence of three-body forces, which play an increasingly important role at the high baryon densities of the outer-core region of a neutron star. (At the lower densities where  ${}^1S_0$  neutron pairing dominates, the three-body force can be safely neglected.) In the case of phase-shift equivalent NN potentials, the models of the 3N force in use have been constrained by the physics of light nuclei, as is the case for the Urbana IX (UIX) 3N interaction (Pudliner *et al.*, 1997). This model has been used in conjunction with the Argonne  $v_{18}$  (AV18) NN interaction to estimate the  ${}^3P_2$ - ${}^3F_2$  pairing gap (Zuo *et al.*, 2008). However, a readjustment of the parameters of UIX interaction, rendering it less repulsive, was required to guarantee agreement with the empirical nuclear-matter saturation properties within Brueckner-Hartree-Fock theory, which in turn was used to obtain the single-particle spectrum entering the gap equation (Zhou *et al.*, 2004). Within this scheme, the triplet gap was found to be slightly reduced from the result for AV18 alone, to a maximum value of the order 0.5 MeV. (We note that upon neglecting the single-particle renormalization, the assumed 3N interaction causes an enhancement of the gap.) The Bonn-B meson-exchange phase-shift equivalent potential including the two- and three-body terms has also been used to estimate the effect of 3N interactions on  ${}^3P_2$ - ${}^3F_2$  pairing (Dong *et al.*, 2013). The maximum of the gap in this study is about 0.6 MeV, but is attained at slightly higher densities (higher neutron  $k_F$  values). Importantly, the authors also considered the effects of wave-function ( $Z$ -factor) renormalization and found a suppression of the gap by an order of magnitude.

The  ${}^3P_2$ - ${}^3F_2$  gap in neutron matter has also been studied for chiral 2N and 3N interactions (Maurizio *et al.*, 2014). Assuming a free single-particle energy spectrum, the 3N force was found to produce an enhancement in third order of the chiral expansion. Introduction of the single-particle renormalization again leads to a moderate suppression of the gap, to a maximal value of order 0.4 MeV. In another recent exploratory study of the effects of a 3N interaction (Papakonstantinou and Clark, 2017), strong sensitivity of the  ${}^3P_2$  gap to the choice of the interactions and the mandatory consistency between the 2N and 3N forces was demonstrated. In summary, these and other similar computational efforts have shown the importance of including 3N interactions for accurate de-

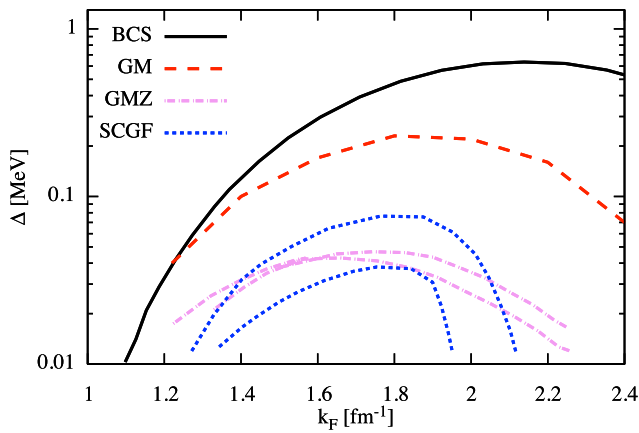


FIG. 21 Dependence of the  ${}^3P_2$ - ${}^3F_2$  pairing gap neutron matter on the Fermi momentum in various many-body theories: “BCS” corresponds to the solution of the BCS gap equation with free single particle spectrum; “GM” is based on solutions of the gap equation with self-energies derived from  $G$ -matrix (Baldo *et al.*, 1998); “GMZ” uses the same theories as GM, but accounts for wave-function renormalization of quasi-particle spectrum (lower maximum curve) plus three-body foci (higher maximum curve) (Dong *et al.*, 2013); “SCGF” correspond to self-consistent GF computations including only short-range correlations (higher-maximum curve) and both short- and long-range correlations (lower maximum curve) (Ding *et al.*, 2016a); The results “BCS”, “GM” and “SCGF” were obtained with the Argonne  $V_{18}$  potential, the “GMZ” - using Bonn-B potential.

termination of the pairing gaps in the spin-triplet channels. Consistent extrapolations of the NN and 3N interactions from nuclear saturation to higher densities, such that these forces are properly constrained by empirical data, will be required, along with microscopic many-body theories that are reliable at high density.

This brings us to remaining aspect of the problem of spin-triplet pairing in high density matter that demands further attention, namely the influence correlations that are not included in BCS theory. Long-range correlations have been found to induce a strong suppression of the gap when non-central Landau interactions are used in conjunction with the weak-coupling formula (Schwenk and Friman, 2004). A more recent computation (Ding *et al.*, 2016a) indicates that the suppression of pairing by short-range correlations is counteracted by enhancement due to long-range correlation, i.e., these two factors tend to compensate each other.

At high densities, isospin-symmetrical nuclear matter should pair in the  ${}^3D_2$  channel, by forming isospin-singlet pairs, the attractive interaction in this channel being stronger than that in the  ${}^3P_2$  channel, as seen in Fig. 1. In much in the same way as one expects a transition from  ${}^3S_1$ - ${}^3D_1$  pairing to  ${}^1S_0$  pairing with rising density, nuclear matter at still higher densities should undergo a transition from  ${}^3D_2$  pairing to  ${}^3P_2$ - ${}^3F_2$  pairing as isospin

asymmetry increases from zero to larger values. However, computations show that already a small imbalance destroys the  $D$ -wave pairing in nuclear matter (Alm *et al.*, 1996), so it can be realized only in nearly symmetrical nuclear matter.

### C. Hyperonic pairing

The inner core of a neutron star may contain a hyperonic component, because the rise of neutron and electron energies with density can be compensated by the onset of lower-energy hyperons. Just as was the case with protons, a relatively low fraction of hyperons implies that they will pair in the  ${}^1S_0$  channel if there is a sufficiently attractive component available in their interaction at low energies (Balberg and Barnea, 1998; Raduta *et al.*, 2017; Takatsuka *et al.*, 2001; Takatsuka *et al.*, 2002, 2006; Vidaña and Tolós, 2004; Wang and Shen, 2010; Xu *et al.*, 2014).

We can exclude from the outset the possibility of hyperon-nucleon pairing and pairing between non-identical hyperons, due to the imbalance between the chemical potentials of baryon components of the core [however, see (Zhou *et al.*, 2005)]. In contrast to the purely nucleonic case considered in Sec. IV, additional imbalance will arise because of the substantial disparity in the masses of different hyperons as well the large difference between the masses of nucleons and hyperons. It cannot be ruled out that the Fermi surfaces of non-identical particles may, for some density, be close enough to support cross-species pairing, but this can only occur in a rather limited density range and depends significantly on the underlying model of composition of matter.

Before discussing the pairing gaps in hypernuclear matter, we need to address the ambient composition and the single-particle energies of hyperons. The complication here is that the non-relativistic theories we have thus far considered fail to account for the measured two-solar mass pulsars (Balberg and Gal, 1997; Baldo *et al.*, 2000; Burgio *et al.*, 2011). The relativistic covariant density-functional (hereafter DF) theory allows for modeling of the properties of hypernuclear matter consistent with the astrophysical constraint on masses of hypernuclear compact stars, as well as with laboratory constraints on the depths of potentials in (hyper)nuclear matter, see e.g. (Colucci and Sedrakian, 2013; Fortin *et al.*, 2016; Marques *et al.*, 2017; Miyatsu *et al.*, 2013; Oertel *et al.*, 2015; Van Dalen *et al.*, 2014). Adopting relativistic DFs, the single-particle energies of hyperons (collectively denoted  $Y$  below) are expressed as

$$E^Y(k) = \sqrt{k^2 + m_Y^{*2}} + g_{\omega Y}\omega + g_{\phi Y}\phi + g_{\rho Y}\tau_{3Y}\rho + \Sigma_R, \quad (106)$$

where  $\Sigma_R$  represents the rearrangement term entering the models with density-dependent couplings,  $\mu_Y = E^Y(k_F)$  stands for the chemical potential, and  $m_Y^* = m_Y - g_{\sigma Y}\sigma - g_{\sigma^* Y}\sigma^*$  is the Dirac effective mass of species  $Y$ . Here  $\sigma$ ,

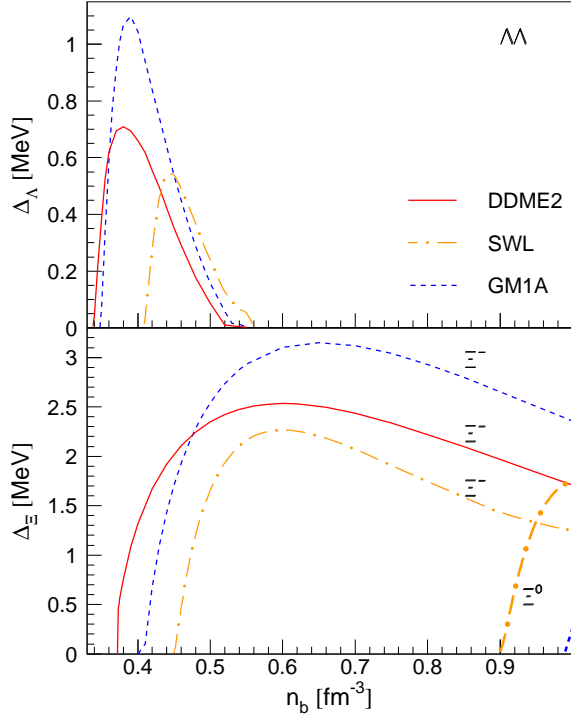


FIG. 22 Dependence of  $^1S_0$  pairing gaps in hyperonic matter on baryonic number density for medium-dependent single-particle energies and composition computed according to DDME2 (solid), NL3 (dashed), GM1A (dash-dotted), and SWL (long-dashed) models. The upper panel refers to the  $\Lambda$  gaps; the lower panel to the  $\Xi^-$  (thin lines) and  $\Xi^0$  (thick lines) gaps. For DDME2 and GM1A functionals,  $\Xi^0$  hyperons do not appear in the density range shown in the figure.

$\sigma^*$ ,  $\rho$ ,  $\omega$  and  $\phi$  refer to the mesonic fields, while the  $g_{\alpha Y}$  with  $\alpha \in (\sigma, \sigma^*, \rho, \omega)$  are the hyperon-meson couplings.

A method for computing the pairing gaps in relativistic DF theories that has been validated in studies of finite nuclei within relativistic Hartree-Fock-Bogolyubov theory (Long *et al.*, 2010) is based on solution of the non-relativistic BCS equation for a given two-nucleon potential (Kucharek and Ring, 1991) using single-particle energies and particle composition computed by the relativistic DF method. While there is a clear inconsistency in treating the unpaired matter and pairing correlations in different theories, this approach is close in the spirit to the decoupling approximation widely applied in the non-relativistic theories discussed previously. In the BCS approximation, it becomes straightforward to solve the gap equation for the pairing of a given type of hyperons. This gap equation can be written as

$$\Delta_Y(k) = -\frac{1}{4\pi^2} \int dk' k'^2 \frac{V_{YY}(k, k') \Delta_Y(k')}{\sqrt{[E^Y(k') - \mu_Y]^2 + \Delta_Y^2(k')}}}, \quad (107)$$

where  $E^Y(k)$  is the single-particle energy of hyperon  $Y$  given by Eq. (106). The pairing interaction, in the BCS

approximation, is given by the interaction in the  $^1S_0$  channel,

$$V_{YY}(k, k') = 4\pi \int dr r^2 j_0(kr) V_{YY}(r) j_0(k'r), \quad (108)$$

where  $j_0(kr) = \sin(kr)/(kr)$  is the spherical Bessel function of order zero and  $V_{YY}(r)$  is the  $YY$  interaction in coordinate space.

Recently, hypernuclear pairing in compact stars was addressed in the context of their cooling (Raduta *et al.*, 2017) using the strategy outlined above. For the  $\Lambda\Lambda$  pairing interaction, the configuration space parameterization of the ESC00 potential (Rijken, 2001) proposed by (Filikhin and Gal, 2002) was adopted. For the  $\Xi^-\Xi^-$  and  $\Xi^0\Xi^0$  interactions, a model presented in (Garcilazo *et al.*, 2016) was selected, specifically the one that corresponds to the Nijmegen Extended Soft Core potential ESC08c (Rijken *et al.*, 2013). These potentials were chosen to maximize the attraction in the respective channels, in order to obtain an upper bound on the pairing gap within BCS theory.

Figure 22 shows the dependence of the pairing gaps for  $\Lambda$  and  $\Xi^{-,0}$  hyperons on the baryon density (Raduta *et al.*, 2017). Because this involves input for the composition of matter and the self-energy effects, the results depend on the chosen DFs, which are labeled as DDME2 (Fortin *et al.*, 2016), NL3 (Miyatsu *et al.*, 2013), GM1A (Gusakov *et al.*, 2014), and SWL (Spinella, 2017). It is interesting that the  $\Lambda$  pairing is restricted to densities  $n_b \leq 0.55 \text{ fm}^{-3}$ ; therefore at higher densities there may exist regions of unpaired  $\Lambda$  matter in the most massive stars. The  $\Xi^-$  hyperons remain paired up to the highest densities considered.

#### D. Overview of neutrino radiation from compact stars

Theoretical modeling of the thermal evolution (cooling) of neutron stars tests neutron-star interior composition predicted by the microscopic theories of dense matter. Such models are confronted with observations of the X-ray emission from the surfaces of nearby neutron stars. The cooling evolution is roughly divided into three stages. (a) There is an initial transient stage during which the core temperature drops to about 0.1 MeV (1 MeV =  $1.16 \times 10^{10}$  K); the subsequent thermal history of the star does not depend on this initial stage. (b) The neutrino cooling era lasts for  $t \leq 10^5$  yr, the main cooling mechanism being neutrino radiation from the stellar interior. This phase controls theoretical predictions of the surface temperatures of the observed thermally emitting stars. The importance of studies of the thermal history of neutron stars lies in its strong dependence of the neutrino emission rates from dense matter during the neutrino cooling era. The rates in turn depend crucially on the particle content and superfluidity of the interior components. (c) The photon cooling era  $t \geq 10^5$  is dominated by radiation of photons from the surface of

the star and heating due to dissipation of rotational and magnetic energy.

In this subsection we briefly review the main processes responsible for neutrino radiation. In particular, we will focus on the effects of superfluidity on these processes to set the stage for a more detailed discussion of microscopic calculations of neutrino emission rates from superfluid matter in the next section.

The various processes or reactions generating neutrinos can be classified according to the number of fermions involved. The rationale of this classification is that each fermion participating in such a reaction introduces a factor  $T/\epsilon_F$ , which is a small parameter when the temperature is much less than the Fermi energy involved. Thus, the processes of leading order in powers of  $T/\epsilon_F$  are given by

$$n \rightarrow p + e + \bar{\nu}, \quad p + e \rightarrow n + \nu, \quad (109)$$

$$N \rightarrow N + \nu + \bar{\nu} \quad (\text{forbidden}), \quad (110)$$

where  $N \in (n, p)$  refers to a nucleon,  $\nu$  and  $\bar{\nu}$  to neutrino and antineutrino. In dealing with the quasiparticle states of nucleons having infinite lifetime, the rates of these reactions are constrained kinematically. The second process (110), known as neutral-current neutrino pair bremsstrahlung, is forbidden by energy/momentum conservation. The Urca reaction (109) is kinematically allowed in matter under  $\beta$ -equilibrium if the proton fraction  $Y_p \geq 11 - 14\%$  (Boguta, 1981; Lattimer *et al.*, 1991). The processes having two baryons in the initial (and final) states obtained from (109) and (110) by adding a nucleon, i.e.,

$$N + n \rightarrow N + p + e + \bar{\nu}, \quad (111)$$

$$N + N' \rightarrow N + N' + \nu + \bar{\nu}, \quad (112)$$

are allowed kinematically but are suppressed by an extra factor  $(T/\epsilon_F)^2$  (Shapiro and Teukolsky, 1983). Estimates of emissivity (power of energy radiated per unit volume) for the processes above are  $\epsilon_{\text{Urca}} \sim 10^{27} \times T_9^6$  for the reaction (109),  $\epsilon_{\text{modUrca}} \sim 10^{21} \times T_9^8$  for the reaction (111) and its inverse, and  $\epsilon_{\nu\bar{\nu}} \sim 10^{19} \times T_9^8$  for reaction (112). Here  $T_9$  is the temperature in units  $10^9$  K. In addition to these nucleonic processes, bremsstrahlung by electrons scattering off nuclei and impurities in the crust contributes to the neutrino radiation; we will not discuss these mechanisms as they are independent of the baryonic superfluidity.

Hyperon-rich matter will emit neutrinos via the hyper-

onic Urca processes (Prakash *et al.*, 1992)

$$\Lambda \rightarrow p + l + \bar{\nu}_l, \quad (113)$$

$$\Sigma^- \rightarrow \begin{pmatrix} n \\ \Lambda \\ \Sigma^0 \end{pmatrix} + l + \bar{\nu}_l, \quad (114)$$

$$\Xi^- \rightarrow \begin{pmatrix} \Lambda \\ \Xi^0 \\ \Sigma^0 \end{pmatrix} + l + \bar{\nu}_l, \quad (115)$$

$$\Xi^0 \rightarrow \Sigma^+ + l + \bar{\nu}_l, \quad (116)$$

where  $l$  stands for a lepton, either electron or muon, and  $\bar{\nu}_l$  is the associated antineutrino. The hyperonic Urca thresholds are much lower than those for nucleons. Once the relative abundances of hyperons exceed a few percent, the hyperonic Urca processes are kinematically allowed. Consequently, the reactions (113)-(116) will operate provided the relevant species of hyperons are present in matter. Since the hyperon abundances increase rapidly once they become energetically favorable, the corresponding threshold densities practically coincide with the onset densities for hyperons.

For completeness we point out here that pion or kaon BECs will radiate via the reactions

$$N + \langle \pi^- \rangle \rightarrow N + e^- + \bar{\nu}_e, \quad (117)$$

$$N + \langle K^- \rangle \rightarrow N + e^- + \bar{\nu}_e, \quad (118)$$

where  $\langle \pi^- \rangle$  and  $\langle K^- \rangle$  refer to the pion and kaon coherent states. The corresponding emissivities are large compared to those of the baryonic processes above, but the Bose-Einstein condensation of pions and kaons is not guaranteed to occur in neutron stars; their discussion is beyond the scope of this review. Finally, once deconfinement takes place, the quark cores of neutron stars will radiate neutrinos predominantly through the quark counterparts of the Urca process (109) (Alford *et al.*, 2008; Anglani *et al.*, 2014; Rajagopal and Wilczek, 2001).

Neutrino radiation is suppressed once superfluid phases are formed in neutron stars, exponentially at asymptotically low temperature by a Boltzmann factor  $\exp[-\Delta_{\text{max}}(0)/T]$  for processes of the Urca type (109), where  $\Delta_{\text{max}}(0)$  is the largest of the gaps of nucleons. A more detailed discussion of this suppression will be given below in Sec. V.G. Similarly, the processes (111) and (112) are suppressed at low temperatures by factors  $\exp\{-[\Delta_N(0) + \Delta_{N'}(0)]/T\}$ , where  $N$  and  $N'$  label the pair of initial (or final) baryons.

Somewhat counterintuitively, superfluidity opens a new channel of neutrino emission, which is due to the process of neutrino-pair bremsstrahlung via the neutral-current Cooper pair-breaking and formation (PBF) process:

$$\{NN\} \rightarrow N + N + \nu + \bar{\nu}, \quad N + N \rightarrow \{NN\} + \nu + \bar{\nu}, \quad (119)$$

where  $\{NN\}$  stand for a nucleonic Cooper pair. The neutrino emission by these two reactions was computed initially neglecting vertex corrections (Flowers *et al.*, 1976; Kaminker *et al.*, 1999; Voskresensky and Senatorov, 1987), which was later revised in a series of works (Kolomeitsev and Voskresensky, 2008, 2010; Leinson and Pérez, 2006; Sedrakian *et al.*, 2007; Steiner and Reddy, 2009).

The first reaction in (119) can be viewed as a breakup of nucleonic Cooper pairs that is accompanied by neutrino-pair emission. The second reaction involves recombination of nucleonic excitations into a Cooper pair. Although at low temperatures the PBF processes are again suppressed exponentially, they are very effective in cooling neutron stars at temperatures not far below the critical temperature  $T_c$  of a relevant nucleonic condensate. These processes are operative also in hyperonic condensates, as discussed below.

### E. Pair-breaking and formation processes

We now turn to a more detailed description of the PBF processes introduced in the previous section. The initial calculations, which did not include vertex corrections, led to the conclusion that the neutrino emission via neutral vector currents is large compared to that via axial vector currents (Flowers *et al.*, 1976; Kaminker *et al.*, 1999; Voskresensky and Senatorov, 1987). More recent work has shown that the vertex corrections substantially suppress the emission via vector currents while they leave the axial vector emission unaffected (Kolomeitsev and Voskresensky, 2008, 2010; Leinson and Pérez, 2006; Sedrakian *et al.*, 2007; Steiner and Reddy, 2009). Accordingly, the axial vector current emission is the dominant one.

The low-energy neutral weak-current interaction Lagrangian describing the interaction of the neutrino field  $\psi$  and baryonic current  $j_\mu$  is given by

$$\mathcal{L}_W = -\frac{G_F}{2\sqrt{2}} j_\mu \bar{\psi} \gamma^\mu (1 - \gamma^5) \psi, \quad (120)$$

where  $G_F$  is the Fermi coupling constant. The baryon current for each  $B$ -baryon is

$$j_\mu = \bar{\psi}_B \gamma_\mu (c_V^{(B)} - c_A^{(B)} \gamma^5) \psi_B, \quad (121)$$

where  $\psi_B$  is the quantum field of the baryon and  $c_V^{(B)}$  and  $c_A^{(B)}$  are its vector and axial vector couplings, respectively.

The rate at which neutrinos are radiated from matter (the neutrino emissivity) can be obtained either by using the optical theorem in finite-temperature field theory (Voskresensky and Senatorov, 1987) or directly from the kinetic equation for neutrinos formulated in terms of real-time propagators (Sedrakian and Dieperink, 2000). Both methods lead to the following expression for the

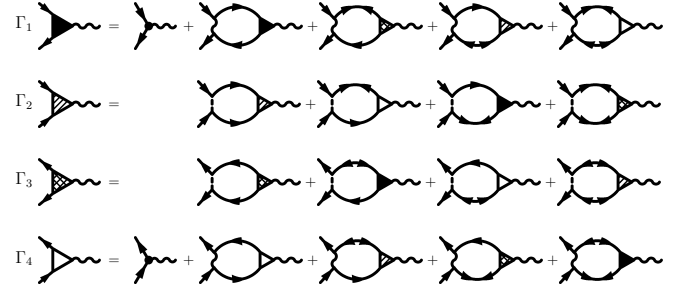


FIG. 23 Coupled integral equations for the three-point weak vertices in a superfluid. The “normal” propagators for particles (holes) are shown as single-arrowed lines directed from left to right (right to left). The double arrowed lines correspond to the “anomalous” propagators  $F$  (two incoming arrows) and  $F^+$  (two outgoing arrows). The “normal” vertices  $\Gamma_1$  and  $\Gamma_4$  are shown as full and empty triangles. The “anomalous” vertices  $\Gamma_2$  and  $\Gamma_3$  are shown as hatched and shaded triangles. Horizontal wavy lines represent the low-energy propagator of the  $Z^0$  gauge boson. Vertical dashed lines stand for the particle-particle interaction  $v_{pp}$ ; wavy lines, the particle-hole interaction  $v_{ph}$ .

neutral-current neutrino pair bremsstrahlung emissivity

$$\begin{aligned} \varepsilon_{\nu\bar{\nu}} = & -2 \left( \frac{G_F}{2\sqrt{2}} \right)^2 \int d^4q g(\omega) \omega \sum_{i=1,2} \int \frac{d^3q_i}{(2\pi)^3 2\omega_i} \\ & \times \Im [L^{\mu\lambda}(q_i) \Pi_{\mu\lambda}(q)] \delta^{(4)}(q - \sum_i q_i), \quad (122) \end{aligned}$$

where  $q_i = (\omega_i, \mathbf{q}_i)$ , with  $i = 1, 2$ , are the neutrino momenta,  $g(\omega) = [\exp(\omega/T) - 1]^{-1}$  is the Bose distribution function,  $\Pi_{\mu\lambda}(q)$  is the retarded polarization tensor of baryons, and

$$\begin{aligned} L^{\mu\nu}(q_1, q_2) = & 4 \left[ q_1^\mu q_2^\nu + q_2^\mu q_1^\nu - (q_1 \cdot q_2) g^{\mu\nu} \right. \\ & \left. - i \epsilon^{\alpha\beta\mu\nu} q_{1\alpha} q_{2\beta} \right] \quad (123) \end{aligned}$$

is the leptonic trace. Here the emissivity is defined per neutrino flavor, i.e., the full rate of neutrino radiation through weak neutral currents is larger by a factor  $N_f$ , the number of neutrino flavors. We will assume  $N_f = 3$  massless neutrino flavors.

The central quantity in (122) is the polarization tensor  $\Pi_{\mu\lambda}(q)$ , which describes the response of the superfluid to electroweak vector and axial currents. A microscopic approach for calculating the response function (or polarization tensor) in superfluid matter was first developed by Abrikosov and Gor'kov in the context of the electrodynamics of superconductors (Abrikosov *et al.*, 1963). In this theory the response of superconductors to external probes is expressed in the language of propagators at non-zero temperature and density, with contact interactions that do not distinguish among the particle-hole and particle-particle channels. It is equivalent to the theories initially advanced for metallic superconductors (Anderson, 1958), which are based on equations of

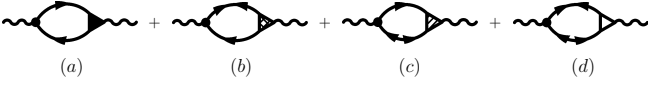


FIG. 24 The sum of polarization tensors contributing to the vector-current neutrino emission rate. Note that diagrams *b*, *c*, and *d* are specific to superfluid systems and vanish in the unpaired state.

motion for second-quantized operators. A more general approach was subsequently developed within the Fermi-liquid theory for superconductors and superfluids (Larkin and Migdal, 1964; Leggett, 1966). The latter method implements wave-function renormalization of the quasiparticle spectrum and higher-order harmonics in the interaction channels, and postulates particle-hole (ph) and particle-particle (pp) interactions having different strengths and/or signs.

Computation of the polarization tensor proceeds in three steps. In the first step, one solves the coupled integral equation for the three-point vertices in the superfluid matter (shown in Fig. 23). Next, the four polarization tensors shown in Fig. 24 are resummed to obtain the full response function. Finally, this function is expanded, to first non-vanishing order, in the small parameter  $v_F/c \ll 1$ , where  $v_F$  is the Fermi velocity of nucleons and  $c$  is the speed of light. In the case of vector-current response, a non-zero contribution is obtained at order  $v_F^4$ , whereas in the case of axial vector coupling, one finds a non-zero contribution at order  $v_F^2$  (here and below we again set  $c = 1$ ). Next, the phase-space integrals in the emissivity (122) are computed after contracting the polarization tensor with the trace over leptonic currents. The final result for three neutrino flavors ( $N_f = 3$ ) can be cast in the form (Kolomeitsev and Voskresensky, 2008; Leinson and Pérez, 2006)

$$\epsilon_{\nu\bar{\nu}}^V = \frac{16G^2 c_V^2 \nu(0) v_F^4}{1215\pi^3} I^V(z) T^7, \quad (124)$$

where  $z = \Delta/T$  and

$$I^V(z) = z^7 \int_1^\infty \frac{dy y^5}{\sqrt{y^2 - 1}} f(zy)^2 [1 + \beta(y) v_F^2], \quad (125)$$

with  $c_V = 1$  for neutrons and  $c_V = 0.08$  for protons,  $\nu(0) = m^* p_F / \pi^2$  is the density of states at the Fermi surface in terms of effective mass  $m^*$  at Fermi momentum  $p_F$ ,  $f(x)$  is the Fermi distribution function. The explicit form of the function  $\beta(y)$  specifying the next-to-lead term in the expansion has been computed elsewhere (Sedrakian, 2012). The order  $v_F^4$  result has been obtained by a number of authors within comparable theoretical frameworks (Kolomeitsev and Voskresensky, 2008; Leinson and Pérez, 2006; Sedrakian, 2012; Steiner and Reddy, 2009). A computation of the vector-current emissivity to order  $v_F^6$  shows that the



FIG. 25 The two diagrams contributing to the axial response of baryonic matter. Conventions are the same as in Fig. 23.

corrections to the leading non-zero term are below 10% for values of  $v_F \leq 0.4$  characteristic of baryons in compact stars (Sedrakian, 2012). This result provides evidence of the convergence of the series expansion of the vector-current polarization tensor in the regime where the momentum transfer is small compared to other relevant scales.

Turning to the axial-vector contribution, we note that the corresponding polarization tensor is unaffected by the vertex corrections; hence it is given by the two diagrams drawn in Fig. 25. The emissivity of this processes is given by (Kolomeitsev and Voskresensky, 2008)

$$\epsilon_{\nu\bar{\nu}}^A = \frac{4G_F^2 g_A^2}{15\pi^3} \zeta_A \nu(0) v_F^2 T^7 I^A, \quad (126)$$

$$I^A = z^7 \int_1^\infty dy \frac{y^5}{\sqrt{y^2 - 1}} f^2(zy) [1 + O(v_F^4)] \quad (127)$$

with  $\zeta_A = 6/7$  and  $g_A \simeq 1.26$ . Note the  $v_F^2$  scaling of the axial neutrino emissivity compared to the  $v_F^4$  scaling found for  $\epsilon_{\nu\bar{\nu}}^V$  in (124). We see that the axial neutrino emissivity dominates the vector current emissivity due to this disparate  $v_F$ -power scaling, other factors being of the same order of magnitude. The temperature dependence of the pair-breaking processes can be understood from dimensional analysis. First, we observe that the initial- and final-state neutrons, being confined to a narrow band  $\sim T$  around the Fermi surface, each contribute a factor  $T$ , while the final-state neutrino and antineutrino contribute each give a factor  $T^3$ . Energy and momentum conservation provide an additional factor  $T^{-2}$ , which is reduced by a factor  $T$  due to the fact that one computes the energy production rate.

The rate as given by Eqs. (126) and (127) is applicable for the  $^1S_0$  neutron condensate in the neutron-star crust and the proton condensate in the core of the star. A calculation similar to that described above can be carried out for the  $^3P_2$ - $^3F_2$  condensate (Leinson, 2013; Yakovlev *et al.*, 1999). The main difference from the  $S$ -wave case is that the leading-order contribution arises already at first order ( $\propto 1$ ) in the small- $v_F$  expansions, with other factors and temperature dependence being the same.

The hyperonic  $S$ -wave condensates introduced above will also contribute to the neutrino radiation through pair-breaking processes, in full analogy to their nucleonic counterparts. These processes were initially considered without vertex corrections (Jaikumar and Prakash, 2001; Yakovlev *et al.*, 1999) and revised later to account for them in (Raduta *et al.*, 2017). Inclusion of vertex corrections implies that the contribution from vector-current

coupling is negligible for  $S$ -wave paired hyperons, compared to that from axial-vector coupling. By the same argument as made for nucleons, the former contribution scales as  $v_{YF}^4$ , where  $v_{YF}$  is the Fermi velocity of a given hyperon, whereas the latter scales as  $v_{YF}^2$ . This last contribution is given, in analogy with the nucleon case, by Eqs. (126) and (127), but with nucleonic quantities replaced by their hyperonic analogs (Raduta *et al.*, 2017; Savage and Walden, 1997).

## F. Collective modes

The set of polarization tensors shown in Fig. 24 also determines the collective modes of the fermionic superfluid. Indeed the vector and axial-vector responses are associated in the non-relativistic limit with the vertices

$$\Gamma_0^{D\mu} = (1, \mathbf{v}_F), \quad \Gamma_0^{S\mu} = (\boldsymbol{\sigma} \mathbf{v}_F, \boldsymbol{\sigma}), \quad (128)$$

which are the same as for the density and density-current (index  $D$ ) and the spin-current and spin-density perturbations (index  $S$ ). By definition the dispersion relations of the collective modes are obtained from the poles of the polarization tensor (Larkin and Migdal, 1964; Leggett, 1966). For single-component neutral superfluid one finds two branches of density modes: the Anderson-Bogolyubov mode, which is an acoustic mode with dispersion  $\omega = uk$ , with  $\omega$  and  $k$  the mode energy and momentum. At low temperatures the mode velocity is given by

$$u = \frac{v_F}{\sqrt{3}}(1 + v_{ph})^{1/2}, \quad (129)$$

where  $v_F$  is the Fermi velocity and  $v_{ph}$  is the particle-hole interaction in the scalar channel. The second mode is the so-called Higgs mode and has a finite threshold as  $k \rightarrow 0$  of the order of the pair-breaking energy  $2\Delta$ . These modes in nuclear matter were studied long ago (Larkin and Migdal, 1964), but the case of neutron matter below saturation density has been considered only recently (Keller and Sedrakian, 2013b; Martin and Urban, 2014). In the neutron-star crust, the modes of the superfluid neutron fluid are coupled to the phonon modes of the lattices, in which case there is a mixing among the modes (Chamel *et al.*, 2013; Cirigliano *et al.*, 2011; Urban and Oertel, 2015).

In the high-density region, corresponding the quantum-liquid core of the star, the nature of modes of the superfluid(s) is affected by the fact that there are plasma modes associated with the oscillations of the proton-electron component, moreover there is a coupling between the neutron and proton fluids that have different Fermi velocities and gaps (Baldo and Ducoin, 2009, 2017). In addition, the  $P$ -wave nature of the neutron superfluid admits modes associated with the spin of the Cooper pairs (Bedaque and Nicholson, 2013; Bedaque *et al.*, 2015; Bedaque and Reddy, 2014; Bedaque *et al.*, 2003b; Leinson, 2011, 2012).

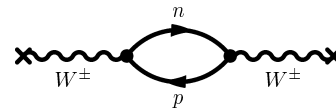


FIG. 26 The lowest order (one-loop) Urca process on charged currents. The second diagram in Fig. 25 is absent at this order by charge conservation in the weak vertex.

Phenomenologically, as new degrees of freedom the collective modes contribute to the thermodynamics of the superfluid. The specific heat is of particular interest for cooling of neutron stars (Keller and Sedrakian, 2013b; Martin and Urban, 2014). The collective modes (phonons) can lose energy by neutrino emission (Bedaque *et al.*, 2003b; Leinson, 2011) and can contribute to the transport (Mannarelli *et al.*, 2013; Manuel *et al.*, 2014; Manuel and Tolos, 2011).

## G. Urca process in superfluid phases

Urca processes involving nucleons (109) or hyperons (113)-(116) are operative at high densities for many models of the equation of state of dense matter. Consequently, it is important to understand how the rates of these processes are affected by superfluidity of the baryons. At asymptotically low temperatures  $T \ll \min(\Delta_n, \Delta_p)$ , where  $\Delta_{n/p}$  are the neutron/proton gaps, the neutrino radiation is suppressed by a Boltzmann factor  $\exp(-\Delta_{\max}/T)$ , with  $\Delta_{\max} = \max(\Delta_n, \Delta_p)$  the larger of the neutron and proton gaps (Lattimer *et al.*, 1991). However, a substantial part of the neutrino cooling of a neutron star occurs in the temperature range  $0.2 \leq T/T_c \leq 1$ , where  $T_c$  is the relevant critical temperature for either neutron or proton pairing. Hence more accurate description of the suppression of the Urca processes is required. Because pairing mainly affects the phase space of nucleons, an initial step is to introduce the BCS spectrum in the distribution functions of nucleons when computing the rate of the Urca process (Levenfish and Yakovlev, 1994). In principle, the matrix element of the process is also modified because one is dealing with a coherent state composed of a superposition of particles and holes as expressed by the coherence factors  $u_p/v_p$  given by Eq. (5). It is convenient to carry out the computation using the Green functions for baryons (Sedrakian, 2005, 2007). To lowest order (i.e. neglecting the vertex corrections discussed above) the one-loop contribution to the Urca process is given by the diagram shown Fig. 26. A new feature in such computation that keeps  $u_p \neq 1$  and  $v_p \neq 0$ , is the emergence of the pair-breaking process in the Urca channel. The polarization tensor computed from the diagram in Fig. 26 contains contributions not only from the scattering processes  $\propto [f_n(\mathbf{p}) - f_p(\mathbf{p} + \mathbf{q})]$ , where  $f_{p/n}$  are the proton and neutron distribution functions and  $\mathbf{q}$  is the momentum transfer, but also from processes

$\propto [1 - f_n(\mathbf{p}) - f_p(\mathbf{p} + \mathbf{q})]$  that are due to the breaking of neutron and proton Cooper pairs. Close to the critical temperature  $0.5 \leq T/T_c \leq 1$  the scattering contribution is dominant, but at lower temperatures the pair-breaking contribution becomes comparable to the scattering contribution.

Neutron stars are seismically active bodies. Density oscillations (more specifically first sound in a superfluid) can induce variations in the chemical potentials of species which can modify the Urca process rate in the superfluid phases. Large enough density oscillations can displace the Fermi seas of nucleons and bridge the gap (Alford and Pangeni, 2017; Alford *et al.*, 2012). This super-thermal effect may strongly enhance the rate of the Urca process in the superfluid up to levels comparable to that of the normal state. In hadronic matter the relative amplitudes of the density oscillations required for this effect to be operative are of the order of  $\Delta n/n \sim 10^{-3}$ . Consequently, an (unstable) growth of oscillation amplitude in a superfluid can saturate due to the dissipation of the energy of oscillations via neutrino emission.

Out-of-equilibrium Urca processes in the superfluid phases are also important for understanding the coupled rotational and chemical evolution of neutron stars, which accounts for changes in the composition of the star due to its deceleration, resulting in a time-dependent centrifugal force (González-Jiménez *et al.*, 2015; Petrovich and Reisenegger, 2011).

## H. Axion radiation from superfluid phases

Superfluid phases of neutron stars may also radiate away energy by emitting particles existing beyond the standard model (SM). The theoretical study of such processes may help constrain the properties of a hypothetical particle by confrontation of their effects on cooling with measurements of X-ray flux from suitable neutron-star candidates. We discuss this possibility using the specific example of axions, which were originally introduced (Peccei and Quinn, 1977; Weinberg, 1978; Wilczek, 1978) to solve the strong-CP problem in QCD ('t Hooft, 1976). In the case of neutron stars, we need to assume that the axion emission, which carries additional energy away from stellar interior, does not significantly alter the agreement between theoretical cooling models and observations.

The computation of the pair-breaking process

$$\{NN\} \rightarrow N + N + a, \quad N + N \rightarrow \{NN\} + a, \quad (130)$$

involving the emission of axion  $a$  is analogous to the axial-current neutrino emission, since the axion couples to the nucleonic axial current; the response function is represented by Fig. 25 where now instead of  $Z_0$  gauge boson an axion is attached to the nucleonic loop.

To set the notation, we start with the interaction Lagrangian

$$\mathcal{L}_{int}^{(B)} = \frac{1}{f_a} B^\mu A_\mu, \quad (131)$$

where  $f_a$  is the axion decay constant, and the baryon and axion currents are given by

$$B^\mu = \sum_N \frac{C_N}{2} \bar{\psi}_N \gamma^\mu \gamma_5 \psi_N, \quad A_\mu = \partial_\mu a, \quad (132)$$

where the  $C_N$  are the Peccei-Quinn (PQ) charges of the baryonic currents and it is convenient to denote nucleons collectively by  $N \in n, p$ . The dimensionless Yukawa coupling can be defined as  $g_{aNN} = C_N m_N / f_a$ , from which it follows that the axionic ‘‘fine-structure’’ constant is written as  $\alpha_{aNN} = g_{aNN}^2 / 4\pi$ .

The charges introduced above are given by generalized Goldberger-Treiman relations

$$C_p = (C_u - \eta)\Delta_u + (C_d - \eta z)\Delta_d + (C_s - \eta w)\Delta_s, \quad (133)$$

$$C_n = (C_u - \eta)\Delta_d + (C_d - \eta z)\Delta_u + (C_s - \eta w)\Delta_s, \quad (134)$$

where  $\eta = (1 + z + w)^{-1}$ , with  $z = m_u/m_d$ ,  $w = m_u/m_s$ , and  $\Delta_u = 0.84 \pm 0.02$ ,  $\Delta_d = -0.43 \pm 0.02$  and  $\Delta_s = -0.09 \pm 0.02$ . The main uncertainty is associated with  $z = m_u/m_d = 0.35\text{--}0.6$ . While there are numerous models of axions, a particularly useful model is the hadronic axion model with  $C_{u,d,s} = 0$ ; in this model the nucleonic charges vary in the range

$$-0.51 \leq C_p \leq -0.36, \quad -0.05 \leq C_n \leq 0.1. \quad (135)$$

The axion mass is related to  $f_a$  by

$$m_a = \frac{z^{1/2}}{1+z} \frac{f_\pi m_\pi}{f_a} = \frac{0.6 \text{ eV}}{f_a / 10^7 \text{ GeV}} \quad (136)$$

in terms of the pion mass  $m_\pi = 135 \text{ MeV}$  and the decay constant  $f_\pi = 92 \text{ MeV}$ , having adopted the value  $z = 0.56$  from the range of  $z$  values quoted. Equation (136) translates a lower bound on  $f_a$  to an upper bound on the axion mass.

Computations analogous to those for neutrinos lead to the axion emissivity from  $S$ -wave condensates (Keller and Sedrakian, 2013a),

$$\epsilon_{aN}^S = \frac{2C_N^2}{3\pi} f_a^{-2} \nu_N(0) v_{FN}^2 T^5 I_{aN}^S, \quad (137)$$

where

$$I_{aN}^S = z_N^5 \int_1^\infty dy \frac{y^3}{\sqrt{y^2 - 1}} f_F^2(z_N y), \quad (138)$$

and  $z_N = \Delta_N^S(T)/T$ ; here  $\Delta_N^S$  refers to the  $S$ -wave  $N$ -nucleonic gap.

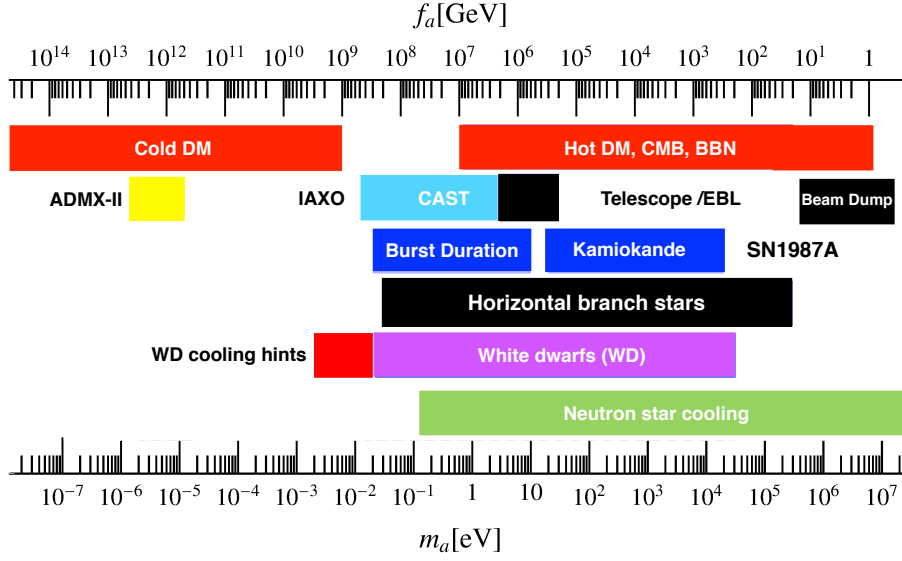


FIG. 27 Regions of exclusion for axion masses and coupling derived from combined experimental and theoretical studies. These regions are organized in rows with regions of exclusion derived from (top to bottom): (1) cosmology, (2) laboratory experiments, (3) supernova 1987A event, (4) horizontal branch stars, (5) physics of white dwarfs, and (6) neutron star cooling. The last result is based on comparison between numerical simulations and X-ray data on surface photon luminosity of thermally emitting neutron stars.

A qualitative bound on  $m_a$  can now be obtained by requiring that the axion cooling does not overshadow the neutrino cooling (which is dominated by the  $S$ -wave neutrino radiation), i.e.,

$$\frac{\epsilon_a^S}{\epsilon_{\nu\bar{\nu}}^S} = \frac{59.2C_N^2}{4f_a^2 G_F^2 \Delta_N^S(T)^2} r(z) \leq 1 \quad (139)$$

where  $r(z)$  is the ratio of the phase-space integral for axions (138) to its counterpart (127) for neutrinos and is numerically bound from above by  $r(z) \leq 1$ . Hence this factor can be dropped from the bound on  $f_a$ . Substituting into Eq. (139) the value of the Fermi coupling constant  $G_F = 1.166 \times 10^{-5} \text{ GeV}^{-2}$  we may convert this bound to

$$\frac{f_a/10^{10}\text{GeV}}{C_N} > 0.038 \left[ \frac{1 \text{ MeV}}{\Delta^S(T)} \right]. \quad (140)$$

Using Eq. (136), this translates to an upper bound on the axion mass of

$$m_a C_N \leq 0.163 \text{ eV} \left( \frac{\Delta_N^S(T)}{1 \text{ MeV}} \right). \quad (141)$$

The nucleon pairing gap on the right-hand side can in fact be replaced by the critical temperature  $T_c$ , because in the temperature range important for pair-breaking processes, i.e.,  $0.5 \leq T/T_c < 1$ , BCS theory predicts  $\Delta(T) \simeq T_c$ .

As explained previously, the presumptive neutron condensate in neutron star cores is paired in the  ${}^3P_2$ - ${}^3F_2$  channel in a state which features an anisotropic gap (Zverev *et al.*, 2003). The corresponding axion emis-

sivity is found to be (Sedrakian, 2016)

$$\epsilon_{an}^P = \frac{2C_n^2}{3\pi} f_a^{-2} \nu_n(0) T^5 I_{an}^P, \quad (142)$$

where

$$I_{an}^P = \int \frac{d\Omega}{4\pi} z_N^5 \int_1^\infty dy \frac{y^3}{\sqrt{y^2-1}} f_F^2(z_N y). \quad (143)$$

Here  $d\Omega$  denotes the integration over the solid angle, and  $z_N = \Delta^P(T, \theta)/T$  depends on the polar angle  $\theta$ , where  $\Delta^P(T, \theta)$  is the pairing gap in the  $P$ -wave channel. Note that  $C_n = 0$  is not excluded; i.e., it is conceivable that axions are not emitted by the neutron  $P$ -wave condensate.

The temperature dependence of axion emission scales with temperature as  $\propto T^5$ . This scaling differs from its neutrino counterpart, which is  $\propto T^7$ . Accordingly, axionic cooling processes would change the slope of the cooling curves in the temperature-age diagram. Detailed numerical simulations of axionic cooling (Sedrakian, 2016) yield the regions of exclusion of axion masses and couplings illustrated in Fig. 27. As seen in this figure, the results from axion cooling simulations of neutron stars and their comparison with the X-ray data on thermally emitting neutron stars, which depend crucially on the axion emission by superfluid phases in neutron stars, are compatible with other constraints derived from stellar physics.

## VI. QUANTUM VORTICITY

### A. Motivation

Motivation for the study of vorticity in nuclear systems derives from the fact that neutron stars are rotating and that neutrons, which form a neutral superfluid, must rotate by forming quantized rotational vortices. Although it has been conjectured that vortex states exist in finite nuclei, the coherence length of the nucleonic condensate, which sets the size of the vortex core, is of the order or larger than the nuclear radius. In neutron stars, rotation at angular velocity  $\Omega$  induces a mesh of neutron vortices with number density

$$n_n = \frac{2\Omega}{\kappa}, \quad \kappa = \frac{\pi}{m_n}, \quad (144)$$

where  $\kappa$  is the quantum of circulation and  $m_n$  is the neutron mass. In the parameter range where the proton superconductor in neutron stars is of type II, electromagnetic vortices are formed with a density

$$n_p = \frac{B}{\phi_0}, \quad \phi_0 = \frac{\pi}{e}, \quad (145)$$

where  $\phi_0$  is the flux quantum and  $B$  is the mean magnetic-field induction. The Abrikosov vortex lattices of neutron and proton superfluids are triangular with the lengths of basis vectors given by

$$d_n = \left( \frac{\kappa}{\sqrt{3}\Omega} \right)^{1/2}, \quad d_p = \left( \frac{2\phi_0}{\sqrt{3}B} \right)^{1/2}, \quad (146)$$

which are of order  $10^{-4}$  cm and  $10^{-9}$  cm respectively, for rotation periods of the order of a fraction of second and fields  $B \sim 10^{12}$  G. The latter scale  $d_p$  is larger than the penetration depth of the magnetic field  $\lambda \simeq 10^{-11}$  cm set by the Meissner mass of a photon inside the proton superconductor.

These length scales define a new mesoscopic scale for description of neutron-star superfluids and superconductors, since an averaging over large number of vortices is required to obtain the hydrodynamical fluid velocity and the macroscopic value of the magnetic field. The microscopic scale is set by the size of the vortex core, which for charged and neutral fermionic superfluids alike is given by the coherence length  $\xi$ . Within the region  $r \leq \xi$ , where  $r$  is the radial cylindrical coordinate, the order parameter of the superfluid is suppressed linearly for  $r \rightarrow 0$ , vanishing at its center. From the microscopic point of view, the core of a vortex contains a new type of excitation – a quasiparticle bound state that emerges from solution of the microscopic Bogolyubov-De-Gennes (BdG) theory. This section is devoted to the physics of these excitations and their interactions with matter, which give rise to mutual friction. The primary motivation for studies of mutual friction in neutron stars is a deeper understanding of the non-stationary dynamics of neutron-star rotation, in particular the phenomena of glitches and post-glitch relaxation in pulsars.

### B. Vortex core quasiparticles

The microscopic theory of bound states of a fermionic vortex was initially developed by Caroli, De-Gennes, and Matricon for a vortex in a type-II superconductor (Caroli *et al.*, 1964). Their approach is based on the solution of the BdG equations for the pairing amplitudes  $u(\mathbf{r})$  and  $v(\mathbf{r})$ , as introduced Sec. II, but in configuration space. These early results were soon adapted to neutron vortices, so as to obtain the coefficients of mutual friction in the core of a neutron star in terms of interactions of the neutron quasiparticles bound in the core of the vortex core with ambient electrons (Feibelman, 1971).

An isolated neutron vortex was studied in Refs. (de Blasio and Elgarøy, 1999; Elgarøy and De Blasio, 2001; Yu and Bulgac, 2003) by solving the BdG equations in neutron matter. Substantial depletion in the region of the core was found in (Yu and Bulgac, 2003), a feature uncharacteristic of condensed-matter vortices. Density depletion in vortex cores is important since it allows the vortices to be detected experimentally in ultra-cold atomic gases (Zwierlein *et al.*, 2006). The vortex profile in an ultra-cold atomic gas was investigated in a population-imbalanced gas (Iskin, 2008; Takahashi *et al.*, 2007; Warringa, 2012; Warringa and Sedrakian, 2011). As discussed in Sec. IV, population imbalances are typically too large in neutron stars to be relevant. However, they could be relevant in super-strong magnetic fields where neutrons become spin-polarized.

The BdG theory can be derived using the Green functions formalism introduced in Sec. III.A, with specialization to configuration space. In this case the Dyson-Schwinger equation for the Nambu-Gor'kov propagator takes the form

$$G^{-1}(X, X') = - \left( \frac{\partial}{\partial \tau} + H \right) \delta(X - X'), \quad (147)$$

where  $X = (\mathbf{r}, \tau)$  is the four-coordinate including the imaginary time  $\tau$ , while

$$H = \begin{pmatrix} h(\Omega) - \mu_{\uparrow} + g n_{\downarrow}(\mathbf{r}) & \Delta(\mathbf{r}) \\ \Delta^*(\mathbf{r}) & -h(\Omega)^* + \mu_{\downarrow} - g n_{\uparrow}(\mathbf{r}) \end{pmatrix}. \quad (148)$$

In this expression,  $h(\Omega)$  denotes the single-particle Hamiltonian in the frame rotating with the frequency  $\Omega$ , and  $\downarrow, \uparrow$  refer to spin-down and spin-up particles with chemical potentials  $\mu_{\downarrow, \uparrow}$  and densities  $n_{\downarrow, \uparrow}$ ,  $g$  being the strength of the assumed four-fermion contact interaction. The solutions of the Dyson-Schwinger equation are obtained by inversion of Eq. (147). This is done by solving the BdG equation

$$H \begin{pmatrix} u_i(\mathbf{r}) \\ v_i(\mathbf{r}) \end{pmatrix} = E_i \begin{pmatrix} u_i(\mathbf{r}) \\ v_i(\mathbf{r}) \end{pmatrix}, \quad (149)$$

for the amplitudes  $u_i(\mathbf{r})$  and  $v_i(\mathbf{r})$ , where the index  $i$  refers to the particle's spin state and the energies  $E_i$  are the eigenvalues of the BdG equation. The functions  $u_i(\mathbf{r})$  and  $v_i(\mathbf{r})$  are normalized by  $\int d^3r [|u_i(\mathbf{r})|^2 + |v_i(\mathbf{r})|^2] = 1$ . The densities of up-spin and down-spin fermions, expressed as

$$n_\uparrow(\mathbf{r}) = \sum_i f(E_i) |u_i(\mathbf{r})|^2, \quad (150)$$

$$n_\downarrow(\mathbf{r}) = \sum_i f(-E_i) |v_i(\mathbf{r})|^2 \quad (151)$$

in terms of the Fermi-Dirac distribution function  $f(E)$ , are to be determined simultaneously with the solution of the BdG equation. The gap function  $\Delta(\mathbf{r})$  is obtained from the anomalous component of the GF, which is given by

$$G_{\uparrow\downarrow}(\mathbf{r}, \tau; \mathbf{r}', \tau) = \sum_i f(E_i) u_i(\mathbf{r}) v_i^*(\mathbf{r}') \quad (152)$$

in the limit  $\mathbf{r}' \rightarrow \mathbf{r}$ . One finds a relation between the gap and the GF in Eq. (152) of the following form

$$G_{\uparrow\downarrow}(\mathbf{r}, \tau; \mathbf{r}', \tau) = -\frac{m\Delta(\vec{x})}{4\pi} \frac{1}{|\mathbf{r} - \mathbf{r}'|} + G_{\uparrow\downarrow}^{\text{reg}}(\mathbf{r}, \tau; \mathbf{r}, \tau), \quad (153)$$

where  $m$  is the (effective) mass of fermions and the regular part  $G_{\uparrow\downarrow}^{\text{reg}}(\mathbf{r}, \tau; \mathbf{r}, \tau)$  of the GF can be found elsewhere (Yu and Bulgac, 2003). The Helmholtz free energy  $F$  can be now evaluated using the solutions of the BdG equation

$$\begin{aligned} F = & -\sum_i \left[ \frac{|E_i|}{2} + \frac{1}{\beta} \log \left( 1 + \exp^{-\beta|E_i|} \right) \right] + \sum_i \epsilon_i \\ & - \int d^3x G_{\uparrow\downarrow}(\mathbf{r}, \tau; \mathbf{r}, \tau)^* \Delta(\vec{x}) \\ & - g \int d^3x n_\uparrow(\mathbf{r}) n_\downarrow(\mathbf{r}) + \mu_\uparrow N_\uparrow + \mu_\downarrow N_\downarrow \end{aligned} \quad (154)$$

where  $\epsilon_i$  are the eigenvalues of the Hartree-Fock Hamiltonian  $H_{\text{HF}} = H(\Omega = 0) - \mu + gn(\mathbf{r})$ .

It should be mentioned that some of the individual terms in the last equation are ultraviolet-divergent, but their sum, and hence the Helmholtz free energy, is ultraviolet-finite. Eq. (154) allows one to determine the parameter space spanned by the coupling  $g$ , the population imbalance, the rotation frequency, and relevant thermodynamic quantities in the phase diagram of the neutron medium and to identify the boundaries of the vortex-supporting phase.

We now present approximate solutions of BdG equations that provide insight into recent numerical work. The states of the vortex core can be approximated as (Caroli and Matricon, 1965)

$$\begin{pmatrix} u_{q_\parallel, \mu}(\mathbf{r}_\perp) \\ v_{p_\parallel, \mu}(\mathbf{r}_\perp) \end{pmatrix} = e^{ip_\parallel z} \begin{pmatrix} e^{i\theta(\mu - \frac{1}{2})} & e^{i\theta(\mu + \frac{1}{2})} \end{pmatrix} \begin{pmatrix} u'_\mu(r) \\ v'_\mu(r) \end{pmatrix}, \quad (155)$$

where the vector  $\mathbf{r} = (r, \theta, z)$  has been decomposed into cylindrical coordinates with the  $z$ -axis along the vortex circulation,  $\parallel$  and  $\perp$  being its components parallel and perpendicular to the vortex circulation. Here  $\mu$  labels the azimuthal quantum number, which assumes half-integer positive values. It is seen that the vortex-core states are plain waves along the vortex circulation, but are quantized in the orthogonal direction. The radial part of the wave function is given by

$$\begin{pmatrix} u'_\mu(r) \\ v'_\mu(r) \end{pmatrix} = 2 \left( \frac{2}{\pi p_\perp r} \right)^{1/2} e^{-K(r)} \begin{pmatrix} \cos(p_\perp r - \frac{\pi\mu}{2}) \\ \sin(p_\perp r - \frac{\pi\mu}{2}) \end{pmatrix}, \quad (156)$$

where  $p_\perp = \sqrt{p^2 - p_F^2}$ ,  $p_F$  being the neutron Fermi momentum. The function in the exponent is

$$K(r) = \frac{p_F}{\pi p_\perp \Delta_\infty} \int_0^r \Delta(r') dr' \simeq \frac{p_F r}{\pi p_\perp \xi} \left( 1 + \frac{\xi e^{-r/\xi}}{r} \right), \quad (157)$$

where  $\Delta_\infty$  is the asymptotic value of the gap far from the vortex core, while  $\xi$  is the coherence length. The eigenstates of neutrons in the core of a vortex for small momentum are given by

$$\epsilon_\mu(p) \simeq \frac{\pi\mu\Delta_\infty^2}{2\epsilon_F} \left( 1 + \frac{p^2}{2p_F^2} \right), \quad (158)$$

where  $\epsilon_F$  is the Fermi energy.

### C. Vortex dynamics and pinning

Following the suggestion by Anderson and Itoh (Anderson and Itoh, 1975) that the neutron superfluid dynamics is driven by the interaction of vortices with the nuclear lattice in the inner crust of a neutron star, many calculations have been performed in efforts to understand the pinning-type interactions between vortices and nuclei. This is in general a time-dependent problem, but the static interactions are of great interest as well. Indeed, the stationary minimum energy state of a neutron vortex could require its pinning to a nucleus (with geometrical overlap), or, alternatively, its pinning in the space between nuclei if the vortex-nucleus interaction is repulsive.

Stationary studies of the pinning in neutron stars compare energy difference between a configuration where nucleus and vortex are well separated with a configuration in which they intersect. A naive picture suggests that the energy required to create the vortex core quasiparticles out of the condensate is gained if the vortex passes through the nucleus (Pines *et al.*, 1980). A more flexible and quantitative basis is offered by Ginzburg-Landau theory (Epstein and Baym, 1988), as other contributions to the Ginzburg-Landau functional besides the condensation can play key roles. In this approach, whether the vortices pin on nuclei or in between them depends on

the density; typically high densities favor pinning to nuclei. Similar conclusions have also been reached in semi-classical models that assume a realistic Argonne interaction (Donati and Pizzochero, 2004, 2006); however, the magnitude of the pinning energy or force is smaller by an order of magnitude than in the Ginzburg-Landau models. Solutions of the BdG equations for the pinning problem exist (Avogadro *et al.*, 2008), but the results for pinning energies are not conclusive.

Dynamical theories of vortex nucleus interactions go beyond static considerations that compare the energy differences between stationary pinned and unpinned configurations. Dynamical studies have included (i) purely hydrodynamical modeling (Link, 2009; Sedrakian, 1995), (ii) modeling based on Gross-Pitaevskii-like equations (Bulgac *et al.*, 2013) and, most recently, (iii) application of time-dependent superfluid density functional theory (Wlazłowski *et al.*, 2016). The last study captures most of the microphysics, and it concludes that nuclei repel vortices in the neutron-star crust, i.e., if they are pinned, vortices reside in between the nuclear clusters.

## D. Mutual friction

Mutual friction arises through interaction of vortices with the ambient non-superfluid components of neutron stars. Analogous phenomena have been investigated extensively in the context of liquid He-II hydrodynamics, but the context of neutron stars is unique because both the ambient fluid and the vorticity are of fermionic nature. We next review the microphysics and kinetics of particle interactions with the bound states in the vortex cores of quantized vortices. Electrons will couple to the core quasiparticles of the neutron vortex via the interaction of the electron charge  $e$  with the neutron magnetic moment  $\mu_n = -1.913\mu_N$ , where (restoring  $\hbar$ )  $\mu_N = e\hbar/2m_p$  is the nuclear magneton (Feibelman, 1971). The relaxation timescale for the electron momentum due to scattering by neutron vortex-core quasiparticles is given by (Bildsten and Epstein, 1989)

$$\tau_{eV}[^1S_0] = \frac{1.6 \times 10^3 \Delta}{\Omega T} \left( \frac{\epsilon_{Fe}}{\epsilon_{Fn}} \right)^2 \times \left( \frac{\epsilon_{Fn}}{2m_n} \right)^{1/2} \exp\left( \frac{\epsilon_{1/2}^0}{T} \right), \quad (159)$$

where  $\epsilon_{Fe}/\epsilon_{Fn}$  are the electron/neutron Fermi energies,  $\Delta$  is the  $S$ -wave neutron pairing gap,  $\epsilon_{1/2}^0$  is given by Eq. (158) with  $\mu = 1/2$ , and  $\Omega$  is the angular velocity of the superfluid, which enters through the number of scattering centers per  $\text{cm}^2$  according to formula (144). We see that the relaxation time is proportional to the Boltzmann factor that measures the probability of finding core quasiparticle states at a given temperature.

The electron dynamics in the stellar core is strongly affected by the proton component, but we assume for

the time being that electrons interact exclusively with neutron vortices in a  $P$ -wave superfluid. The order parameter in the  $P$ -wave case has a tensor character and can be written as a traceless and symmetric function  $A_{\mu\nu}$ ,  $\mu, \nu = 1, 2, 3$ . This function can be decomposed in cylindrical coordinates  $(r, \phi, z)$  as (Sauls *et al.*, 1982)

$$A_{\mu\nu} = \frac{\Delta}{\sqrt{2}} e^{i\phi} \left\{ [f_1 \hat{r}_\mu \hat{r}_\nu + f_2 \hat{\phi}_\mu \hat{\phi}_\nu - (f_1 + f_2) \hat{z}_\mu \hat{z}_\nu + ig(r_\mu \hat{\phi}_\nu + r_\nu \hat{\phi}_\mu)] \right\}, \quad (160)$$

where  $g(r)$  and  $f_{1,2}(r)$  are the radial functions describing the vortex profile and  $\Delta$  is the average value of the gap in the  $^3P_2$  channel. The new aspect emerging in the core of a neutron star is that  $P$ -wave vortices possess intrinsic magnetization because the relevant Cooper pairs are spin-1 objects. Their magnetization is given by (Sauls *et al.*, 1982)

$$\mathbf{M}_V(\mathbf{r}) = (\gamma_n \hbar) \frac{\boldsymbol{\sigma}(\mathbf{r})}{2} = g_n \mu_N \frac{\boldsymbol{\sigma}(\mathbf{r})}{2} \quad (161)$$

where  $\gamma_n = g_n \mu_N \hbar^{-1}$  is the gyromagnetic ratio of the neutron with  $g_n = 3.826$ . For a  $P$ -wave vortex, the spin density  $\hbar \boldsymbol{\sigma}/2$  may be estimated from

$$\sigma(r) = \frac{\nu_n \Delta_n^2}{3} \ln\left( \frac{\Lambda}{T_c} \right) g(r) [f_1(r) - f_2(r)], \quad (162)$$

where  $\Lambda$  is the BCS cutoff and  $\nu_n$  is the neutron density of states at the Fermi surface. The magnitude of the vortex magnetization that follows from Eq. (162) is in turn estimated as

$$|M_V(^3P_2)| = \frac{g_n \mu_N}{2} n_n \left( \frac{\Delta}{\epsilon_{Fn}} \right)^2 \simeq 10^{11} \text{ G}. \quad (163)$$

The interaction of electrons with  $P$ -wave superfluid vortices is driven by the interaction  $-e\boldsymbol{\gamma} \cdot \mathbf{A}(\mathbf{r})$ , with  $\mathbf{A}(\mathbf{r}) = A(r) \hat{\phi}$  derived from magnetization according to

$$A(r) = \frac{1}{r} \int_0^r |M_V(r')| r' dr'. \quad (164)$$

Finally, the relaxation time for the electron-vortex scattering is obtained as (Sauls *et al.*, 1982)

$$\tau_{eV}[^3P_2] \simeq \frac{7.91 \times 10^8}{\Omega} \left( \frac{k_{Fn}}{\text{fm}} \right) \left( \frac{\text{MeV}}{\Delta_n} \right) \left( \frac{n_e}{n_n} \right)^{2/3}. \quad (165)$$

In contrast to the case of scattering off the quasiparticles, the relaxation time (165) is nearly independent of temperature, the only temperature-dependent quantity being the gap. The result (165) sets a lower limit on the scattering rate at low temperatures ( $T \ll \Delta$ ), where the relaxation time  $\tau_{eV}[^1S_0]$  of Eq. (159) is exponentially suppressed.

Allowing now for a proton component, we identify additional interaction channels, which turn out to be dominant in most cases. Let us first consider the case of non-superfluid protons, since at sufficiently high densities the proton  $^1S_0$  gap closes. The neutron quasiparticles in the cores of vortices will then couple to proton excitations, in much the same way as they coupled to the electron component (Feibelman, 1971). However, an important distinction is that the protons will couple to neutrons by the strong nuclear force, instead of much weaker electromagnetic interaction. The corresponding relaxation time becomes (Sedrakian, 1998)

$$\begin{aligned} \tau_{pV}[^1S_0] &= \frac{0.71}{\Omega_s} \frac{m_n^* m_p^*}{m_n \mu_{pn}^*} \left( \frac{\epsilon_{Fp}}{\epsilon_{Fn}} \right)^2 \frac{\epsilon_{1/2}^0}{T} \\ &\times \exp \left( \frac{\epsilon_{1/2}^0}{T} \right) \frac{\xi_n^2}{\langle \sigma_{np} \rangle}, \end{aligned} \quad (166)$$

where  $\mu_{pn}^* = m_p^* m_n^* / (m_n^* + m_p^*)$  is the reduced mass of the neutron-proton system (entering the relation between the cross-section and the scattering amplitude squared),  $\epsilon_{1/2}^0$  is the lowest eigenstate of vortex-core excitations according to Eq. (158), and  $\langle \sigma_{np} \rangle$  can be viewed as an average neutron-proton cross-section. Eq. (166) suggests a much stronger coupling between the electron-proton plasma and the neutron vortices than implied by any of the previously quoted timescales.

Consider next the case of superconducting protons, in which no quasiparticle excitations are available for coupling to vortex-core quasiparticles. Nevertheless, in this case there is an entrainment effect that induces a new type of magnetization of the neutron vortex (Alpar *et al.*, 1984; Vardanyan and Sedrakyan, 1981). In effect, neutron vortices carry a non-integral multiple of the flux quantum,

$$\phi^* = k\phi_0, \quad k = \frac{m_p^*}{m_p}, \quad (167)$$

which leads to a  $B$  field larger by four orders of magnitude than that due to the spontaneous magnetization considered above. The relaxation timescales are correspondingly shorter. It is now convenient to define the full relaxation time in terms of a zero-range relaxation time

$$\tau_0^{-1} = \frac{2n_v}{k_{eF}} \left( \frac{\pi^2 \phi_*^2}{4\phi_0^2} \right). \quad (168)$$

The term in parentheses is an approximation to the exact Aharonov-Bohm scattering result, in which  $\sin^2(\pi/2)(\phi_*/\phi_0)$  appears instead (Alford and Wilczek, 1989). The finite range result then can be written as (Alpar *et al.*, 1984)

$$\tau_{e\phi}^{-1} = \frac{3\pi}{32} \left( \frac{\epsilon_{Fe}}{m_p} \right) \frac{\tau_0^{-1}}{k_{eF}\lambda}, \quad (169)$$

where  $\lambda$  is the penetration depth. We note the weak dependence of the scattering relaxation time on the temperature, reflecting the fact that coupling is to the  $B$ -field and not to the thermally excited quasiparticles.

A more complete discussion of mutual friction requires addressing the interaction between neutron and proton vortices and their intertwined dynamics, which however is beyond the scope of our focus on microphysics. We refer the reader to a recent review (Haskell and Sedrakian, 2017) for such a discussion.

## VII. CONCLUSIONS

This review has covered a range of topics on nucleonic superfluidity with an emphasis on extended systems such as neutron stars and matter created in nuclear collisions. The pairing problem at the level of mean-field BCS theory, in which the pairing interaction is extracted directly from free-space nuclear interactions, is essentially solved within the density range corresponding to energies where the scattering phase shifts are known. There still exist discrepancies between various methods for microscopic many-body calculation of pairing properties, notably in relation to the issue of suppression of  $S$ -wave pairing in neutron matter by long-range collective fluctuations in the nuclear medium. Theories that incorporate such fluctuation corrections as well as the effects of short-range correlations due to the repulsion of the two-nucleon potential at short distances have been emerging in recent years. The goal of achieving convergent results for pairing in low-density nuclear matter appears to be within sight. Other important objectives that arise at higher densities are harder to handle. These include especially the challenge of accurate evaluation of pairing gaps in the  $^3P_2$ - $^3F_2$  channel, which is complicated by their characteristically small magnitude, high sensitivity to the two-body pairing interaction, which is not well constrained theoretically, and the increasingly important role of the three-nucleon forces. Additionally, the off-shell behavior of the pairing gap and its impact on the phenomenology of nucleonic superfluids remain largely unexplored.

Superfluid phases with broken space-time symmetries have received much attention from theorists during the past two decades. Recent experimental realization of imbalanced superfluids in ultracold fermionic atomic gases has created the possibility of laboratory tests of the predictions of many-body theory under highly controlled conditions. There are excellent prospects for future cross-fertilization of nuclear theory and experimental activity in cold atomic gases, especially in identifying the phases of imbalanced superfluids and in exploring the physics of the BCS-BEC crossover. The phase diagram of imbalanced superfluids, as outlined in this review, offers a rich arena for mutual interaction and enrichment of quantum many-body theories and experimental studies of trapped atomic gases.

As discussed in detail in this review, the physics of the

thermal evolution of neutron stars is a sensitive probe of their interior physics, particularly their composition. Accurate weak-interaction rates in the superfluid phases of neutron stars are of great importance for reliable modeling of neutron-star cooling. The quantum many-body methods involved in computations of these rates, some of which existed already in the 1960s, have been recently applied to compute the the weak response of nucleonic superfluids, thereby providing accurate rates of neutrino emission from nucleonic and hyperonic superfluids. Future observational progress in measuring and modeling the surface radiation of neutron stars, in conjunction with improved theoretical input and simulations of neutron stars, can yield further clues on their interior composition and on the couplings of non-standard-model particles (e.g. axions) to matter.

Quantum vortex states, reviewed in the last section, are fundamental to an understanding of the rich spectrum of observed rotational anomalies in pulsars. This is yet another area in which models and theories developed for nuclear systems can be tested in laboratory experiments on ultra cold atomic gases. Further theoretical studies of vortex dynamics, combined with pulsar timing observations, can be expected to shed new light on the internal structure of the superfluid phases of neutron stars, especially on the microphysics of mutual friction as surveyed in this review.

## Acknowledgments

A.S. acknowledges the support by the DFG (Grants No. SE 1836/3-2 and No. SE 1836/4-1), by the Helmholtz International Center for FAIR, and by the NewCompStar COST Action MP1304. J.W.C. acknowledges support from the McDonnell Center for the Space Sciences and is grateful for the hospitality of the Centro de Investigação em Matemática e Aplicações, University of Madeira, Funchal, Portugal.

## References

- Abe, T., and R. Seki, 2009, Phys. Rev. C **79**(5), 054002.
- Abrikosov, A., L. Gor'kov, and I. Dzyaloshinski, 1963, *Methods of quantum field theory in statistical physics* (Dover, New York, N.Y.).
- Ainsworth, T. L., J. Wambach, and D. Pines, 1989, Phys. Lett. B **222**, 173.
- Alford, M. G., and K. Pangeni, 2017, Phys. Rev. C **95**(1), 015802.
- Alford, M. G., S. Reddy, and K. Schwenzer, 2012, Phys. Rev. Lett. **108**(11), 111102.
- Alford, M. G., A. Schmitt, K. Rajagopal, and T. Schäfer, 2008, Rev. Mod. Phys. **80**, 1455.
- Alford, M. G., and F. Wilczek, 1989, Phys. Rev. Lett. **62**, 1071.
- Alm, T., B. L. Friman, G. Röpke, and H. Schulz, 1993, Nucl. Phys. A **551**, 45.
- Alm, T., G. Röpke, and M. Schmidt, 1990, Zeitschrift für Physik A Hadrons and Nuclei **337**, 355.
- Alm, T., G. Röpke, A. Sedrakian, and F. Weber, 1996, Nucl. Phys. A **604**, 491.
- Alpar, M. A., S. A. Langer, and J. A. Sauls, 1984, ApJ **282**, 533.
- Anderson, P. W., 1958, Phys. Rev. **112**, 1900.
- Anderson, P. W., and N. Itoh, 1975, Nature **256**, 25.
- Anglani, R., R. Casalbuoni, M. Ciminale, N. Ippolito, R. Gatto, M. Mannarelli, and M. Ruggieri, 2014, Rev. Mod. Phys. **86**, 509.
- Arellano, H. F., F. Isaule, and A. Rios, 2016, Eur. Phys. J. A **52**, 299.
- Avogadro, P., F. Barranco, R. A. Broglia, and E. Vigezzi, 2008, Nucl. Phys. A **811**, 378.
- Babu, S., and G. E. Brown, 1973, Ann. Phys. (NY) **78**, 1.
- Bäckman, S.-O., G. E. Brown, and J. A. Niskanen, 1985, Phys. Rep. **124**, 1.
- Bäckman, S.-O., C.-G. Källman, and O. Sjöberg, 1973, Phys. Lett. B **43**, 263.
- Balberg, S., and N. Barnea, 1998, Phys. Rev. C **57**, 409.
- Balberg, S., and A. Gal, 1997, Nucl. Phys. A **625**, 435.
- Baldo, M., I. Bombaci, and U. Lombardo, 1992a, Phys. Lett. B **283**, 8.
- Baldo, M., G. F. Burgio, and H.-J. Schulze, 2000, Phys. Rev. C **61**(5), 055801.
- Baldo, M., J. Cugnon, A. Lejeune, and U. Lombardo, 1992b, Nucl. Phys. A **536**, 349.
- Baldo, M., and C. Ducoin, 2009, Phys. Rev. C **79**(3), 035801.
- Baldo, M., and C. Ducoin, 2017, Phys. Rev. C **96**(2), 025811.
- Baldo, M., Ø. Elgarøy, L. Engvik, M. Hjorth-Jensen, and H.-J. Schulze, 1998, Phys. Rev. C **58**, 1921.
- Baldo, M., U. Lombardo, and P. Schuck, 1995, Phys. Rev. C **52**, 975.
- Balian, R., H. Flocard, and M. Veneroni, 1998, eprint cond-mat/9802006.
- Bardeen, J., L. N. Cooper, and J. R. Schrieffer, 1957, Phys. Rev. **108**, 1175.
- Barranco, F., P. F. Bortignon, R. A. Broglia, G. Colò, P. Schuck, E. Vigezzi, and X. Viñas, 2005, Phys. Rev. C **72**, 054314.
- Baym, G., C. Pethick, and D. Pines, 1969a, Nature **224**, 673.
- Baym, G., C. Pethick, D. Pines, and M. Ruderman, 1969b, Nature **224**, 872.
- Bedaque, P. F., H. Caldas, and G. Rupak, 2003a, Phys. Rev. Lett. **91**(24), 247002.
- Bedaque, P. F., and A. N. Nicholson, 2013, Phys. Rev. C **87**(5), 055807.
- Bedaque, P. F., A. N. Nicholson, and S. Sen, 2015, Phys. Rev. C **92**(3), 035809.
- Bedaque, P. F., and S. Reddy, 2014, Phys. Lett. B **735**, 340.
- Bedaque, P. F., G. Rupak, and M. J. Savage, 2003b, Phys. Rev. C **68**(6), 065802.
- Benhar, O., and G. De Risi, 2017, J. Low. Temp. Phys. **189**, 250.
- Bertsch, G. F., 2013, *Nuclear Pairing: Basic Phenomena Revisited* (World Scientific Publishing Co), pp. 26–39.
- Bethe, H. A., 1971, Ann. Rev. Nucl. Part. Sci. **21**, 93.
- Bildsten, L., and R. I. Epstein, 1989, ApJ **342**, 951.
- Bloch, I., J. Dalibard, and W. Zwerger, 2008, Rev. Mod. Phys. **80**, 885.
- Bogoliubov, N. N., 1958, Soviet Physics Doklady **3**, 279.
- Bogoliubov, N. N., 1958, Il Nuovo Cimento **7**, 794.
- Boguta, J., 1981, Phys. Lett. B **106**, 255.

- Bohr, A., B. R. Mottelson, and D. Pines, 1958, Phys. Rev. **110**, 936.
- Botermans, W., and R. Malfliet, 1990, Phys. Rep. **198**, 115.
- Bożek, P., 2000, Phys. Rev. C **62**(5), 054316.
- Bożek, P., 2002, Phys. Rev. C **65**(3), 034327.
- Bożek, P., 2003, Phys. Lett. B **551**, 93.
- Bożek, P., and P. Czerski, 2002, Phys. Rev. C **66**(2), 027301.
- Brogia, R. A., and V. Zelevinsky, 2013, *Fifty Years of Nuclear BCS: Pairing in Finite Systems* (World Scientific Publishing Company).
- Brueckner, K. A., and J. L. Gammel, 1958, Phys. Rev. **109**, 1023.
- Bulgac, A., M. M. Forbes, and R. Sharma, 2013, Phys. Rev. Lett. **110**(24), 241102.
- Burgio, G. F., H.-J. Schulze, and A. Li, 2011, Phys. Rev. C **83**(2), 025804.
- Cao, L. G., U. Lombardo, and P. Schuck, 2006, Phys. Rev. C **74**(6), 064301.
- Carbone, A., A. Cipollone, C. Barbieri, A. Rios, and A. Polls, 2013, Phys. Rev. C **88**(5), 054326.
- Caroli, C., P. G. De Gennes, and J. Matricon, 1964, Physics Letters **9**, 307.
- Caroli, C., and J. Matricon, 1965, Physik der Kondensierten Materie **3**, 380.
- Cederwall, B., F. G. Moradi, T. Bäck, A. Johnson, J. Blomqvist, E. Clément, G. de France, R. Wadsworth, K. Andgren, K. Lagergren, A. Dijon, G. Jaworski, *et al.*, 2011, Nature **469**, 68.
- Chamel, N., D. Page, and S. Reddy, 2013, Phys. Rev. C **87**(3), 035803.
- Chandrasekhar, B. S., 1962, Applied Physics Letters **1**, 7.
- Chao, N.-C., J. W. Clark, and C.-H. Yang, 1972, Nucl. Phys. A **179**, 320.
- Chen, J. M. C., J. W. Clark, R. D. Davé, and V. V. Khodel, 1993, Nucl. Phys. A **555**, 59.
- Chen, J. M. C., J. W. Clark, E. Krotscheck, and R. A. Smith, 1986, Nucl. Phys. A **451**, 509.
- Cirigliano, V., S. Reddy, and R. Sharma, 2011, Phys. Rev. C **84**(4), 045809.
- Clark, J. W., C.-G. Källman, C.-H. Yang, and D. A. Chakkalakal, 1976, Phys. Lett. A **61**, 331.
- Clark, J. W., A. Sedrakian, M. Stein, X.-G. Huang, V. A. Khodel, V. R. Shaginyan, and M. V. Zverev, 2016, in *Journ. Phys. Conf. Ser.*, volume 702, p. 012012.
- Clogston, A. M., 1962, Phys. Rev. Lett. **9**, 266.
- Colucci, G., and A. Sedrakian, 2013, Phys. Rev. C **87**(5), 055806.
- Combescot, R., 2001, EPL **55**, 150.
- Cooper, L. N., 1956, Phys. Rev. **104**, 1189.
- de Blasio, F. V., and Ø. Elgarøy, 1999, Phys. Rev. Lett. **82**, 1815.
- Dean, D. J., and M. Hjorth-Jensen, 2003, Rev. Mod. Phys. **75**, 607.
- Delaroche, J.-P., M. Girod, J. Libert, H. Goutte, S. Hilaire, S. Péru, N. Pillet, and G. F. Bertsch, 2010, Phys. Rev. C **81**(1), 014303.
- Dickhoff, W. H., 1988, Phys. Lett. B **210**, 15.
- Ding, D., A. Rios, H. Dussan, W. H. Dickhoff, S. J. Witte, A. Carbone, and A. Polls, 2016a, Phys. Rev. C **94**(2), 025802.
- Ding, D., A. Rios, H. Dussan, W. H. Dickhoff, S. J. Witte, A. Carbone, and A. Polls, 2016b, Phys. Rev. C **94**(2), 025802.
- Donati, P., and P. M. Pizzochero, 2004, Nucl. Phys. A **742**, 363.
- Donati, P., and P. M. Pizzochero, 2006, Phys. Lett. B **640**, 74.
- Dong, J. M., U. Lombardo, and W. Zuo, 2013, Phys. Rev. C **87**(6), 062801.
- Drischler, C., T. Krüger, K. Hebeler, and A. Schwenk, 2017, Phys. Rev. C **95**(2), 024302.
- Eagles, D. M., 1969, Phys. Rev. **186**, 456.
- Elgarøy, Ø., and F. V. De Blasio, 2001, A&A **370**, 939.
- Elgarøy, Ø., L. Engvik, M. Hjorth-Jensen, and E. Osnes, 1996a, Nucl. Phys. A **604**, 466.
- Elgarøy, Ø., L. Engvik, M. Hjorth-Jensen, and E. Osnes, 1996b, Phys. Rev. Lett. **77**, 1428.
- Elgarøy, Ø., L. Engvik, M. Hjorth-Jensen, and E. Osnes, 1996c, Nucl. Phys. A **607**, 425.
- Elgarøy, Ø., and M. Hjorth-Jensen, 1998, Phys. Rev. C **57**, 1174.
- Eliashberg, G. M., 1960, Sov. Phys. JETP **11**, 696.
- Emery, V. J., 1959, Nucl. Phys. A **12**, 69.
- Emery, V. J., 1960, Nucl. Phys. A **19**, 154.
- Epstein, R. I., and G. Baym, 1988, ApJ **328**, 680.
- Fabrocini, A., S. Fantoni, A. Y. Illarionov, and K. E. Schmidt, 2005, Phys. Rev. Lett. **95**(19), 192501.
- Fabrocini, A., S. Fantoni, A. Y. Illarionov, and K. E. Schmidt, 2008, Nucl. Phys. A **803**, 137.
- Fan, H.-H., E. Krotscheck, and J. W. Clark, 2017, J. Low. Temp. Phys. **189**, 470.
- Fantoni, S., 1981, Nucl. Phys. A **363**, 381.
- Feibelman, P. J., 1971, Phys. Rev. D **4**, 1589.
- Fetter, A. L., 2009, Rev. Mod. Phys. **81**, 647.
- Filikhin, I., and A. Gal, 2002, Nucl. Phys. A **707**(3), 491, ISSN 0375-9474.
- Finelli, P., S. Maurizio, and J. W. Holt, 2015, in *Eur. Phys. J. Web Conf.*, volume 95, p. 04021, eprint 1411.7504.
- Flowers, E., M. Ruderman, and P. Sutherland, 1976, ApJ **205**, 541.
- Forbes, M. M., E. Gubankova, W. V. Liu, and F. Wilczek, 2005, Phys. Rev. Lett. **94**(1), 017001.
- Fortin, M., C. Providência, A. R. Raduta, F. Gulminelli, J. L. Zdunik, P. Haensel, and M. Bejger, 2016, Phys. Rev. C **94**, 035804.
- Frick, T., and H. Müther, 2003, Phys. Rev. C **68**(3), 034310.
- Frick, T., H. Müther, and A. Polls, 2004, Phys. Rev. C **69**(5), 054305.
- Fulde, P., and R. A. Ferrell, 1964, Phys. Rev. **135**, 550.
- Galitskii, V. M., 1958, Sov. Phys. JETP **7**, 104.
- Gandolfi, S., A. Gezerlis, and J. Carlson, 2015, Ann. Rev. Nucl. Part. Sci. **65**, 303.
- Gandolfi, S., A. Y. Illarionov, S. Fantoni, F. Pederiva, and K. E. Schmidt, 2008, Phys. Rev. Lett. **101**(13), 132501.
- Gandolfi, S., A. Y. Illarionov, F. Pederiva, K. E. Schmidt, and S. Fantoni, 2009a, Phys. Rev. C **80**(4), 045802.
- Gandolfi, S., A. Y. Illarionov, K. E. Schmidt, F. Pederiva, and S. Fantoni, 2009b, Phys. Rev. C **79**(5), 054005.
- Garcilazo, H., A. Valcarce, and J. Vijande, 2016, Phys. Rev. C **94**(2), 024002.
- Gezerlis, A., and J. Carlson, 2008, Phys. Rev. C **77**(3), 032801.
- Gezerlis, A., and J. Carlson, 2010, Phys. Rev. C **81**(2), 025803.
- Gezerlis, A., C. J. Pethick, and A. Schwenk, 2014, ArXiv eprints eprint 1406.6109.
- Gezerlis, A., and R. Sharma, 2012, Phys. Rev. C **85**(1), 015806.

- Ginzburg, V. L., and D. A. Kirzhnits, 1965, *Sov. Phys. JETP* **20**, 1346.
- Giorgini, S., L. P. Pitaevskii, and S. Stringari, 2008, *Rev. Mod. Phys.* **80**, 1215.
- Gold, T., 1968, *Nature* **218**, 731.
- González-Jiménez, N., C. Petrovich, and A. Reisenegger, 2015, *MNRAS* **447**, 2073.
- Goriely, S., N. Chamel, and J. M. Pearson, 2013, *Phys. Rev. C* **88**(6), 061302.
- Goriely, S., N. Chamel, and J. M. Pearson, 2016, *Phys. Rev. C* **93**(3), 034337.
- Gor'kov, L. P., 1958, *Sov. Phys. JETP* **9**(6), 505.
- Gor'kov, L. P., and T. K. Melik-Barkhudarov, 1961, *Sov. Phys. JETP* **13**, 1018.
- Greiner, M., C. A. Regal, and D. S. Jin, 2005, *Phys. Rev. Lett.* **94**(7), 070403.
- Gubankova, E., W. V. Liu, and F. Wilczek, 2003, *Phys. Rev. Lett.* **91**(3), 032001.
- Gulminelli, F., and A. R. Raduta, 2015, *Phys. Rev. C* **92**(5), 055803.
- Gusakov, M. E., P. Haensel, and E. M. Kantor, 2014, *MNRAS* **439**(1), 318.
- Haskell, B., and A. Sedrakian, 2017, *ArXiv e-prints eprint 1709.10340*.
- He, L., M. Jin, and P. Zhuang, 2006, *Phys. Rev. B* **74**(21), 214516.
- Heckel, S., P. P. Schneider, and A. Sedrakian, 2009, *Phys. Rev. C* **80**(1), 015805.
- Hempel, M., and J. Schaffner-Bielich, 2010, *Nucl. Phys. A* **837**, 210.
- Hewish, A., S. J. Bell, J. D. H. Pilkington, P. F. Scott, and R. A. Collins, 1968, *Nature* **217**, 709.
- Hoffberg, M., A. E. Glassgold, R. W. Richardson, and M. Ruderma, 1970, *Phys. Rev. Lett.* **24**, 775.
- Hornreich, R. M., 1980, *Journal of Magnetism and Magnetic Materials* **15**, 387.
- Huang, X.-G., 2010, *Phys. Rev. C* **81**(3), 034007.
- Isaule, F., H. F. Arellano, and A. Rios, 2016, *Phys. Rev. C* **94**(3), 034004.
- Isayev, A. A., 2008, *Phys. Rev. C* **78**(1), 014306.
- Iskin, M., 2008, *Phys. Rev. A* **78**(2), 021604.
- Jaikumar, P., and M. Prakash, 2001, *Phys. Lett. B* **516**, 345.
- Jin, M., L. He, and P. Zhuang, 2007, *Int. J. Mod. Phys. E* **16**, 2363.
- Jin, M., M. Urban, and P. Schuck, 2010, *Phys. Rev. C* **82**(2), 024911.
- Kadanoff, L., and G. Baym, 1962, *Quantum statistical mechanics: Green's function methods in equilibrium and nonequilibrium problems* (W.A. Benjamin).
- Kaiser, N., T. Nikšić, and D. Vretenar, 2005, *Eur. Phys. J. A* **25**, 257.
- Kaminker, A. D., P. Haensel, and D. G. Yakovlev, 1999, *A&A* **345**, L14.
- Kanada-En'yo, Y., N. Hinohara, T. Suhara, and P. Schuck, 2009, *Phys. Rev. C* **79**(5), 054305.
- Keller, J., and A. Sedrakian, 2013a, *Nucl. Phys. A* **897**, 62.
- Keller, J., and A. Sedrakian, 2013b, *Phys. Rev. C* **87**(4), 045804.
- Khodel, V. A., J. W. Clark, M. Takano, and M. V. Zverev, 2004, *Phys. Rev. Lett.* **93**(15), 151101.
- Khodel, V. A., J. W. Clark, and M. V. Zverev, 2001a, *Phys. Rev. Lett.* **87**(3), 031103.
- Khodel, V. A., V. V. Khodel, and J. W. Clark, 1996, *Nucl. Phys. A* **598**, 390.
- Khodel, V. V., V. A. Khodel, and J. W. Clark, 2001b, *Nucl. Phys. A* **679**, 827.
- Kolomeitsev, E. E., and D. N. Voskresensky, 2008, *Phys. Rev. C* **77**(6), 065808.
- Kolomeitsev, E. E., and D. N. Voskresensky, 2010, *Phys. Rev. C* **81**(6), 065801.
- Krotscheck, E., 2000, *J. Low. Temp. Phys.* **119**, 103.
- Krotscheck, E., and J. W. Clark, 1979, *Nucl. Phys. A* **328**, 73.
- Krotscheck, E., and J. W. Clark, 1980, *Nucl. Phys. A* **333**, 77.
- Krotscheck, E., R. A. Smith, and A. D. Jackson, 1981, *Phys. Rev. B* **24**, 6404.
- Kucharek, H., and P. Ring, 1991, *Zeitschrift fur Physik A Hadrons and Nuclei* **339**, 23.
- Kuckei, J., F. Montani, H. Müther, and A. Sedrakian, 2003, *Nucl. Phys. A* **723**, 32.
- Lacombe, M., B. Loiseau, J. M. Richard, R. V. Mau, J. Côté, P. Pirès, and R. de Tournel, 1980, *Phys. Rev. C* **21**, 861.
- Larkin, A. I., and A. B. Migdal, 1964, *Sov. Phys. JETP* **17**(5), 1146.
- Larkin, A. I., and Y. N. Ovchinnikov, 1965, *Sov. Phys. JETP* **20**, 762.
- Lattimer, J. M., M. Prakash, C. J. Pethick, and P. Haensel, 1991, *Phys. Rev. Lett.* **66**, 2701.
- Leggett, A. J., 1966, *Phys. Rev.* **147**, 119.
- Leggett, A. J., and S. Zhang, 2012, in *Lecture Notes in Physics, Berlin Springer Verlag*, edited by W. Zwerger, volume 836, p. 33.
- Leinson, L. B., 2011, *Phys. Rev. C* **83**(5), 055803.
- Leinson, L. B., 2012, *Phys. Rev. C* **85**(6), 065502.
- Leinson, L. B., 2013, *Phys. Rev. C* **87**(2), 025501.
- Leinson, L. B., and A. Pérez, 2006, *Phys. Lett. B* **638**, 114.
- Levenfish, K. P., and D. G. Yakovlev, 1994, *Astron. Lett.* **20**, 43.
- Link, B., 2009, *Phys. Rev. Lett.* **102**(13), 131101.
- Liu, W. V., and F. Wilczek, 2003, *Phys. Rev. Lett.* **90**(4), 047002.
- Lombardo, U., P. Nozières, P. Schuck, H.-J. Schulze, and A. Sedrakian, 2001, *Phys. Rev. C* **64**(6), 064314.
- Lombardo, U., and H.-J. Schulze, 2001, in *Physics of Neutron Star Interiors*, edited by D. Blaschke, N. K. Glendenning, and A. Sedrakian, volume 578, p. 30, eprint astro-ph/0012209.
- Long, W. H., P. Ring, N. V. Giai, and J. Meng, 2010, *Phys. Rev. C* **81**(2), 024308.
- Machleidt, R., 2001, *Phys. Rev. C* **63**(2), 024001.
- Machleidt, R., and D. R. Entem, 2011, *Phys. Rep.* **503**, 1.
- Mannarelli, M., C. Manuel, and L. Tolos, 2013, *Ann. Phys. (NY)* **336**, 12.
- Manuel, C., S. Sarkar, and L. Tolos, 2014, *Phys. Rev. C* **90**(5), 055803.
- Manuel, C., and L. Tolos, 2011, *Phys. Rev. D* **84**(12), 123007.
- Mao, S., X. Huang, and P. Zhuang, 2009, *Phys. Rev. C* **79**(3), 034304.
- Margueron, J., H. Sagawa, and K. Hagino, 2007, *Phys. Rev. C* **76**(6), 064316.
- Marques, M., M. Oertel, M. Hempel, and J. Novak, 2017, *Phys. Rev. C* **96**(4), 045806.
- Martin, N., and M. Urban, 2014, *Phys. Rev. C* **90**(6), 065805.
- Matsuo, M., 2006, *Phys. Rev. C* **73**(4), 044309.
- Maurizio, S., J. W. Holt, and P. Finelli, 2014, *Phys. Rev. C* **90**(4), 044003.
- Migdal, A., 1967, *Theory of Finite Fermi Systems: And Ap-*

- plications to Atomic Nuclei* (Interscience Publishers).
- Migdal, A. B., 1959, Nucl. Phys. A **13**, 655.
- Migdal, A. B., 1962, Nucl. Phys. A **30**, 239.
- Miyatsu, T., M.-K. Cheoun, and K. Saito, 2013, Phys. Rev. C **88**, 015802.
- Müther, H., and W. H. Dickhoff, 2005, Phys. Rev. C **72**(5), 054313.
- Müther, H., and A. Sedrakian, 2002, Phys. Rev. Lett. **88**(25), 252503.
- Müther, H., and A. Sedrakian, 2003, Phys. Rev. C **67**(1), 015802.
- Nambu, Y., 1960, Phys. Rev. **117**, 648.
- Nozières, P., and S. Schmitt-Rink, 1985, J. Low. Temp. Phys. **59**, 195.
- Oertel, M., A. F. Fantina, and J. Novak, 2012, Phys. Rev. C **85**(5), 055806.
- Oertel, M., C. Providência, F. Gulminelli, and A. R. Raduta, 2015, Journal of Physics G Nuclear Physics **42**(7), 075202.
- Page, D., J. M. Lattimer, M. Prakash, and A. W. Steiner, 2013, ArXiv e-prints eprint 1302.6626.
- Pais, H., S. Chiacchiera, and C. Providência, 2015, Phys. Rev. C **91**(5), 055801.
- Pankratov, S. S., M. Baldo, and E. E. Saperstein, 2015, Phys. Rev. C **91**(1), 015802.
- Papakonstantinou, P., and J. W. Clark, 2017, J. Low. Temp. Phys. **189**, 361.
- Partridge, G. B., W. Li, R. I. Kamar, Y.-a. Liao, and R. G. Hulet, 2006, Science **311**, 503.
- Pavlou, G. E., E. Mavrommatis, C. Moustakidis, and J. W. Clark, 2017, Eur. Phys. J. A **53**, 96.
- Peccei, R. D., and H. R. Quinn, 1977, Phys. Rev. Lett. **38**, 1440.
- Petrovich, C., and A. Reisenegger, 2011, A&A **528**, A66.
- Pines, D., J. Shaham, M. A. Alpar, and P. W. Anderson, 1980, Prog. Theor. Phys. Suppl. **69**, 376.
- Prakash, M., M. Prakash, J. M. Lattimer, and C. J. Pethick, 1992, ApJ Lett. **390**, L77.
- Pudliner, B. S., V. R. Pandharipande, J. Carlson, S. C. Pieper, and R. B. Wiringa, 1997, Phys. Rev. C **56**, 1720.
- Raduta, A. R., and F. Gulminelli, 2010, Phys. Rev. C **82**(6), 065801.
- Raduta, A. R., A. Sedrakian, and F. Weber, 2017, ArXiv e-prints eprint 1712.00584.
- Rajagopal, K., and F. Wilczek, 2001, *The Condensed Matter Physics of QCD* (World Scientific Publishing Co), pp. 2061–2151.
- Ramanan, S., S. K. Bogner, and R. J. Furnstahl, 2007, Nucl. Phys. A **797**, 81.
- Ramanan, S., and M. Urban, 2013, Phys. Rev. C **88**(5), 054315.
- Regal, C., and D. Jin, 2007 (Academic Press), volume 54 of *Advances In Atomic, Molecular, and Optical Physics*, pp. 1 – 79.
- Reinhard, P.-G., 2017, ArXiv e-prints eprint 1710.05667.
- Rijken, T. A., 2001, Nucl. Phys. A **691**, 322.
- Rijken, T. A., M. M. Nagels, and Y. Yamamoto, 2013, Few-Body Systems **54**(7), 801, ISSN 1432-5411.
- Ring, P., and P. Schuck, 1980, *The nuclear many-body problem* (Springer-Verlag, New York).
- Rios, A., A. Polls, and W. H. Dickhoff, 2017a, J. Low. Temp. Phys. **189**, 234.
- Rios, A., A. Polls, and W. H. Dickhoff, 2017b, J. Low. Temp. Phys. **189**, 234.
- Rios, A., A. Polls, A. Ramos, and H. Müther, 2006, Phys. Rev. C **74**(5), 054317.
- Rios, A., A. Polls, and I. Vidaña, 2009, Phys. Rev. C **79**(2), 025802.
- Röpke, G., A. Schnell, P. Schuck, and P. Nozières, 1998, Phys. Rev. Lett. **80**, 3177.
- Rubtsova, O. A., V. I. Kukulin, V. N. Pomerantsev, and H. Müther, 2017, Phys. Rev. C **96**(3), 034327.
- Sadhukhan, J., W. Nazarewicz, and N. Schunck, 2016, Phys. Rev. C **93**(1), 011304.
- Salasnich, L., 2011, Phys. Rev. C **84**(6), 067301.
- Sarma, G., 1963, Journal of Physics and Chemistry of Solids **24**, 1029.
- Sauls, J. A., D. L. Stein, and J. W. Serene, 1982, Phys. Rev. D **25**, 967.
- Savage, M. J., and J. Walden, 1997, Phys. Rev. D **55**, 5376.
- Schmidt, M., G. Röpke, and H. Schulz, 1990, Ann. Phys. (NY) **202**, 57.
- Schulze, H.-J., J. Cugnon, A. Lejeune, M. Baldo, and U. Lombardo, 1996, Phys. Lett. B **375**, 1.
- Schulze, H.-J., A. Polls, and A. Ramos, 2001, Phys. Rev. C **63**(4), 044310.
- Schwenk, A., and B. Friman, 2004, Phys. Rev. Lett. **92**(8), 082501.
- Schwenk, A., B. Friman, and G. E. Brown, 2003, Nucl. Phys. A **713**, 191.
- Sedrakian, A., 1998, Phys. Rev. D **58**(2), 021301.
- Sedrakian, A., 2001, Phys. Rev. C **63**(2), 025801.
- Sedrakian, A., 2003, Phys. Rev. C **68**(6), 065805.
- Sedrakian, A., 2005, Phys. Lett. B **607**, 27.
- Sedrakian, A., 2007, Prog. Part. Nucl. Phys. **58**, 168.
- Sedrakian, A., 2012, Phys. Rev. C **86**(2), 025803.
- Sedrakian, A., 2016, Phys. Rev. D **93**(6), 065044.
- Sedrakian, A., T. Alm, and U. Lombardo, 1997, Phys. Rev. C **55**, R582.
- Sedrakian, A., and J. W. Clark, 2006a, *Nuclear Superconductivity in Compact Stars: BCS Theory and Beyond* (World Scientific Publishing Co), p. 135.
- Sedrakian, A., and J. W. Clark, 2006b, Phys. Rev. C **73**(3), 035803.
- Sedrakian, A., and A. E. L. Dieperink, 2000, Phys. Rev. D **62**(8), 083002.
- Sedrakian, A., T. T. S. Kuo, H. Müther, and P. Schuck, 2003, Phys. Lett. B **576**, 68.
- Sedrakian, A., and U. Lombardo, 2000, Phys. Rev. Lett. **84**, 602.
- Sedrakian, A., J. Mur-Petit, A. Polls, and H. Müther, 2005, Phys. Rev. A **72**(1), 013613.
- Sedrakian, A., H. Müther, and A. Polls, 2006, Phys. Rev. Lett. **97**(14), 140404.
- Sedrakian, A., H. Müther, and P. Schuck, 2007, Phys. Rev. C **76**(5), 055805.
- Sedrakian, A., G. Röpke, and T. Alm, 1995, Nucl. Phys. A **594**, 355.
- Sedrakian, A. D., 1995, MNRAS **277**, 225.
- Shang, X.-l., and W. Zuo, 2013, Phys. Rev. C **88**(2), 025806.
- Shapiro, S. L., and S. A. Teukolsky, 1983, *Black holes, white dwarfs, and neutron stars: The physics of compact objects*.
- Shen, C., U. Lombardo, and P. Schuck, 2005, Phys. Rev. C **71**(5), 054301.
- Sinha, M., and A. Sedrakian, 2015, Phys. Rev. C **91**(3), 035805.
- Spinella, W., 2017, *A systematic investigation of exotic matter in neutron stars*, Ph.D. thesis, Claremont Graduate University/San Diego State University.

- Srinivas, S., and S. Ramanan, 2016, *Phys. Rev. C* **94**(6), 064303.
- Stein, H., A. Schnell, T. Alm, and G. Röpke, 1995, *Zeitschrift für Physik A Hadrons and Nuclei* **351**, 295.
- Stein, M., X.-G. Huang, A. Sedrakian, and J. W. Clark, 2012, *Phys. Rev. C* **86**(6), 062801.
- Stein, M., A. Sedrakian, X.-G. Huang, and J. W. Clark, 2014a, *Phys. Rev. C* **90**(6), 065804.
- Stein, M., A. Sedrakian, X.-G. Huang, and J. W. Clark, 2016, *Phys. Rev. C* **93**(1), 015802.
- Stein, M., A. Sedrakian, X.-G. Huang, J. W. Clark, and G. Röpke, 2014b, in *Journ. Phys. Conf. Ser.*, volume 496, p. 012008, eprint 1401.4651.
- Steiner, A. W., and S. Reddy, 2009, *Phys. Rev. C* **79**(1), 015802.
- Stoks, V. G. J., R. A. M. Klomp, C. P. F. Terheggen, and J. J. de Swart, 1994, *Phys. Rev. C* **49**, 2950.
- Stoof, H. T. C., M. Houbiers, C. A. Sackett, and R. G. Hulet, 1996, *Phys. Rev. Lett.* **76**, 10.
- Su, R. K., S. D. Yang, and T. T. S. Kuo, 1987, *Phys. Rev. C* **35**, 1539.
- Sumiyoshi, K., and G. Röpke, 2008, *Phys. Rev. C* **77**(5), 055804.
- Sun, B. Y., and W. Pan, 2013, *Nucl. Phys. A* **909**, 8.
- Sun, B. Y., H. Toki, and J. Meng, 2010, *Phys. Lett. B* **683**, 134.
- Sun, T. T., B. Y. Sun, and J. Meng, 2012, *Phys. Rev. C* **86**(1), 014305.
- 't Hooft, G., 1976, *Phys. Rev. Lett.* **37**, 8.
- Takahashi, M., T. Mizushima, K. Machida, and M. Ichioka, 2007, *J. Low. Temp. Phys.* **148**, 423.
- Takatsuka, T., S. Nishizaki, Y. Yamamoto, and R. Tamagaki, 2001, *Prog. Theor. Phys.* **105**(1), 179.
- Takatsuka, T., S. Nishizaki, Y. Yamamoto, and R. Tamagaki, 2002, *Prog. Theor. Phys. Suppl.* **146**, 279.
- Takatsuka, T., S. Nishizaki, Y. Yamamoto, and R. Tamagaki, 2006, *Prog. Theor. Phys.* **115**, 355.
- Takatsuka, T., and R. Tamagaki, 1971, *Prog. Theor. Phys.* **46**, 114.
- Takatsuka, T., and R. Tamagaki, 1981, *Prog. Theor. Phys.* **65**, 1333.
- Takatsuka, T., and R. Tamagaki, 1993, *Prog. Theor. Phys. Suppl.* **112**, 27.
- Thompson, C., and R. C. Duncan, 1995, *MNRAS* **275**, 255.
- Thouless, D. J., 1960, *Ann. Phys. (NY)* **10**, 553.
- Turolla, R., S. Zane, and A. L. Watts, 2015, *Reports on Progress in Physics* **78**(11), 116901.
- Typel, S., G. Röpke, T. Klähn, D. Blaschke, and H. H. Wolter, 2010, *Phys. Rev. C* **81**, 015803.
- Urban, M., and M. Oertel, 2015, *Int. J. Mod. Phys. E* **24**, 1541006.
- Van Dalen, E., G. Colucci, and A. Sedrakian, 2014, *Phys. Lett. B* **734**, 383.
- Vardanyan, G. A., and D. M. Sedrakyan, 1981, *Sov. Phys. JETP* **54**, 919.
- Vidaña, I., and L. Tolós, 2004, *Phys. Rev. C* **70**(2), 028802.
- Voskresensky, D. N., and A. V. Senatorov, 1987, *Sov. J. Nucl. Phys.* **45**, 657.
- Wambach, J., T. L. Ainsworth, and D. Pines, 1993, *Nucl. Phys. A* **555**, 128.
- Wang, Y. N., and H. Shen, 2010, *Phys. Rev. C* **81**(2), 025801.
- Warringa, H. J., 2012, *Phys. Rev. A* **86**(4), 043615.
- Warringa, H. J., and A. Sedrakian, 2011, *Phys. Rev. A* **84**(2), 023609.
- Weinberg, S., 1978, *Phys. Rev. Lett.* **40**, 223.
- Wilczek, F., 1978, *Phys. Rev. Lett.* **40**, 279.
- Wiringa, R. B., V. G. J. Stoks, and R. Schiavilla, 1995, *Phys. Rev. C* **51**, 38.
- Wlazłowski, G., K. Sekizawa, P. Magierski, A. Bulgac, and M. M. Forbes, 2016, *Phys. Rev. Lett.* **117**(23), 232701.
- Wu, X.-H., S.-B. Wang, A. Sedrakian, and G. Röpke, 2017, *J. Low. Temp. Phys.* **189**, 133.
- Xu, R., C. Wu, and Z. Ren, 2014, *Int. J. Mod. Phys. E* **23**, 1450078.
- Yakovlev, D. G., A. D. Kaminker, and K. P. Levenfish, 1999, *A&A* **343**, 650.
- Yang, C.-H., and J. W. Clark, 1971, *Nucl. Phys. A* **174**, 49.
- Yu, Y., and A. Bulgac, 2003, *Phys. Rev. Lett.* **90**(16), 161101.
- Zhou, X. R., G. F. Burgio, U. Lombardo, H.-J. Schulze, and W. Zuo, 2004, *Phys. Rev. C* **69**(1), 018801.
- Zhou, X.-R., H.-J. Schulze, F. Pan, and J. P. Draayer, 2005, *Phys. Rev. Lett.* **95**(5), 051101.
- Zuo, W., C. X. Cui, U. Lombardo, and H.-J. Schulze, 2008, *Phys. Rev. C* **78**(1), 015805.
- Zverev, M. V., J. W. Clark, and V. A. Khodel, 2003, *Nucl. Phys. A* **720**, 20.
- Zwierlein, M. W., A. Schirotzek, C. H. Schunck, and W. Ketterle, 2006, *Science* **311**, 492.